GEOTECHNICAL SPECIAL PUBLICATION NO. 196

New Technologies in Construction and Rehabilitation of Portland Cement Concrete Pavement and Bridge Deck Pavement

Edited by
Moon Won
Yoon Ho Cho
Shiraz Tayabji
Jianbo Yuan

ASCE
GEO INSTITUTE

GEOTECHNICAL SPECIAL PUBLICATION NO. 196

NEW TECHNOLOGIES IN CONSTRUCTION AND REHABILITATION OF PORTLAND CEMENT CONCRETE PAVEMENT AND BRIDGE DECK PAVEMENT

SELECTED PAPERS FROM THE 2009 GEOHUNAN INTERNATIONAL CONFERENCE

August 3–6, 2009
Changsha, Hunan, China

HOSTED BY
Changsha University of Science and Technology, China

CO-SPONSORED BY
ASCE Geo-Institute, USA
Asphalt Institute, USA
Central South University, China
Chinese Society of Pavement Engineering, Taiwan
Chongqing Jiaotong University, China
Deep Foundation Institute, USA
Federal Highway Administration, USA
Hunan University, China
International Society for Asphalt Pavements, USA
Jiangsu Transportation Research Institute, China
Korea Institute of Construction Technology, Korea
Korean Society of Road Engineers, Korea
Texas Department of Transportation, USA
Texas Transportation Institute, USA
Transportation Research Board (TRB), USA

EDITED BY
Moon Won
Yoon Ho Cho
Shiraz Tayabji
Jianbo Yuan

Published by the American Society of Civil Engineers

Library of Congress Cataloging-in-Publication Data

New technologies in construction and rehabilitation of Portland cement concrete pavement and bridge deck pavement : selected papers from the 2009 GeoHunan International Conference, August 3-6, 2009, Changsha, Hunan, China / hosted by Changsha University of Science and Technology, China ; co-sponsored by ASCE Geo-Institute, USA … [et al.] ; edited by Moon Won … [et al.].
p. cm. -- (Geotechnical special publication ; no. 196)
Includes bibliographical references and indexes.
ISBN 978-0-7844-1048-6
1. Pavements, Concrete--Design and construction--Congresses. 2. Pavements, Concrete--Maintenance and repair--Congresses. 3. Concrete bridges--Floors--Design and construction--Congresses. 4. Concrete bridges--Floors--Maintenance and repair--Congresses. 5. Portland cement--Analysis--Congresses. I. Won, Mooncheol. II. Changsha li gong da xue. III. American Society of Civil Engineers. Geo-Institute. IV. GeoHunan International Conference on Challenges and Recent Advances in Pavement Technologies and Transportation Geotechnics (2009 : Changsha, Hunan Sheng, China)

TE278.N485 2009
625.8'4--dc22 2009022666

American Society of Civil Engineers
1801 Alexander Bell Drive
Reston, Virginia, 20191-4400

www.pubs.asce.org

ISBN 978-0-7844-1048-6
Manufactured in the United States of America.

Geotechnical Special Publications

1 *Terzaghi Lectures*
2 *Geotechnical Aspects of Stiff and Hard Clays*
3 *Landslide Dams: Processes, Risk, and Mitigation*
7 *Timber Bulkheads*
9 *Foundations & Excavations in Decomposed Rock of the Piedmont Province*
11 *Dynamic Response of Pile Foundations - Experiment, Analysis and Observation*
14 *Geotechnical Aspects of Karst Terrains*
15 *Measured Performance Shallow Foundations*
16 *Special Topics in Foundations*
17 *Soil Properties Evaluation from Centrifugal Models*
18 *Geosynthetics for Soil Improvement*
19 *Mine Induced Subsidence: Effects on Engineered Structures*
21 *Hydraulic Fill Structures*
22 *Foundation Engineering*
23 *Predicted and Observed Axial Behavior of Piles*
24 *Resilient Moduli of Soils: Laboratory Conditions*
25 *Design and Performance of Earth Retaining Structures*
27 *Geotechnical Engineering Congress*
28 *Detection of and Construction at the Soil/Rock Interface*
29 *Recent Advances in Instrumentation, Data Acquisition and Testing in Soil Dynamics*
32 *Embankment of Dams - James L. Sherard Contributions*
33 *Excavation and Support for the Urban Infrastructure*
34 *Piles Under Dynamic Loads*
35 *Geotechnical Practice in Dam Rehabilitation*
37 *Advances in Site Characterization: Data Acquisition, Data Management and Data Interpretation*
39 *Unsaturated Soils*
40 *Vertical and Horizontal Deformations of Foundations and Embankments*
41 *Predicted and Measured Behavior of Five Spread Footings on Sand*
42 *Serviceability of Earth Retaining Structures*
43 *Fracture Mechanics Applied to Geotechnical Engineering*
44 *Ground Failures Under Seismic Conditions*
45 *In Situ Deep Soil Improvement*
46 *Geoenvironment 2000*
47 *Geo-Environmental Issues Facing the Americas*
48 *Soil Suction Applications in Geotechnical Engineering*
49 *Soil Improvement for Earthquake Hazard Mitigation*
50 *Foundation Upgrading and Repair for Infrastructure Improvement*
51 *Performance of Deep Foundations Under Seismic Loading*
52 *Landslides Under Static and Dynamic Conditions - Analysis, Monitoring, and Mitigation*
53 *Landfill Closures - Environmental Protection and Land Recovery*
54 *Earthquake Design and Performance of Solid Waste Landfills*
55 *Earthquake-Induced Movements and Seismic Remediation of Existing Foundations and Abutments*
56 *Static and Dynamic Properties of Gravelly Soils*
57 *Verification of Geotechnical Grouting*
58 *Uncertainty in the Geologic Environment*
59 *Engineered Contaminated Soils and Interaction of Soil Geomembranes*
60 *Analysis and Design of Retaining Structures Against Earthquakes*
61 *Measuring and Modeling Time Dependent Soil Behavior*
62 *Case Histories of Geophysics Applied to Civil Engineering and Public Policy*
63 *Design with Residual Materials: Geotechnical and Construction Considerations*
64 *Observation and Modeling in Numerical Analysis and Model Tests in Dynamic Soil-Structure Interaction Problems*
65 *Dredging and Management of Dredged Material*
66 *Grouting: Compaction, Remediation and Testing*
67 *Spatial Analysis in Soil Dynamics and Earthquake Engineering*
68 *Unsaturated Soil Engineering Practice*
69 *Ground Improvement, Ground Reinforcement, Ground Treatment: Developments 1987-1997*
70 *Seismic Analysis and Design for Soil-Pile-Structure Interactions*
71 *In Situ Remediation of the Geoenvironment*
72 *Degradation of Natural Building Stone*
73 *Innovative Design and Construction for Foundations and Substructures Subject to Freezing and Frost*

74 ***Guidelines of Engineering Practice for Braced and Tied-Back Excavations***
75 ***Geotechnical Earthquake Engineering and Soil Dynamics III***
76 ***Geosynthetics in Foundation Reinforcement and Erosion Control Systems***
77 ***Stability of Natural Slopes in the Coastal Plain***
78 ***Filtration and Drainage in Geotechnical/Geoenvironmental Engineering***
79 ***Recycled Materials in Geotechnical Applications***
80 ***Grouts and Grouting: A Potpourri of Projects***
81 ***Soil Improvement for Big Digs***
82 ***Risk-Based Corrective Action and Brownfields Restorations***
83 ***Design and Construction of Earth Retaining Systems***
84 ***Effects of Construction on Structures***
85 ***Application of Geotechnical Principles in Pavement Engineering***
86 ***Big Digs Around the World***
87 ***Jacked Tunnel Design and Construction***
88 ***Analysis, Design, Construction, and Testing of Deep Foundations***
89 ***Recent Advances in the Characterization of Transportation Geo-Materials***
90 ***Geo-Engineering for Underground Facilities***
91 ***Special Geotechnical Testing: Central Artery/Tunnel Project in Boston, Massachusetts***
94 ***Performance Confirmation of Constructed Geotechnical Facilities***
95 ***Soil-Cement and Other Construction Practices in Geotechnical Engineering***
96 ***Numerical Methods in Geotechnical Engineering: Recent Developments***
97 ***Innovations and Applications in Geotechnical Site Characterization***
98 ***Pavement Subgrade, Unbound Materials, and Nondestructive Testing***
99 ***Advances in Unsaturated Geotechnics***
100 ***New Technological and Design Developments in Deep Foundations***
101 ***Slope Stability 2000***
102 ***Trends in Rock Mechanics***
103 ***Advances in Transportation and Geoenvironmental Systems Using Geosynthetics***
104 ***Advances in Grouting and Ground Modification***
105 ***Environmental Geotechnics***
106 ***Geotechnical Measurements: Lab & Field***
107 ***Soil Dynamics and Liquefaction 2000***
108 ***Use of Geophysical Methods in Construction***
109 ***Educational Issues in Geotechnical Engineering***
110 ***Computer Simulation of Earthquake Effects***
111 ***Judgment and Innovation: The Heritage and Future of the Geotechnical Engineering Profession***
112 ***Soft Ground Technology***
113 ***Foundations and Ground Improvement***
114 ***Soils Magic***
115 ***Expansive Clay Soils and Vegetative Influence on Shallow Foundations***
116 ***Deep Foundations 2002: An International Perspective on Theory, Design, Construction, and Performance***
117 ***Discrete Element Methods: Numerical Modeling of Discontinua***
118 ***A History of Progress: Selected U.S. Papers in Geotechnical Engineering***
119 ***Soil Behavior and Soft Ground Construction***
120 ***Grouting and Ground Treatment***
121 ***Probabilistic Site Characterization at the National Geotechnical Experimentation Sites***
122 ***Sinkholes and the Engineering and Environmental Impacts of Karst***
123 ***Recent Advances in Materials Characterization and Modeling of Pavement Systems***
124 ***GeoSupport 2004: Drilled Shafts, Micropiling, Deep Mixing, Remedial and Specialty Foundation Systems***
125 ***Current Practices and Future Trends in Deep Foundations***
126 ***Geotechnical Engineering for Transportation Projects***
127 ***Recycled Materials in Geotechnics***
128 ***Soil Constitutive Models: Evaluation, Selection, and Calibration***
129 ***Advances in Designing and Testing Deep Foundations***
130 ***Advances in Pavement Engineering***
131 ***Contemporary Issues in Foundation Engineering***
132 ***Advances in Deep Foundations: In Memory of Michael W. O'Neill***
133 ***Earthquake Engineering and Soil Dynamics***
134 ***Soil Dynamics Symposium in Honor of Professor Richard D. Woods***
135 ***Erosion of Soils and Scour of Foundations***

136 *Innovations in Grouting and Soil Improvement*
137 *Legal and Liability Issues in Geotechnical Engineering*
138 *Site Characterization and Modeling*
139 *Calibration of Constitutive Models*
140 *Slopes and Retaining Structures under Seismic and Static Conditions*
141 *International Perspectives on Soil Reinforcement Applications*
142 *Waste Containment and Remediation*
143 *Geomechanics: Testing, Modeling, and Simulation*
144 *Sinkholes and the Engineering and Environmental Impacts of Karst*
145 *Seismic Performance and Simulation of Pile Foundations in Liquefied and Laterally Spreading Ground*
146 *Asphalt Concrete: Simulation, Modeling and Experimental Characterization*
147 *Unsaturated Soils 2006*
148 *Advances in Unsaturated Soil, Seepage, and Environmental Geotechnics*
149 *Site and Geomaterial Characterization*
150 *Soil and Rock Behavior and Modeling*
151 *Advances in Earth Structures: Research to Practice*
152 *Ground Modification and Seismic Mitigation*
153 *Foundation Analysis and Design: Innovative Methods*
154 *Pavement Mechanics and Performance*
155 *Underground Construction and Ground Movement*
156 *Geomechanics II: Testing, Modeling, and Simulation*
157 *Computer Applications in Geotechnical Engineering*
158 *Contemporary Issues in Deep Foundations*
159 *Case Studies in Earth Retaining Structures*
160 *Dynamic Response and Soil Properties*
161 *Embankments, Dams, and Slopes: Lessons from the New Orleans Levee Failures and Other Issues*
162 *Problematic Soils and Rocks and In Situ Characterization*
163 *Geoenvironmental Engineering*
164 *Innovative Applications of Geophysics in Civil Engineering*
165 *Geosynthetics in Reinforcement and Hydraulic Applications*
166 *Educational Activities in Geotechnical Engineering*
167 *Geotechnics of Soil Erosion*
168 *Grouting for Ground Improvement: Innovative Concepts and Applications*
169 *Soil and Material Inputs for Mechanistic-Empirical Pavement Design*
170 *Probabilistic Applications in Geotechnical Engineering*
171 *Advances in Shallow Foundations*
172 *Soil Improvement*
173 *Advances in Measurement and Modeling of Soil Behavior*
174 *Designing Our Underground Space*
175 *Field Measurements in Geomechanics 2007*
176 *Analysis of Asphalt Pavement Materials and Systems: Emerging Methods*
177 *GeoCongress 2008: Geotechnics of Waste Management and Remediation*
178 *GeoCongress 2008: Geosustainability and Geohazard Mitigation*
179 *GeoCongress 2008: Characterization, Monitoring, and Modeling of GeoSystems*
180 *From Research to Practice in Geotechnical Engineering*
181 *Geotechnical Earthquake Engineering and Soil Dynamics IV*
182 *Pavements and Materials: Characterization, Modeling, and Simulation*
183 *Sinkholes and the Engineering and Environmental Impacts of Karst*
184 *Pavements and Materials: Modeling, Testing, and Performance*
185 *Contemporary Topics in Deep Foundations*
186 *Contemporary Topics in In-Situ Testing, Analysis, and Reliability of Foundations*
187 *Contemporary Topics in Ground Modification, Problem Soils, and Geo-Support*
188 *Advances in Ground Improvement: Research to Practice in USA and China*
189 *Characterization, Modeling, and Performance of Geomaterials*
190 *Asphalt Material Characterization, Accelerated Testing, and Highway Management*
191 *Road Pavement Material Characterization and Rehabilitation*
192 *Recent Advancement in Soil Behavior, In Situ Test Methods, Pile Foundations, and Tunneling*
193 *Material, Design, Construction, Maintenance, and Testing of Pavement*
194 *Soils and Rock Instrumentation, Behavior, and Modeling*
195 *Performance Modeling and Evaluation of Pavement Systems and Materials*

This page intentionally left blank

Preface

The GeoHunan Conference has come at an opportune moment for the bridge construction and concrete pavement areas. In concrete pavement area, the last few years have seen significant enhancements in design and construction methodologies. In addition, the durability aspect of concrete pavement, which has been neglected for so many years, has finally started getting the attention it deserves. Current concrete pavement design procedures have been criticized for the lack of accuracy and obscure definitions of input variables in the design procedures. Papers submitted to this Conference reflect the efforts that researchers have made to address the deficiencies in the current concrete pavement design procedures. Since substantial portions of existing concrete pavement systems in some countries are approaching the end of their structural lives, rational methods for rehabilitation have become more important. The durability aspect of concrete pavement is becoming more important in many countries as well, since concrete pavements usually provide much longer performance period than asphalt pavement, and quite often, durability is the limiting factor to concrete pavement performance. Excellent papers were submitted in this area, which will help practitioners worldwide in improving the efficiency of their operations in rehabilitation designs and developing more durable concrete.

Bridges represent essential and important elements in the infrastructure system in any nation. Engineers have faced a number of issues related to optimum bridge designs and material selections, along with construction techniques. Different bridge types, design methods and construction techniques have been used in different parts of the world. Engineers should share their expertise and experience in this area so that better ideas and practices can be developed. The papers submitted in this area represent substantial information that researchers and practitioners have developed and gathered over the years. This information will undoubtedly enhance the state of knowledge in bridge design, materials selection and construction technique.

The editor wishes to thank the authors for their willingness to share valuable information with other professionals in this area and to spend their valuable time developing high quality papers. The editor also believes that the Proceedings will provide valuable resources for both researchers and practitioners and a reference for future research in this area.

Moon Won
Editor

This page intentionally left blank

Contents

Innovative Techniques for Bridge Deck Pavement Design and Construction

A Long Life Pavement for Orthotropic Bridge Decks in China 1
Robert Gaul

Optimization Design of Long-Span Steel Bridge Deck Pavement System 9
Lei Zhang, Wei Huang, and Zhendong Qian

An Innovative Rehabilitation Approach for the Bridge Deck Pavement 19
Hyung Bae Kim and Kwang-Ho Lee

Special Considerations and Analysis for the Bascule Bridge Pavement..... 28
Lei Zhang, Zhendong Qian, and Yun Liu

Structure Mechanical Study on Overlay of the Tied Arch Concrete Bridge Deck..... 35
Xue-lian Li and Yu-liang Chen

Project Design and Mechanical Analysis for Sutong Bridge Deck Pavement..... 45
Jian-jun Yang and Jian-long Zheng

Study on the Interface Treatment of Concrete Deck Pavement 52
Youqiang Pan, Zhongyin Guo, and Chen Ling

Effects of Material Design Parameters on Mechanical States of Bridge Deck Pavement 61
Tao Xu and Xiaoming Huang

Mechanic Analysis of Bridge Reinforcement with Mesh and Steel Fiber Reinforced Concrete and Experimental Construction Technology 68
Wen-xian Zhang, Bing Luo, and Shu-yang Jin

New Composite Pavement System for Orthotropic Steel Bridge Decks..... 76
Xue-lian Li and Yu-liang Chen

New Analysis Techniques and Materials for Portland Cement Concrete Pavement System

Stress Analysis of Portland Cement Concrete Pavement Slab under Various Supporting Conditions..... 85
Hongyuan Fu, Yang Zhang, and Bo Kuang

The Reliability Calculation Program and the Parameter Sensitivity Analysis of Airfield Cement Concrete Pavement..... 93
Le Li and Guo-ping Cen

Initial Behavior of Thin-Bonded Continuously Reinforced Concrete Overlay (CRCO) on Aged Jointed Concrete Pavement..... 101
Sung Woo Ryu, Min-Young Park, Jung-Hee Nam, ZuOg An, Jong-Oh Bae, Yoon-Ho Cho, and Seung Woo Lee

Physical Properties of Rapid-Setting Concrete Using Ultra Fine Fly Ash 107
Sungil Jeon, Jeong-Hee Nam, Ji-Hwan An, and Soo-Ahn Kwon

Repair of Longitudinal Joints and Cracks **119**
Dar Hao Chen, Taylor Crawford, David W. Fowler, James Jirsa, Megan Stringer, David Whitney, and Moon Won

Analysis on Criterion for Void Identifying under Cement Concrete Pavement Corner **125**
Sheng Zeng, Jia Xu, and Xiaojun Zeng

Differential Settlement Control Criterion of Bridge-Approach on People-Vehicle-Road Interaction **133**
Xiang-hua Tao

Deflection and Stress Analysis of Concrete Slab under Temperature and Axle Load Coupling **140**
Xinkai Li, Songlin Ma, and Xiangshen Hou

Sensitivity Analysis of Transverse Cracking for Continuously Reinforced Concrete Pavement **147**
Xudong Zha

Estimation of the Compressive Strength of Concrete Using Shear Wave Velocity **154**
Ji-Hwan An, Jeong-Hee Nam, Soo-Ahn Kwon, and Sung-Ho Joh

Performance of Continuously Reinforced Concrete Pavement Containing Recycled Concrete Aggregate **165**
Seongcheol Choi and Moon Won

Indexes

Author Index **173**

Subject Index **175**

A LONG LIFE PAVEMENT FOR ORTHOTROPIC BRIDGE DECKS IN CHINA

Robert Gaul*

*Vice President, ChemCo Systems, Inc.
2800 Bay Road
Redwood City, CA
Tel. 650-261-3790
gaul@chemcosystems.com

ABSTRACT

Pavements on orthotropic steel bridge decks in China have typically lasted three to seven years until the introduction of Epoxy Asphalt at the 2nd Yangtze River Bridge at Nanjing. The thermoset nature of Epoxy Asphalt compared to the thermoplastic bitumen paving materials previously used accounts for its ability to satisfy the requirements of skid resistance, a uniform riding surface and steel deck waterproofing for extended years even under severe ambient and load conditions. As of the end of 2008 over 500,000 square meters of Epoxy Asphalt have been installed on 20 orthotropic steel bridges in China. These installations are performing very well with few problems. Extensive laboratory test programs have been conducted to characterize the properties of this unique paving material. Although there are strict time and temperature constraints in the construction of Epoxy Asphalt pavements Chinese contractors have quickly learned how to install these pavements without significant problems.

INTRODUCTION

Since the beginning of widespread construction of orthotropic steel deck bridges in the middle of the last century most of these bridges throughout the world have experienced pavement life problems (Touran & Okereke, 1991). Cracking, rutting, and shoving have been commonplace on bridges that have employed polymer modified asphalt, SMA or mastic asphalt pavements. Orthotropic bridge decks in China have been no exception. With plate thickness as low as 12 mm and subjected to deck temperatures up to 70°C (158°F) during prolonged hot summers and with frequent overloads, orthotropic deck pavements in China have typically lasted only three to seven years. (Xu 2008, Yao & Cheng 2008). The need for an improved pavement in China has been rapidly growing as more orthotropic steel deck bridges have been built. In only in the last fifteen years China has built twenty bridges with orthotropic steel decks longer than 100 meters and there are at least another dozen under construction. This is in comparison to only twelve such bridges built in the United States in the last forty years.

PURPOSE OF THE PAVEMENT

The surfacing applied to orthotropic steel decks has three main purposes:

- provide a riding surface with suitable skid resistance
- provide a flat riding surface by varying its thickness to compensate for distortion of the steel deck plate
- protect the deck plate by providing a waterproofing layer.

(Medani, 2001)

To be successful on heavily traveled bridge decks a pavement must satisfy these requirements and be durable enough to withstand millions of loadings and overload under the severe ambient conditions of summer and winter without cracking, losing bond, rutting or shoving. Based on their performance since they were introduced in China in the year 2000 Epoxy Asphalt pavements appear to be able to meet these requirements and have the necessary durability. All of the installations are performing very well with a few very minor localized exceptions that are attributed to installation difficulties.

MAJOR BRIDGES IN CHINA PAVED WITH EPOXY ASPHALT

The first installation of ChemCo Systems' Type V Epoxy Asphalt in China was on the 2nd Yangtze River Bridge at Nanjing (Fig.1). By the end of 2008 twenty orthotropic decks totaling over 500,000 m^2 have been paved with this material including the world's longest cable stay Sutong Bridge (Fig. 2); the North (Fig. 3) and South cable stay bridges on the 36 km long Hangzhou Bay crossing; China's longest suspension bridge, the 1650 meter main span Xihoumen Bridge (Fig.4) near Zhoushan; and both the 708 meter cable stay and 1108 meter main span suspension bridge at HuangPu.

Table 1. Major Orthotropic Steel Decks Paved with Type V Epoxy Asphalt

BRIDGE	*LOCATION*	*YEAR PAVED*	*AREA M^2* *Approximate*
Nanjing 2nd Yangtze River	Nanjing	2000	37,140
Taoyaomen	Zhoushan	2003	20,600
Runyang Cable Stay	Zhenjiang	2004	22,740
Runyang Suspension	Zhenjinag	2004	44,700
Dagu	Tianjin	2004	3,700
Nanjing 3d Yangtze River	Nanjjing	2005	38,640
Pingsheng	Foshan	2006	14,000
Nanhuan	Beijing	2006	10,800
Zhanjiang	Zhanjiang	2006	20,500
Fenghua	Tianjin	2006	10,500
Yanglou	Wuhan	2007	38,400
Hangzhou Bay North	Cixi City- Jiaxing.	2007	32,000
Hangzhou Bay South	Cixi City- Jiaxing	2007	23,000
Sutong	Nantong-Sozhou	2007	65,000
HuangPu Cable Stay	Guangzhou	2008	24,400
HuangPu Suspension	Guangzhou	2008	34,700
Xihoumen	Zhoushan	2008	59,400
Jingtan	Zhoushan	2008	43,560

Fig 1. 2nd Yangtze River Bridge

Fig 2. Sutong Bridge

Fig 3. Hangzhou Bay North Bridge

Fig 4. Xihoumen Bridge

CHARACTERISTICS OF EPOXY ASPHALT

Epoxy Asphalt fulfills the purpose of a pavement for orthotropic steel decks because of its unique characteristics. Epoxy Asphalt is polymer concrete formed by first combining epoxy resin with a hardener that is extended with asphalt and then mixing with asphalt concrete aggregates. This process makes a polymer concrete that looks like asphalt concrete. The highest quality aggregate for conventional asphalt paving that is available is used in Epoxy Asphalt concrete. However, the physical properties are quite different than the various types of

asphalt concrete that have been used to pave orthotropic steel decks such as polymer-modified asphalt SMA and Gussasphalt (mastic asphalt).

Epoxy Asphalt is fundamentally different because it is a thermoset material that will not melt after it is cured, unlike the thermoplastic asphalt materials that will melt if heated again. A thermoplastic material can repeatedly soften and melt when heated and harden when cooled. A thermoset material undergoes a chemical change during curing to become permanently insoluble and infusible. The chemical cross-linking is the principal difference between a thermoset and a thermoplastic material. Thermoset materials have far better fatigue resistance and heat resistance than thermoplastic materials and those characteristics provide much better resistance to the cracking, rutting and shoving that have plagued orthotropic steel deck pavements worldwide. (Read & Whiteoak 2003)

The Epoxy Asphalt polymer is a two-phase chemical system with the polymerized epoxy resin/hardener being the continuous phase and the asphalt extender being the discontinuous phase. Thus the characteristics of epoxy/hardener continuous phase predominate. Epoxy Asphalt looks like asphalt because it contains asphalt whose black color masks all other appearance. The liquid Epoxy Asphalt is used as the binder for aggregate and as a bond coat to the steel deck and between layers of pavement.

How Epoxy Asphalt Satisfies the Purpose of the Pavement

Skid Resistance.

Epoxy Asphalt meets fulfills the purpose of adequate skid resistance because it incorporates the best available non-polishing aggregate and because the Epoxy Asphalt binder does not bleed. Unlike thermoplastic binders such as Guss Asphalt and SMA, Epoxy Asphalt does not melt at high temperature. Once cured Epoxy Asphalt binder is worn off of the trafficked surface so that the aggregate is exposed and remains exposed. This provides the maximum possible long term skid resistance over the life of the pavement. In 1995 the California Department of Transportation conducted skid tests on the then nineteen year old Epoxy Asphalt pavement on the San Francisco-Oakland Bay Bridge. This bridge carried over 25,000 vehicles per lane per day at that time including heavy trucks.

The results of the towed trailer ASTM E-274 test are shown in Table 2. (Seim & Gaul 1995)

Upper Deck Skid Numbers					Lower Deck Skid Numbers				
Lane 1	Lane 2	Lane 3	Lane 4	Lane 5	Lane 1	Lane 2	Lane 3	Lane 4	Lane 5
47.46	45.00	45.67	45.67	45.67	42.31	38.31	40.00	39.19	42.14

Provide a Flat Riding Surface

Epoxy Asphalt is installed with conventional asphalt paving equipment. (Figs 5&6) It can be laid in lifts as low as 19 mm with this equipment. Orthotropic steel decks are much flatter as installed today compared to the early installations of Epoxy

Asphalt where the pavement was utilized to make up for swales and dips as great as 50 mm.


Fig. 5 Laying Epoxy Asphalt


Fig. 6 Compacting Epoxy Asphalt

Protect the Deck as a Waterproofing Layer
Most decks that receive Epoxy Asphalt are first painted with a zinc rich primer as a backup for long term corrosion protection. Epoxy Asphalt bond coat that also acts as membrane is then applied at a thickness of about 0.67 mm. The Epoxy Asphalt pavement is then compacted to less than 3% voids. The system does not allow the passage of water or water vapor to the deck

To demonstrate the impervious nature of an Epoxy Asphalt pavement, Construction Technology Laboratory conducted Chloride ion penetration tests according to AASHTO Test Method T259. Epoxy Asphalt bond coat at a thickness of .67 mm and 25 mm of pavement were installed on four concrete slabs. After the Epoxy Asphalt cured, a 3% solution of sodium chloride was ponded on top of the Epoxy Asphalt for 90 days. The concrete under the Epoxy Asphalt was then analyzed for the presence of chloride ions by potentiometric titration with silver nitrate. No Chloride was found in any of the twelve slabs.

Durability- Resistance to Cracking
The primary cause of cracking of pavements on orthotropic steel decks is the negative moment resulting when the deck is loaded by wheels traveling adjacent to the longitudinal stiffeners. The resulting strains can be severe as the radius of curvature over the stiffener is relatively small. This curvature is determined by the size of the load, deck plate thickness and the width and spacing of the stiffeners.

In the United States the San Mateo-Hayward Bridge orthotropic deck has been in service for over forty years with no significant cracking. Epoxy Asphalt pavements have lasted for over 20 years without significant cracking on the San Diego-Coronado and Golden Gate Bridges.

In China the decks are subjected to higher summer time temperatures than in the United States. For that reason, prior to the first installation of Epoxy Asphalt on the 2nd Yangtze River Bridge at Nanjing Southeast University conducted a fatigue

crack test program formulated in conjunction with T.Y. Lin International. The program included comprehensive fatigue testing of composite beams of Epoxy Asphalt pavement on steel plates that simulated the construction and loading of the actual steel deck. (Figs 7 & 8) The tests were conducted at 0 deg C, 18 deg C and 60 deg C. They included overloads expected on the deck. All tests were extended to 12 million load cycles. There was no fatigue cracking under any of the conditions tested. (Test Report of Epoxy Asphalt Surfacing Materials Used For Nanjing Second Yangtze Bridge, 2000, unpublished report by Transportation College Southeast University). Subsequent tests at Southeast University have demonstrated the ability of the pavement to withstand 20 million load cycles without cracking (Yao & Cheng 2008). With few exceptions the installed pavements in China have shown little or no cracking.

Fig. 7 Fatigue Test Machine

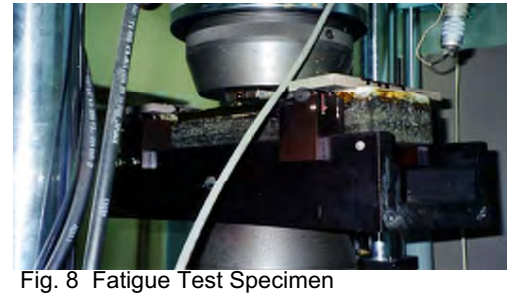
Fig. 8 Fatigue Test Specimen

Durability- Rutting and Shoving

None of the Epoxy Asphalt pavements in China have shown evidence of rutting or shoving. Laboratory rutting tests showed negligible rutting. This is to expected because of the thermoset nature of Epoxy Asphalt. It does not soften nearly as much as the bitumen pavements previously used. The Marshall Strength tests demonstrate that at 40 to 70 KN Epoxy Asphalt is 6 to 8 times more stable than conventional asphalt. (Read & Whiteoak 2003)

CONSTRUCTION OF EPOXY ASPHALT PAVEMENTS

Paving with Epoxy Asphalt is the same as paving with conventional asphalt except that the Epoxy Asphalt bonder takes the place of asphalt binder. Before the pavement is placed, a bond coat of Epoxy Asphalt is sprayed on to the steel deck and between layers of pavement. Trucks transport the paving mix to the bridge deck and dump into the paving machine. The pavement is usually installed in two 25 mm (total of 50 mm) lifts to assure compaction to less than 3% voids. For maximum fatigue cracking resistance the pavement must be compacted to below 3% air voids. Standard asphalt rollers compact the pavement. The temperature of every batch is measured and recorded. The average temperature of the batches in each truckload determines the time before which the load must be discharged into the paving machine. Breakdown rolling must be completed before the temperature of the mat drops below 82°C and final rolling must be completed before the mat temperature drops below 65°C.

EQUIPMENT REQUIREMENTS

In addition to the standard asphalt paving machine and rollers two special mixers for the installation are required.

- A special “Spray Distributor” machine is required that proportions and mixes the two components of the bond coat and delivers them at a controlled rate (Fig. 9).
- The two components of the Epoxy Asphalt polymer systems are premixed and injected into the pug-mill of the batch plant by a “Meter/Mix” machine. This machine uses mass flow meters to accurately proportion the two components and then mixes them and delivers the required amount for each batch (Fig. 10).

Fig. 9 Spray of Bond Coat

Fig. 10 Meter/Mix Machine (Red)

Four major paving contractors in China have acquired the special mixing equipment that is required. The Chinese contractors have also made important innovations in materials handling that have improved the construction of Epoxy asphalt pavements.

CONSTRUCTION CONSTRAINTS

Trucks transport the paving mix to the bridge deck and dump into the paving machine before the cure of the mix has advanced too far. This time can be as long as 90 minutes and as short as 60 minutes depending on the temperature of the mix. The temperature of every batch is measured and recorded. In order to achieve a maximum 3% voids in the compacted pavement the breakdown rolling must be completed before the temperature of the mat drops below 82°C and final rolling must be completed before the mat temperature drops below 65°C

CONCLUSION

Epoxy Asphalt has successfully fulfilled the purposes of skid resistance, uniform riding surface and waterproofing for orthotropic steel bridge decks in China and has proven to be a durable pavement on most of the major orthotropic steel bridges in China in recent years. The thermoset character of the Epoxy Asphalt binder provides the resistance to fatigue cracking and rutting that is important because of the high deck temperatures and overloads to which the pavements are subjected. Although the Epoxy Asphalt binder and bond coat required special mixing equipment and the reactive nature of these materials imposes time and temperature constraints on the installation Chinese contractors have learned how to successfully install Epoxy Asphalt.

REFERENCES

Touran, Ali and Okereke, Alex (1991) *Journal of Performance of Constructed Facilities*, Vol. 5, No. 2, May 1991, pp. 134-148.

Medani, T.O., (2001)*."* Asphalt Surfacing Applied to Orthotropic Steel Bridge Decks". *Report 7-01-127-1, Road and Railway Research Laboratory, Faculty of Civil Engineering*, Delft University of Technology, the Netherlands.

Yao, Bo and Cheng, Cheng, (2008) "Design of a Deck Surface for the Longest Cable Stay Bridge in the World: the Sutong Bridge"*, 2008 International Orthotropic Bridge Conference,* Sacramento, CA

Read, John and Whiteoak, David *Shell Bitumen Handbook, Fifth Edition 2003* ,pp 87-89 Thomas Tedford Publishing, London,

Seim, Charles and Gaul, Robert 1997 "San Francisco-Oakland Bay Bridge Surfacing Revisited", *SP-169 In Place Performance of Polymer Concrete Overlays,* American Concrete Institute, Detroit Michigan

Optimization Design of Long-span Steel Bridge Deck Pavement System

Lei Zhang[1], Wei Huang[2], and Zhendong Qian[3]

[1]Lecturer, Intelligent Transportation System Engineering Research Center, Southeast University, Nanjing
210096, China; lei800@163.com

[2]Professor, Intelligent Transportation System Engineering Research Center, Southeast University, Nanjing 210096, China; hwei@seu.edu.cn

[3]Professor, Intelligent Transportation System Engineering Research Center, Southeast University, Nanjing 210096, China; qzd@seu.edu.cn

ABSTRACT: Asphalt mixtures have been widely used for wearing surfaces on steel decks of long-span bridges. Due to the unique mechanical and environmental conditions of steel decks, requirements for paving materials and paving patterns are different from those for regular road pavements. Currently there are no commonly adopted design theories or procedures for steel bridge deck surfacing. Premature failures of deck pavements have often been observed on steel bridges, particularly on the newly-built long-span bridges in China. Therefore, two main objectives are identified in this paper as: 1) *integrating the separate design processes for the bridge structure and the deck pavement into one interactive process*; 2), *establishing the methodology of determining pavement system parameters*. Systematic research has been conducted to develop the design theory and procedure, from many aspects including pavement materials and structure, mechanistic characteristics of the wearing surfaces on steel decks, fatigue properties, axle-load equivalency conversion, and optimization design procedure. The *empirical-mechanistic approach* is employed for the optimization of design. The case study shows that it is more feasible to consider the orthotropic deck and its pavement as a whole structural system during bridge design.

INTRODUCTION

Since the 1990's, many long-span cable-stayed and suspension bridges have been built in the world, particularly in Japan and China. Orthotropic steel decks are usually applied on these bridges. Since systematic design theory and procedure for surfacing long-span steel bridge decks had not been developed before, severe premature distresses have been found in the wearing surfaces on most newly-built long-span bridges in China. Some of the bridges have been repaved several times during the

short period after opening to the traffic. Therefore, significant resources have been spent recently in developing the appropriate surfacing technology.

The conditions and requirements of surfacing on the steel deck, as seen in Figure 1 (*left part of the Figure cited from* Medani 2001), are far more stringent than those for the ordinary road pavement,. The typical properties of deck pavements are listed below.

1) Mechanics of orthotropic deck pavement system. Long-span bridges are more flexible than simply supported or continuous bridges. The orthotropic steel deck complicates the mechanistic analysis of the wearing surface. Supported by the stiffening structures under the deck plate, negative bending moment of pavement will be present above the top of stiffening ribs, transverse clapboard and longitudinal clapboard, consequently the longitudinal fatigue cracking will appear at these surface points and will extend through the pavement thickness downward, which is different from the reflection crack pattern and contraction crack pattern of the road surfacing.

2) The material properties. The thermal expansion coefficients of the pavement materials with respect to the high and low temperature will cause the problem of deformation consistence between the pavement and the steel deck.

3) Independent designs of the bridge and the wearing surface. Until now, except its mass, pavement layer has been ignored in the design of bridge structures with orthotropic steel deck. This adds more difficulties for the pavement designer. It is easily understood that an optimized design of both the bridge structure and the wearing surface can not only benefit the mechanistic analysis of the wearing surface but also reduce the cost of the whole structure.

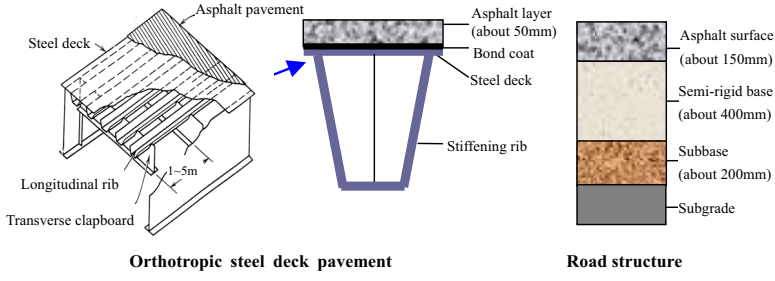

Figure 1 Difference between the Orthotropic Deck Pavement and Road

According to the mechanical characteristics and working conditions of steel deck pavement on the long-span bridges, the *empirical approach based on laboratory tests* was first employed to achieve the asphalt components and mixture design, and then the *mechanistic approach* was used to simulate and evaluate the working state of orthotropic deck pavement system. Finally, combined with these two steps, an

optimization design method of long-span steel bridge deck pavement system was established.

MIXTURE DESIGN REQUIREMENT AND FATIGUE PROPERTIES

The three typical pavement patterns applied on the long-span steel bridge deck are a single layer of one material, two layers of the same material, and two layers of different materials. In particular, because two-layer pavements can be designed jointly to overcome inconsistent properties (high temperature stability and low temperature anti-cracking ability) of material, it is more widely applied on long-span steel bridges.

The choices of layer pattern and material depend on the deck pavement characteristic as (Deck pavement group 2004, Huang 2003): 1) comparative higher strength and suitable thickness; 2) good bond attachment between the deck and the pavement; 3) high temperature stability and low temperature anti-cracking ability; 4) good durability, i.e., anti-aging, waterproof and fatigue resistance; 5) roughness, slipping and wearing abilities；6) water permeation；and 7) construction technique and quality control.

For asphalt mixture design, the *empirical approach containing laboratory tests* is employed. Due to paper length limitation, only the fatigue test is taken into account, which is especially important for the evaluation and prediction of pavement service life. Based on the data from extensive laboratory tests (Deck pavement group 2004), the results can be expressed in the form of a power function such as Eq.1.

$$N = A_1 \sigma^{-c_1} \tag{1}$$

Where, N : equivalent action times of standard axle-load； A_1, c_1:material constant. The coefficients obtained are listed in Table 1.

Table 1. Regression Coefficients for Fatigue Life evaluation

Mixture type	A_1	c_1	R^2
SMA	1547.3	5.319	0.9335
Gussasphalt	22.7	4.348	0.9935
Epoxy asphalt	8176.3	6.252	0.9870

MCHANIC ANALYSIS OF STEEL DECK PAVEMENT SYSTEM

Regarding the orthotropic steel deck, research has been done with many analytical methods; the main methods include the Fourier series method, the finite difference method, and the P-E method. However, when taking the pavement influence, particularly the partial interaction between the steel deck and asphalt surfacing layer, into account, it is difficult to obtain a pure analytical solution. Finite

element method (FEM) is selected to analyze the orthotropic steel deck pavement system in this study. The static analysis results follow.

For simplicity and representative brevity, a steel box girder model was adopted in the analysis. In this model, four diaphragms were contained. Considering the complexity of the steel deck pavement system, solid elements were used to simulate different material. In addition, two terminals of steel deck, pavement and longitudinal stiffening ribs were assumed to be completely fixed.

To analyze the stress variation on the steel deck pavement, three to seven transverse loading positions were selected on the transverse orientation of the deck with respect to the relative location of the load and the stiffening ribs, and simultaneously four to nine loading positions were selected on longitudinal orientation with regard to the distance between the load and longitudinal clapboards.

According to the FEM calculation, the maximum stress or strain of the pavement were obtained for three recently built bridges in China. Some results are listed in Table 2.

Table 2 FEM Computing Results of Steel Bridges Deck Pavement

Bridge Name	Max transversal tensile stress/strain (MPa/με)	Max longitudinal tensile stress/ strain (MPa/με)	Max transversal shear stress / longitudinal shear stress (MPa)	Max vertical displacement (mm)
Nanjing Second Yangtze River Bridge	0.821 / 753.3	0.521 / 477.9	0.249 / 0.077	0.840
Taoyaomen Bridge	0.804 / 724.5	0.498 / 454.1	0.251 / 0.078	0.812
Runyang Bridge	0.502 /402.6	0.365 / 238.1	0.434 / 0.189	0.722

The results indicate that the transversal tensile stress is the worst stress, and many research projects (Deck pavement group 2004, Zhang 2006) show that the FEM results and dual wheels load can be regressed in the form of a power function shown in Eq.2:

$$\sigma_x = a_1 P^{b_1} \tag{2}$$

Where, σ_x : maximum tensile stress on the surface of the pavement (MPa);
P: single-axle- dual wheels load (kN), a_1, b_1: regression coefficients.

Taking dual wheel load as an example, the simulation results show that a_1=0.0021, b_1=0.9967. The regression coefficients are very useful when the axle-equivalent method is carried out.

EQUIVALENT AXLE LOAD DETERMINATION

Based on Eq.1 and Eq.2, which are obtained from fatigue test results and FEM results respectively, the axle-equivalent method of steel deck pavement was summarized as follows (Zhang 2006):

$$\frac{N_1}{N_2} = \left(\left(\frac{P_1}{P_2} \right)^{b_1} \right)^{-c_1} = \left(\frac{P_2}{P_1} \right)^{b_1 c_1} = \left(\frac{P_2}{P_1} \right)^{n_1} \tag{3}$$

Where, P_1: standard axle-load (kN), P_2: axle-load to be exchanged (kN), N_1: equivalent repetitions of standard axle-load, N_2: applied repetitions of different axle-load to be exchanged, $n_1 = b_1 \cdot c_1$.

Coefficient b_1 can be obtained from Eq.2 by the analysis of FEM as mentioned before. And coefficient c_1 can be gained from Eq.1 as listed in Table 1. Substituting two coefficients into Eq.3, it is known that n_1 is 4.34, 5.310 and 6.241 for the Gussasphalt pavement, Epoxy asphalt pavement and SMA respectively.

Through the analysis above it can be seen that combined with the *empirical approach* for the mixture design and the *mechanistic approach* for the stress computation, the axle equivalent method can be achieved. This is the important step of the optimization design procedure for the steel deck pavement system.

DESIGN OPTIMIZATION OF STEEL DECK PAVEMENT SYSTEM

A steel box girder deck pavement system is a complicated composite structure because the components affect each other. However, the present design of deck pavement is separated from that of the steel deck and usually the deck pavement design is carried out after completing the design of the long-span bridge structure. This would easily lead to harsh requirements for the bridge deck pavement, greatly increase the difficulty of pavement design, and subsequently influence its service life. Therefore, the optimization of the whole steel deck system, including pavement, gradually becomes one of the focuses of the pavement researchers.

Structural optimization is the process to meet the minimum objective function by changing the design variables' value within the constraints of the state variables.

Design Variables

For design optimization of the steel deck pavement system, the design variables mainly include the geometry of the steel plate and the paving structure, transverse clapboard's position and the pavement material properties, etc. Based on the structural design parameters of the long span steel box girder bridges which have been constructed since 1990's, the structural optimization design variables of the steel deck pavement system are chosen as: thickness of the upper pavement $T1_1$, thickness of the

lower pavement $T1_2$, the steel plate thickness T_2 , modulus of the upper pavement $E1_1$, modulus of the lower pavement $E1_2$, lower bottom width of the longitudinal stiffening rib b, distance between of the longitudinal stiffening ribs d_{sp}, height of the longitudinal stiffening rib h, thickness of the longitudinal stiffening ribs t, span of transverse clapboard L.

State Variables

State variables (such as force, bending moment, stress and displacement etc.) control the design. Only when the state variables satisfy the given restrictive conditions (for example: the onsite stress is below the allowed stress, the deformation does not surpass allowed level), can the design be called a feasible design, which should be the precondition of the optimized design.

The parameters should meet the following requirements of the pavement system:

•Safety Constraint

When the design optimization of the steel beck pavement system is discussed, one of the criteria is not to exceed the tensile stress limit of the pavement:

$$\sigma_{\text{xmax}} \leq [\sigma_f]_{\text{allowance}} \tag{4}$$

Where: σ_{xmax}: the most disadvantageous stress which is obtained from the steel bridge deck pavement analysis, $[\sigma_f]_{\text{allowance}}$: the allowable tensile stress which may be gotten according to the fatigue test results of the pavement material.

•Performance Requirement

In order to enhance the ride comfort, safety and to control the surface strain level of the pavement, the ratio of central deflection to the span of trapezoid stiffening ribs(i.e. d/l) needs to be controlled, and the central deflection is calculated at the center point of these ribs. It is suggested that the allowed ratio of the steel deck deflection to the span of the ribs(i.e. $[d/l]_{\text{allowance}}$) should be smaller than about 1/500 according to Japanese Steel Bridge Guide and Euro Steel Bridge Code. Considering the fact that in recent years the asphalt mixture surface layer cannot be compliant with the large deformation of the steel deck, the range of $[d/l]_{\text{allowance}}$ should be 1/800 to 1/1700.

Hence, another criterion of the pavement design during the optimization process is to meet the deformation constraint of the pavement in terms of the ratio described above:

$$d/l_{\text{max}} \leq [d/l]_{\text{allowance}} \tag{5}$$

Where, d/l_{max}: the maximum ratio of the steel deck deflection to the span of the ribs, which is obtained from the steel bridge deck pavement analysis.

Objective Function

The objective function is often expressed by a function of design variables as $G_i=fi(x_1,x_2,\cdots,x_i)$, where G_i is the ith objective function, and $x_1,x_2,\cdots,x_i$ are members of design variables. In the structural design, and the objective function can be chosen for one or more different design requirements, such as the maximum weight, maximum

bearing capacity, the lowest cost of construction, and so on.

According to the structural design requirements of the steel deck pavement system, and the previous research projects, the objective functions can be constructed by two objectives of the lowest cost and the longest pavement service life, both of which are described as follows.

• The Lowest Cost

The total expense of the steel deck pavement system mainly contains two parts. One is the initial investment of construction. The other one is the cost caused by the maintenance and rehabilitation or resurfacing during pavement service life. The initial investment of construction and the other cost can be expressed by the following two equations, respectively.

$$F_1 = \sum_{i=1}^{n} C_{1i} V_{1i} + C_2 \mathrm{V}_2 \tag{6}$$

$$F_2 = p_f \cdot \sum_{i=1}^{n} C'_{1i} V_{1i} \tag{7}$$

Where, F_1: the initial investment expense, V_{1i} and C_{1i}: the volume of the ith layer of pavement and corresponding construction cost for unit volume, V_2 and C_2: the volume of the steel deck including steel plate and stiffening ribs, corresponding construction cost for unit volume, F_2: the pavement reconstruction expense at the end of its design service life, C'_{1i}: the rehabilitation cost of unit volume for the ith layer of pavement, and p_f: the pavement failure probability of the pavement layer's failure.

Obviously, the total cost can be expressed by $F_1 + F_2$. It is noted that the structure volume V_{1i} and V_2 can be expressed as the function of the dimensions (including length, width, thickness).

• The Longest Pavement Service Life

$$Y = \frac{N_f}{N_{eq}} \tag{8}$$

Where, Y: service life (year), N_f : fatigue life of the pavement (number of load repetitions), N_{eq}: accumulative times of equivalent axle load in a year (number of repetitions per year).

Here, N_f can be obtained from the fatigue test, but it should be modified due to the difference between the field performance and laboratory result. N_{eq} can be gained through the axle equivalent method mentioned previously, such as Eq.3. Of course, the axle equivalent equation is a function of the geometric dimensions.

From the discussion above, it is easy to know that both of the objective functions can be expressed in the geometric dimensions. Therefore, the dimensions are chosen as design variables. The solutions of the proposed method can be found in the textbooks (Jünger, M. 2001). It should be pointed out, when optimization procedure is carried out, parameters N_f and N_{eq} contain the connection between the *empirical approach including laboratory tests* and the *mechanistic approach.*

Example of the Steel Deck Pavement System Optimization

Taking Runyang Bridge, the longest-span bridge in China with steel box-girders, as an example, the optimization design model of the double-layer deck pavement system was established. Some parameters of the orthotropic steel deck are assumed as follows.

Steel deck Young's modulus E_2=210000MPa, Poisson's ratio μ_2=0.30, the thickness of the transverse clapboard and longitudinal clapboard t_2=10mm, the density of the upper layer pavement is 2.58g/cm^3, the density of lower layer pavement is 2.52g/cm^3, Poisson's ratio μ_1=0.25, and the density of the steel plate is 7.8g/cm^3. Other structural design variables' range and initial values are showed in Table 3.

Table 3 Initialization and Optimal results of steel deck pavement system

Parameters*	**$T1_1$ (mm)**	**$T1_2$ (mm)**	**T2 (mm)**	***u* (MPa)**	***b* (MPa)**	***d_sp* (mm)**	***h* (mm)**	***L* (mm)**	***t* (mm)**	**Y (year)**	***W* (1000 $/m)**
Initial	25	30	12	280	180	600	300	3200	8	13.47	31.7
Lower limit	20	20	8	200	150	500	240	2400	6	--	--
Upper limit	40	40	16	500	230	700	320	4000	10	--	--
Mode number	5	5	0.5	5	5	50	10	50	0.5	--	--
Empirical Design	25	35	14	300	170	600	280	3750	8	17.44	32.44
Reference **	21	26.5	11.4	289	170	600	319.9	3466	12	14.15	34.65
Optimized	20	35	14	300	190	500	320	3400	6	20.08	30.92

Note* : The meaning of parameters in the first line is already listed in the previous section *Design variables.*

** : the value from Reference (Deck pavement group 2004)

In the calculation, the maximum allowed tensile stress of the pavement is set to 0.7Mpa, and the maximum allowed ratio of the deflection to longitudinal rib span is set to 1/900. According to these constraints settings, the optimization design can be performed. After 10 iterations, the solution is converged, and the results are also listed in Table 3.

The parameter value from *Reference* (Deck pavement group 2004) is gained by the single-objective optimization design (only take the lowest deck system weight as objective function). The iteration number is about 80 based on an ordinary searching algorithm. Compared with it, the ant system is better for taking both construction cost and service life into account. The computing time of the system is also shorter than the ordinary searching algorithm. From Table 4， it is obvious that optimization design cannot only reduce the total cost of the structure but also increase service life of the pavement. These results indicate that it is feasible to use the proposed optimization model to solve the structural optimization problem of the steel bridge deck pavement

system. Furthermore, when there are more design variables, the structural computation model is more complex. Therefore, the fine algorithm employed in this paper would significantly improve the design method's efficiency. At the same time, owing to the use of the ant searching optimal strategy, the final parameter value is made out in the form of the mode number (discrete interval of the parameter) and thus it is convenient to apply it in the actual pavement projects.

CONCLUSIONS

This research tried to establish a feasible optimization design method for long-span steel bridge deck pavement system. The major results and findings are summarized as follows:

1) The analysis results indicated that the transverse tensile stress is the index which controls the mechanical state of the pavement and usually leads to longitudinal pavement cracks.

2) Combined with the *empirical approach* for the mixture design and the *mechanistic approach* for the pavement stress analysis, the axle load equivalent method was achieved. It should be pointed out that the axle equivalent method is one of the important steps during the optimization design, which connects the mixture design and the pavement structural design.

3) The proposed optimization design method took the steel deck and the pavement as an integral system, which is different to traditional design method. The final results indicated that when the pavement thickness is near 55 mm and the steel deck thickness is about 14 mm, the objective function achieves optimization. In general, if this design method is adopted in the practical projects, it can, not only reduce the total cost of the structure, but also increase service life of the pavement.

ACKNOWLEDGEMENTS

The authors wish to thank the National Science Foundation of China for providing the funds and support for this research through Project No. 50578038.

REFERENCES

AASHTO (2004). "AASHTO Guide for Design of Pavement Structures. Association of State Highway and Transportation Officials. " Washington, D.C.

Deck pavement group (2004). "Technical Study for Steel Deck Pavement on Runyang Yangtze River Highway Bridge." Report102, College of Transportation Southeast University, Nanjing, China.

Huang, W. (2003). “Epoxy Asphalt Concrete Paving on the Deck of Long-span Steel Bridges. ” Chinese Science Bulletin (English Version), Vol.47, No.24, pp1894-1897.

Jünger, M., Naddef, D. (2001). “Computational Combinatorial Optimization. ” Springer(1 edition), pp108-124.

Medani, T. O., Sc, M. (2001). “Asphalt Surfacing Applied to Orthotropic Steel Bridge Decks. ” Report 7-01-127-1, Faculty of Civil Engineering and Geosciences of Delft University of Technology, Delft, Netherlands.

Zhang lei, Qian Z. D. (2006). “Axle-equivalent Method of Steel-deck Pavement. ” Journal of Southeast University (English Version), Vol.26, No.1, pp85-90.

An Innovative Rehabilitation Approach for the Bridge Deck Pavement

Hyung Bae Kim and Kwang-Ho Lee

Senior Researcher, Expressway & Transportation Technology Institute, Korea Expressway Corporation, 50-5 San-Chuck-ri, Dong-tan, Hwa-Sung-shi, Kyungki-do 445-812, Korea, 445-812, E-mail: kimhyun3@ex.co.kr
R&D Director, Expressway & Transportation Technology Institute, Korea Expressway Corporation, 50-5 San-Chuck-ri, Dong-tan, Hwa-Sung-shi, Kyungki-do 445-812, Korea, 445-812, E-mail: LKH@ex.co.kr

Abstract. This study presents a rehabilitation method for the bridge deck pavement which has been damaged due to a moisture related failure of the asphalt concrete. In order to quickly drain the water which has infiltrated into the bridge deck pavement, this rehabilitation method adopts a new drainage system including a porous asphalt concrete layer and a polymer concrete based waterproofing layer so that the water cannot stay and cause moisture-related failure on the bridge deck. The most important factors for this drainage system are to meet satisfactory performance of the repairing material for the damaged concrete bridge deck, the waterproofing layer, and to develop a fast-track construction technique with a limited traffic blocking time. The porous asphalt mixtures for the new drainage system was suggested with the maximum aggregate size of 10mm, and was validated through various physical and mechanical laboratory tests to confirm its performance characteristics. In this study, methyl methacrylate (MMA)-type material was introduced for the water-proofing on the concrete bridge deck and damaged bridge deck repairing, and the results from a series of mechanical tests for evaluating the performance of the MMA material shows it has good capability for waterproofing and repairing of the concrete bridge deck which is subject to a moisture-induced neutralization of the cement concrete. In addition, to evaluate the field performance of the new rehabilitation method, a field study was conducted on a real bridge. Field performance observations on both the MMA and pavement materials indicated that the new method performs much better than traditional methods in draining water that has infiltrated into pavement layers.

Keywords: Bridge Deck Pavement, Moisture Damage, Waterproof, Drainage Layer, MMA

1.Introduction

Bridge deck pavements play an important role in providing comfortable and safe ride quality to the public by maintaining smoothness and surface friction of the bridge deck and protecting the structure against moisture damage. In Korea, premature failure and significant damage to the bridge deck due to infiltrated water has been considerably reduced by introducing waterproofing layers in the pavement system since the early

1980s. However, problems still remain, because water that has penetrated into the pavement may not drain out quickly but remains in the structure for a long time. Consequently, structural integrity of the bridge deck has often been degraded due to neutralization of the cement material, which has resulted in a premature failure of the bridge deck pavement. Therefore, there is a pressing need to develop better bridge deck paving systems that can quickly drain water and mitigate the neutralization of cement concrete bridge deck. Currently, drain channels buried under asphaltic layers are used to drain infiltrated water from the bridge deck pavement system in Korea. This drainage approach was not quite satisfactory and did not solve the premature failure of the pavement as demonstrated in Fig. 1. Fig. 1 presents the number of maintenances performed on each long-span bridge in Seoul during the year 2003 (Lee et al. 2005). Fig. 1 indicates that the potholes are the most frequent form of distress inferring that the currently used drain method for bridge deck pavements in Korea is somewhat inappropriate for mitigating moisture damage.

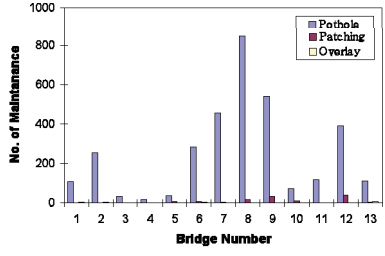

Fig. 1. Primary types of distress observed from bridge deck pavements in Seoul

In the current drain method, the infiltrated water located around the center of the pavement is not effectively transported and drained through the drain channel but most probably stays in the pavement system, which results in premature potholes and cracks due to significant moisture damage. To overcome the aforementioned problems observed from the current draining system, this study proposes the use of porous asphalt mixture to form a draining layer, as shown in Fig. 2. The draining layer of porous asphalt mixture is placed between a waterproofing layer and a top wearing course so that the water that penetrates into the pavement structure can be quickly drained out without causing any significant impact on the bridge deck.

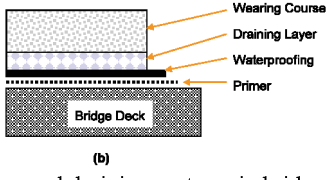

Fig. 2. New proposed draining systems in bridge deck pavements

The most important factors for the new bridge deck pavement drainage system would be to ensure the performance of a new type of waterproofing materials applied, and to

develop appropriate construction techniques for the thin drainage layer with less than 10mm maximum aggregate size. For the new type of waterproofing layer, methyl methacrylate (MMA)-type material was introduced, and a series of mechanical tests were performed to judge the applicability of the MMA material for waterproofing. To evaluate the field performance of the new drainage system proposed in this study, a field study has been conducted on a real bridge.

2. Development of the porous asphalt

2.1 Determination of mixture gradation

To determine allowable upper- and lower-gradation limits for the porous asphalt mixtures designed with the maximum aggregate size of 10mm, several Marshall specimens designed with different trial gradations were fabricated, and air voids of each specimen were monitored. Fig. 3 presents a finally determined gradation band composed of the upper-gradation to meet 17–18% air voids and the lower-gradation targeting 20–21% void content. The lower gradation was determined by simply shifting a gradation curve that has been typically used in Korea to produce porous asphalt mixtures with 13mm maximum aggregate size.

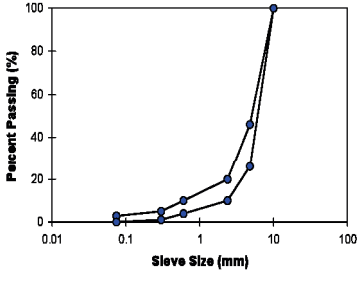

Fig. 3 Upper- and lower-gradation limits for porous asphalt mixtures with 10-mm maximum aggregate size

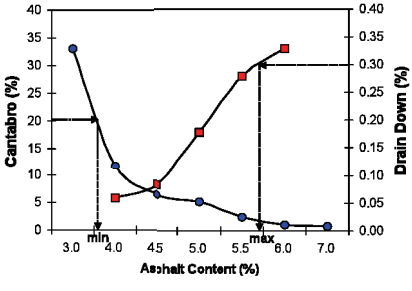

Fig. 4 Determination of maximum and minimum allowable asphalt content for the porous asphalt mixtures

2.2 Determination of optimum asphalt content

Based on the National Center for Asphalt Technology (NCAT) mixture design guide (Kandhal and Mallick 1999), an optimum asphalt content was determined in this study by performing two tests: the Cantabro test and the draindown test (AASHTO 2001), with a variation of trial asphalt contents from 3 to 7%. As demonstrated in Fig. 4, a minimum of 3.6% and a maximum of 5.7% of asphalt can be obtained from specification requirements: maximum allowable Cantabro loss is 20% and draindown is 0.3%, respectively. Within the range of asphalt content allowable, 5.2% was finally determined as the optimum asphalt content because it is at 20% air voids.

2.3 Laboratory tests results

Table 1 summarizes the laboratory test results. All test results met specification requirements (Korea Highway Corporation 2004). Average dynamic stability was 3342 cycles/mm, which was greater than the required value of 3000 cycle/mm, and moisture damage resistance of the mixture represented by the TSR was also satisfactory.

Table 1 Laboratory test results from porous asphalt mixtures and corresponding requirements in specification

Properties	*Specification*	*Test results*
Air void (%)	20 min.	20
Dynamic stability (cycle/mm)	3000 min.	3442
Cantabro loss (%)	20 max.	3.15
Draindown (%)	0.3 max.	0.208
Permeability coefficient (cm/sec)	0.02 min.	0.04
Moisture damage (TSR, %)	70 min.	80.3

3. MMA mortar and waterproofing

3.1 Characteristics of MMA and its composition

MMA is a reactive resin that is produced through a polymerization of acrylic and methacrylic acid ester. MMA resin is a very fast curing (typically less than one hour) material. Its fatigue performance and bonding strength to bridge deck are outstanding. Thus, it has long been used as a waterproofing material in Europe because of its excellent performance. However it has not been widely used in other regions including Korea because of its relative high cost compared to other types of waterproofing materials. The curing time of MMA resin is controlled by curing compound. Typically one or two percent of benzoyl peroxide is added to control the curing time of MMA resin. For the waterproofing, a liquid type of MMA resin is applied 2mm thick on top of the bridge deck, or MMA resin mixed with $CaCO_3$ and glass bid finer than 0.03mm is applied 5mm thick on the bridge deck. The latter is better if the unevenness of the bridge deck surface is severe and is the one used in this study. MMA resin can also be used as a repairing material for the deteriorated concrete bridge deck since its mechanical characteristics are better than typical cement concretes. In Germany, MMA resin mortar has been used for repair work (Silikal 2000). Although the cost of MMA resin mortar is more expensive than conventional cement concretes, when the rehabilitation time is limited, MMA resin mortar can be a good option for the repair work due to its fast curing characteristics. In this study, two different types of MMA resins were used for waterproofing and for repairing, respectively as follows:

• MMA waterproofing: MMA resin (1.00kg) + curing compound (0.02kg) + filler (5.00kg)
• MMA mortar: MMA resin (1.00kg) + curing compound (0.02kg) + filler (5.00kg) + fine aggregate (6.00kg)

3.2 Laboratory tests

MMA Mortar for Repairing
MMA mortar for repairing old bridge deck surfaces needs appropriate strength, durability, and bonding characteristics with existing cement concrete surfaces. In addition, the coefficient of thermal expansion of the mortar almost seven times larger than that of cement concrete so that the mortar should be flexible enough. In an attempt to estimate these required physical–mechanical characteristics, several laboratory tests were performed: uniaxial tensile tests to estimate bonding characteristics between the MMA mortar and the existing cement concrete surface, uniaxial compressive tests to obtain elastic modulus and strength of the mortar, and tests to monitor the coefficient of thermal expansion of the MMA mortar.
For the uniaxial tensile testing, each cement concrete cylinder fabricated (30mm tall and 50mm diameter) was subjected to treatment with a primer after removing laitance on top of the cylinder specimen. MMA mortar was then added to the cement concrete specimen to produce a 30mm long cylinder. A gluing jig and a uniaxial testing apparatus were developed to provide precise alignment of a cylindrical specimen with respect to the loading axis and to minimize eccentric stress concentration during tests. All tests were conducted using a servo-hydraulic closed-loop testing machine at both -20 ^{o}C and 20^{o}C. Each specimen was glued to the end plates that were connected to the loading frame through a load cell.
Similar to the uniaxial tensile testing, uniaxial compressive tests of MMA mortar were also performed with cylinder specimens of 100mm height and 150mm diameter. Each specimen was cured for a day before testing. Test results are summarized in Table 2. Properties of fast-curing cement mortar are also presented in Table 2 for comparisons. The fast-curing cement mortar has been traditionally used to fix old and deteriorated bridge deck surfaces.

Table 2 Mechanical testing results of MMA mortar

Properties	*PCC pavement*	*Fast-curing cement mortar*	*MMA mortar*
Tensile adhesion (MPa) -20 ^{o}C	-	-	14.1
Tensile adhesion (MPa) 20 ^{o}C	-	-	13.9
Compressive strength (MPa)	20 – 30	20 – 30	40-70
Elastic modulus (GPa)	22 – 30	25 – 35	6
Thermal expansion coefficient (/^{o}C)	1.2×10^{-5}	$1 - 3\times10^{-5}$	7×10^{-5}

MMA Waterproofing Layer
As demonstrated in a later section (Field Study of the New Drainage System), MMA materials were also applied to the waterproofing layer that connects the MMA mortar placed on top of the cement concrete bridge deck surfaces and the draining layer composed of the porous asphalt mixture. To estimate the mechanical performance, in

particular the bending characteristics and resistance to cracking of the MMA waterproofing layer, three-point bending beam tests at low temperatures (-10, 0, 10°C) were conducted, and test data from MMA specimens were compared to the test results from Guss asphalt mixtures that have often been used for waterproofing of bridge deck pavements in Korea. Specimen dimensions were 300mm long, 50mm wide, and 10mm for the both mixtures. Although the 10mm thickness is not representing the actual thickness, this test was performed for a comparison purpose. Test results from two replicates of each case were averaged and are illustrated in Figs. 5(a) and 5(b). As shown in Fig. 5, flexural strength decreased, while failure strain increased when specimens were tested at higher temperatures. The MMA mixtures generally experienced higher values in both flexural strength and failure strain than the Guss asphalt mixtures, which implies that the MMA materials perform better than Guss asphalt mixtures because of higher toughness and better resistance to low-temperature cracking.

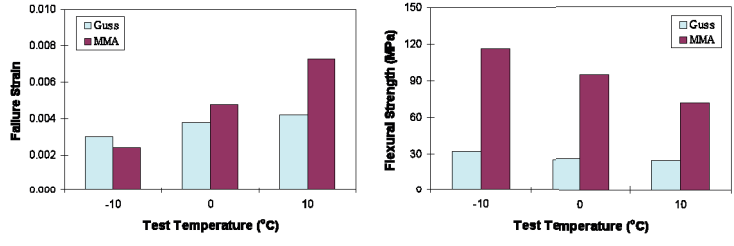

(a) (b)

Fig. 5 Test results comparing MMA waterproofing materials with Guss asphalt mixtures: (a) flexural strength at different test temperatures; (b) failure strain at different test temperatures

4. Field application of suggested rehabilitation method for the bridge deck pavement

4.1 Overview

In an attempt to implement the new rehabilitation method suggested in this paper into field construction and to estimate its performance characteristics and economic efficiency in the field, a trial construction was conducted on an existing bridge (210m long and 11.2m wide) in October 2007. It started its service in 1996 with an asphalt bridge deck pavement (8cm thick). As shown in Fig. 6, the bridge surface had been severely deteriorated with cracking and stripping inferring that the water had been infiltrated into the bridge deck pavement and was not well drained. From the extended field testing, it is found that the concrete deck was also widely damaged. The field trial bridge is located in a heavy snow area. Use of calcium chloride to melt snow in the winter season may accelerate the deterioration of the bridge deck. The regional maintenance office decided to rehabilitate both the bridge deck and pavement structure with a new drain system. The MMA material was applied to repair all deteriorated

cement concrete decks after the deteriorated areas were completely removed as well as provide the waterproof on the bridge deck. In addition, a variety of pavement structures including SMA, epoxy modified asphalt concrete, and porous asphalt concrete were applied to evaluate their performance in accompany with the new drain system and MMA materials as shown in Fig. 7.

Fig. 6 Distress on bridge deck pavement

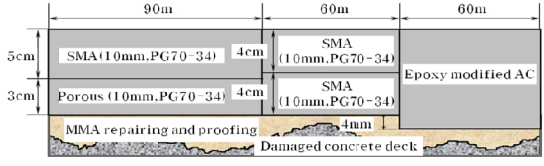

Fig. 7 Cross section of the in-field trial construction

The specific objectives of this field study are to investigate efficiency of the newly designed draining layer to drain water, determine locations for installation of drain channels and drip pipes, and estimate in-field applicability of MMA materials for repairing and waterproofing. Fig. 8illustrates a section view and a plan view of the bridge deck pavement with the new drainage system implemented.

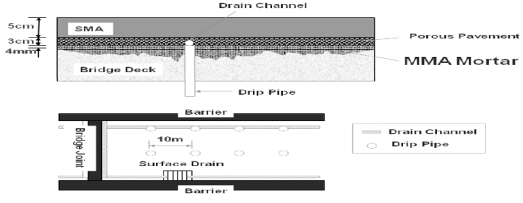

Fig. 8 Section view and plan view of bridge deck pavements with the new drainage system installed

A MMA mortar was placed on the deteriorated cement concrete deck at one time for both repairing and waterproofing saving significant construction time and labor cost. Top surfaces of the MMA layer were then treated with chipping aggregates followed by polymer-modified emulsifiers for tack-coating. Then, 30mm thick porous asphalt mixtures were placed to act as the draining layer. Finally, SMA mixtures were compacted to produce the 50mm thick wearing (surface) course. In order to accelerate draining of water that had penetrated into pavement layers, plastic drain channels of 15mm diameter and drip pipes of 10mm diameter were also installed within the draining layer. Fig. 8 also demonstrates that the drain channel with the diameter of 15mm was installed along the boundary between the concrete structure and the pavement. In addition to the use of drain channel, drip pipes (10mm in diameter) were also installed at every 10m interval to improve draining efficiency, which simply followed the methodology presented in Denmark guidelines (Vibeke 2000).

4.2 Performance evaluation of the new drainage system implemented in the field

Performance evaluation of the new drainage system was conducted after construction. On-site performance investigation was conducted twice: after three months (i.e., January 2007) and twenty months (i.e., June 2008) of public service. Fig. 9 shows pictures taken after three days of snowfall in June 2008. As shown in Fig. 9 pavement surfaces were completely dry, while water in the pavement was still drained through the drain channel. The field study clearly demonstrated that the new bridge deck pavement rehabilitation method performed very well without causing any significant moisture-related damage. Therefore, one can expect better-performing and longer-lasting pavements with the new rehabilitation method.

Fig.9 Investigation of in-field water draining after 20 months(June 2008) with the traditional bridge deck paving system

5. Conclusions

A rehabilitation method for the bridge deck pavement with a more quick drainage system and a MMA based material for waterproofing and repairing on the damaged bridge deck was developed in this study. Some of the important findings from this study can be summarized as follows:

1. The porous asphalt mixture design with the maximum aggregate size of 10mm was developed, and various physical and mechanical laboratory tests confirmed that the porous asphalt mixture satisfied all the specification requirements to form a thin drainage layer within the bridge deck pavement structure.
2. In order to overcome limitations observed from traditional waterproofing materials such as waterproofing sheets, MMA type waterproofing materials were employed in this study, and it was found that the MMA could be a good option for the repairing and waterproofing of deteriorated bridge decks.
3. A field study has been conducted to evaluate field performance of the new rehabilitation method for damaged bridge decks and pavement systems. It has been found that the suggested drainage system works quite well to drain the water that penetrates into pavement layers and MMA based waterproofing layer performs well. Based on field performance evaluation for twenty months after construction, it can be concluded that the new rehabilitation method performed very well due to better draining.

Acknowledgments

The study was conducted under the support of the research program for "Development of Long-lasting and Environmental Friendly Pavement Materials and Design-build Technology" funded by Korea Institute of Construction and Transportation Technology Evaluation and Planning.

6. References

AASHTO T283. 1999. *Resistance of Compacted Bituminous Mixture to Moisture-Induced Damage*. AASHTO Standards. Washington, D.C.

AASHTO T305. 2001. *Determination of Draindown Characteristics in Uncompacted Asphalt Mixtures*. AASHTO Standards. Washington, D.C.

Kandhal, P. S.; Mallick, R. B. 1999. *Design of New Generation Open-Graded Friction Courses*. Research Report No. 99-3. National Center for Asphalt Technology (NCAT). Auburn. Alabama.

Korea Highway Corporation. 2004. *Special Specification for Highway Construction*.

Lee, S. K.; Lee, H. J.; Park, S. W.; Seo, Y. C. 2005. *Strategic Research to Improve Road Pavement Quality in Seoul Metropolitan*. Research Report. Seoul Metropolitan Government. Korea.

Park, H. Y. 2005. *Development of a Drainage Method to Prevent Bridge Deck Pavement from Moisture Damage*. Master's Thesis. Sejong University. Seoul. Korea.

Silikal. 2000. *Reactive Resin and Polymer Concrete for Industrial Flooring and Civil Engineering*. Technical Documentation. Silikal. Germany.

Vibeke, W. 2000. *Surfacing of Concrete Bridge*. Research Report No. 106. Danish Road Institute. Denmark.

Special Considerations and Analysis for the Bascule Bridge Pavement

Lei Zhang[1], Zhendong Qian[2], and Yun Liu[3]

[1]Lecturer, Intelligent Transportation System Engineering Research Center, Southeast University, Nanjing 210096, China; lei800@gmail.com

[2]Professor, Intelligent Transportation System Engineering Research Center, Southeast University, Nanjing 210096, China; qzd@seu.edu.cn

[3]Ph.D., Intelligent Transportation System Engineering Research Center, Southeast University, Nanjing 210096, China; seuliuyun@126.com

ABSTRACT: The bascule bridge is one of the most appropriate bridges for ports and inland rivers from structural and economic viewpoints. However, the difficulty in successfully paving steel deck pavement remains to be solved for its wide applications. Serious premature failures of the pavements are found on many bascule bridges. So far, there is little discussion about this issue. In this study, the dynamic response of bascule bridge deck pavement was analyzed based on the different rotation velocities and different pavement elastic modulus for the Haihe Bridge being built in Tianjin, China, one of the largest bascule type bridges in the world. The results indicate that the shear stress of the pavement will increase greatly when the main girder opens wide, and simultaneously the girder rotation angle and rotation speed will lead to the non-uniform distribution of the shear stress. Since it is hard to control the pavement modulus due to the changing environmental temperature in the real world, an appropriate rotation velocity is suggested for reducing the shear stress between the pavement and the steel deck.

INTRODUCTION

Since there is no limitation on ship navigation clearance, the bascule bridge has become one of the most suitable bridges for ports and inland rivers and is widely applied in the world particularly in the United States and China. Compared with the ordinary bridge, the bascule bridge is unique in that: (1) the moveable girder leads to long cantilever span; (2) in order to reduce the total weight, the high strength steel is often used for main span, but this will cause a decrease in the stiffness; (3) it has two work states, i.e., the normal closed phase for traffic to pass by and the special opening (rotating) phase for the ships to pass through; and (4) special structural strengthening members should applied nearby the rotation axle (i.e., trunnion and hub). However, the girder rotation angle and rotation speed will lead to complicated distribution of the pavement stress and cause premature pavement failures, during the opening process. For example, as Evers (1977) recorded that, in Unite States, the Indian River Bridge at Port Carling, is a bascule bridge of orthotropic design and the first time the deck was raised, better than 50% of the asphalt concrete surface slid off. Therefore, the working state of the deck pavement on the bascule bridge has become a worldwide issue for decades.

This paper analyzed this issue from the structural aspects. Using the Haihe Bridge, one of the longest bascule bridges, as an example, the mechanical properties of the deck pavement

on the bascule bridge was studied. The Haihe Bridge links the new central business district and the old urban area in Tianjin. It has two flaps with a width of 20m on each side of the river. Two main longitudinal steel-box beams and perpendicular fourteen cross-girders clapboard support orthotropic steel decks. Each flap has about 819 tons in weight, and also has the counterweight which balances the flap about the main bearings. Each flap has a four lane traffic road, spanning 33.45m, as it can be seen in Fig. 1. and Fig. 2.

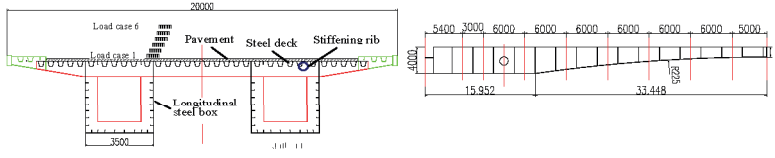

a) cross-section and load cases b) elevation drawing

FIG. 1. The general sketch of the structure

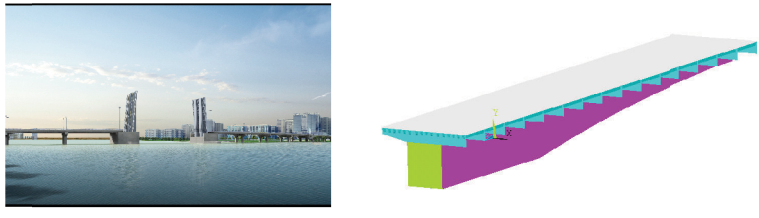

a) effective drawing b) Finite Element model

FIG. 2. The effective drawing of the Haihe Bridge and its FE model

ANALYSIS MODEL

Traditional methods such as Fourier series method and P-E method (Pelikan 1957) which need some hypothesis and further simplification were widely applied in mast planning or design of the main structure. However, in the case of deck pavement, the performance of the thin layer on the top of the main girder greatly relies on the defection of the supporting orthotropic deck. If some structural details are neglected, the local effect of the deck pavement will be omitted. This may lead to the similar results as that of the ordinary road pavement, which cannot interprete the more severe premature failures occurred in deck pavement. Therefore, the finite element method (FEM) was employed to analyze the deck pavement on the selected bascule bridge.

To simulate the deck pavement more precisely, solid element type was chosen. Since the steel plates such as the deck, the web and the flange are thin-walled structures, shell elements were selected to consider the membrane effect and reduce the total number of elements. Between the shell and solid elements, transition elements were used to link the two types of elements, i.e. to make the shells with an additional rotation degree of freedom and the solids

with only translational degree of freedom consistent. Because of the structural symmetry, half of the main span was set up as shown in Fig. 2. The geometry and material parameters are listed in Table 1.

Table 1. Geometry and material parameters

Parameter	Value	Parameter	Value
Deck thickness(mm)	20	Distance between U ribs (mm)	500
Transverse clapboard space(mm)	3200	U Stiffening rib height (mm)	251
Transverse clapboard thickness(mm)	16	Pavement thickness(mm)	50
U-shaped Stiffening rib thickness(mm)	6	Steel Poisson's ratio	0.3
U-shaped Stiffening rib top width(mm)	294	Steel elastic modulus (MPa)	210000
U Stiffening rib bottom width(mm)	171	Pavement modulus (MPa)	1000

NUMERICAL SIMULATION

The bascule bridge has two work states: normal closed phase and opening (rotating) phase. Correspondingly, both static analysis and dynamic analysis were carried out as follows.

Static Analysis

While the main span of the bascule bridge is closed for traffic, the mechanical properties of deck pavement are similar to those on the unmovable steel bridge with the similar dimensions of the orthotropic deck, so the method for the static analysis of orthotropic decks was adopted. To obtain the worst tensile stress of the pavement, six transverse load cases were selected on the transverse orientation of the deck with respect to the relative location of the load and the stiffening ribs or longitudinal web plate. At the same time, five loading positions were selected on longitudinal orientation with regard to the distance between the load and the transverse clapboard.

According to the FEM calculation, the maximum tensile stress on the pavement surface and the maximum shear stress between the pavement and the steel deck are listed in Table 2. The results indicate that the maximum transversal tensile stress is greater than the maximum longitudinal tensile stress and the maximum transversal shear stress is greater than the maximum longitudinal shear stress.

Table 2. The max stress of the pavement

Transversal Load Case	1	2	3	4	5	6
Max transversal tensile stress (MPa)	0.430	0.441	0.491	0.439	0.294	0.259
Max longitudinal tensile stress (MPa)	0.281	0.294	0.289	0.319	0.185	0.331
Max transversal shear stress (MPa)	0.185	0.272	0.265	0.133	0.200	0.143

Dynamic rotation analysis

While the main span of the bascule bridge is opening for ship navigation, the effect of the gravity and the rotation movement will affect the mechanical properties of the whole bridge including deck pavement. In this circumstance, dynamic rotation analysis was carried out. Before studying the influences of different aspects on the pavement response, the damping matrix should be determined first.

Damping coefficients

Rayleigh damping was adopted here. The damping matrix is expressed as a linear combination of the mass and stiffness matrices as $C = \alpha M + \beta K$. The coefficients α and β are constants which can be obtained from the equations below, if two mode-damping ratios ξ_i and ξ_j are available.

$$\alpha = \frac{2\left(\xi_i\omega_j - \xi_j\omega_i\right)}{\left(\omega_j^2 - \omega_i^2\right)}\omega_i\omega_j \qquad \beta = \frac{2\left(\xi_j\omega_j - \xi_i\omega_i\right)}{\left(\omega_j^2 - \omega_i^2\right)} \tag{1}$$

In civil engineering, the damping ratio of the bridge is normally selected between the range from 0.01 to 0.2, and it is assumed as 0.02 for the Haihe Bridge. Then the damping coefficients α and β can be obtained by substituting the damping ratio and the first two natural frequencies to Eq.1.

Influence of different opening angles

According to the design of the bridge, the maximum of opening angle of the main girder is 87°. During the rotation of the main girder (flap), the calculation results show that the longitudinal tensile stress of the pavement is larger than the transversal tensile stress, and the longitudinal shear stress is larger than the transversal shear stress, indicating the quite different mechanical states in the pavement of the bascule bridge during the opening process as those of the static analysis. Figure 3 illustrates the results of the longitudinal tensile stress and longitudinal shear stress versus flap opening angle.

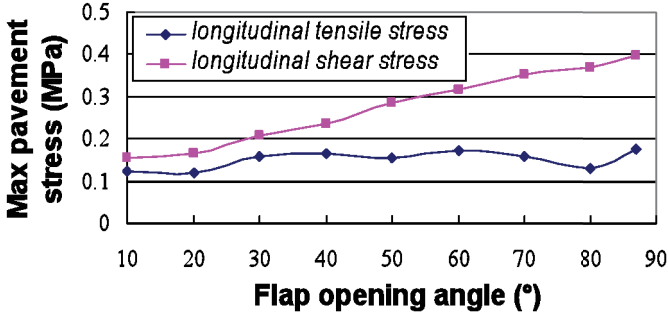

FIG. 3. Longitudinal stress vs. flap opening angle

It can be seen that longitudinal shear stress increases with the opening angle but the longitudinal tensile stress only fluctuates slightly with respect to the opening angle. The maximum longitudinal tensile stress is much smaller than the longitudinal shear stress during opening process. Therefore, the longitudinal shear stress was taken as the control stress in further research, and the case when the flap is fully opened at 87° was studied.

Influence of different rotation velocities

The dynamic responses of the pavement were analyzed under 0.15^{o}/s, 0.3^{o}/s, 0.5^{o}/s, 1^{o}/s, respectively. Assuming the pavement modulus is 1000MPa, the contour plotting and maximum value of the shear stress are list in Figure 4 and Table 3.

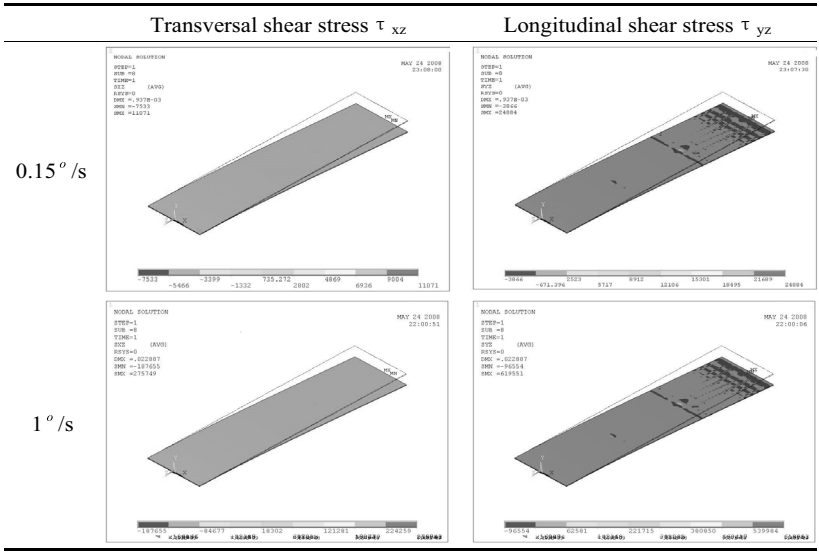

FIG. 4. Pavement shear stress results due to different rotation velocities

Table 3. Max pavement shear stress due to different rotation velocities

Rotation velocity	Vertical shear stress (MPa)	Transversal shear stress (MPa)	Longitudinal shear stress (MPa)
0.15^{o}/s	0.005	0.011	0.025
0.3^{o}/s	0.019	0.045	0.100
0.5^{o}/s	0.075	0.177	0.397
1^{o}/s	0.116	0.276	0.620

It is found the maximum shear stress occurs at the interface between the pavement and the steel deck, and increases rapidly with the growing of the rotation velocity. When the rotation velocity is low, the shear stress is inconspicuous. Comparably, when the velocity is high, the shear stress becomes notable, which is greater than the most disadvantage stress during closed phase by 26%.

The severer longitudinal shear stress confirms Evers' (1977) findings and becomes the main cause of the failure for deck pavement slid off.

Influence of different pavement elastic modulus

Due to the changing environmental temperature, the epoxy asphalt pavement modulus varies between the range from 500 to 2000MPa (Liu 2004, Huang 2003). Thus the dynamic

responses of the pavement were analyzed with the pavement modulus of 500MPa, 1000MPa, 1500MPa, 2000MPa respectively, and some of the results are listed in Table 4.

Table 4. Max pavement shear stress due to different pavement modulus

Pavement Modulus	Vertical shear stress (MPa)	Transversal shear stress (MPa)	Longitudinal shear stress (MPa)
Rotation velocity 0.3°/s			
500Mpa	0.010	0.022	0.049
1000Mpa	0.019	0.045	0.100
1500Mpa	0.027	0.066	0.149
2000Mpa	0.036	0.087	0.196
Rotation velocity 1°/s			
500Mpa	0.091	0.223	0.519
1000Mpa	0.116	0.276	0.620
1500Mpa	0.141	0.327	0.723
2000Mpa	0.165	0.374	0.831

Table 4 shows that the maximum shear stress increases with the enlargement of the pavement modulus. When the rotation velocity is relatively low (0.3°/s), the stress increases slightly, whereas it increases greatly when the rotation velocity is relatively high (1°/s). Supposed that the flap rotation velocity is 1°/s and the pavement modulus is 2000Mpa, the maximum shear stress exceeds the most disadvantage stress during the closed phase by 68%. The extreme shear stress 0.831MPa may cause bond failure between the pavement and the steel deck. To avoid this, the effective way is to decrease the rotation velocity, because little can be done to change the temperature. Furthermore, considering that the practical time requirements should be smaller than 5 minutes from the closed phase to the fully opened phase (87°)，the appropriate rotation velocity is suggested as 0.3°/s. At least, the rotation velocity should not be greater than 1°/s.

CONCLUSIONS

This research shows that the mechanical characteristics of the pavement on the bascule bridges are more complicated than those of pavement on the ordinary steel bridge deck. Static and dynamic approaches were employed respectively for analyzing two bascule bridge phases including closed and opening. The major results and findings are summarized as below.

1) According to the static analysis for the closed phase of the bascule bridge, the maximum stress was obtained. Analysis of the pavement indicates that the transverse tensile stress is the most disadvantageous factor that controls the mechanical state of the pavement.

2) The pavement state during opening phase is quite different to that of the ordinary closed phase. The maximum longitudinal tensile stress is much smaller than the longitudinal shear stress during opening phase.

3) The pavement response during the opening phase is sensitive to the rotation velocity of the main girder and pavement modulus. The maximum shear stress increases rapidly with the increase in the rotation velocity. When the rotation velocity is high, the maximum shear stress is greater than the most disadvantage stress during closed phase by 26%. The maximum shear stress also increases with the enlargement of the pavement modulus. Supposed the rotation velocity is relatively high (1^{o}/s) and the pavement modulus is 2000Mpa, the maximum shear stress will exceed the most disadvantage stress during closed phase by 68%.

4) To meet the requirements of practical application and the pavement safety, the appropriate rotation velocity of the main girder is suggested as 0.3^{o}/s. At least, the rotation velocity should not be greater than 1^{o}/s.

It should be pointed out that the bond coat between the pavement and the steel deck must be constructed carefully to provide enough shear resistance.

REFERENCES

Chopra Anil K. (2006). “Dynamics of Structures (3rd Edition).” *Prentice Hall*, New Jersey.

Evers R.C. (1977). “Dense Mastic Surfacing of an Orthotropic Bascule Bridge” *Ontario Ministry of Transportation & Communication*, pp73-125.

Huang, W., Qian Z. D., Cheng, G., Yang, J. (2003). “Epoxy Asphalt Concrete Paving on the Deck of Long-span Steel Bridges. ” *Chinese Science Bulletin* (English Version), Vol.47, No.24, pp1894-1897.

Pelikan W., Esslinger M.(1957). Die Stahlfahrbahn berechnung und konstruktion. *M.A.N. Forsch- Hft*, No.7, pp305-345(in German).

Liu Zhenqing (2004). “Research on Key Technology of Long-span Steel Bridges Deck Surfacing Design.” Doctoral Dissertation, *College of Transportation at Southeast University*, Nanjing, China.

Structure Mechanical Study on Overlay of the Tied Arch Concrete Bridge Deck

Li Xue-lian[1], Chen Yu-liang[2]

[1]Lecturer and PhD, School of Communication and Transportation Engineering, Changsha University of Science and Technology, Chiling Road 45#, Changsha, Hunan, China, 410076. E-mail: lixuelianfj@yahoo.com.cn

[2]Lecturer, School of Engineering & Architecture, East China Jiaotong University, Nanchang, Jiangxi, China, 330013. E-mail: chenyuliangjx@yahoo.com.cn

ABSTRACT: The structural behavior of the double-layered asphalt concrete Huanghe bridge was analyzed by the FEM (Finite Element Method). The most critical loading location for the bridge pavement was determined, and the control indexes for the asphalt pavement established. For the most adverse loading cases, the variations of asphalt overlays around wheel paths were analyzed and the corresponding three-dimensional graphs presented. To determine the influences of horizontal cyclic loads on the control index, different asphalt overlays under various horizontal cyclic loads were analyzed. To simulate the boundary conditions, the bridge, including beams, arch ribs, suspenders, and pavement were analyzed. Experiments were conducted in coordination with the finite element analysis. A relationship between shearing and bonding strength under varying temperatures was established, also, the interlayer stable control index, and bonding strength under 15℃, were determined. An in-situ pullout test was performed using the pullout apparatus designed by the research team to verify the stability of inter-layers. (You need to provided the specific finding and results in the abstract)

KEYWORDS:FEM; tied arch bridge; bridge deck overlays; waterproof-and-binding layer; shearing strength; bonding strength

INTRODUCTION

The quality of a bridge is reflected in part by the performance of its pavement. Thus, it is critical to minimize deterioration caused by traffic, environmental impacts, and/or hidden construction defects or faults. The quality of the pavement directly affects the driving quality and durability. However no standard for the design of concrete bridge deck pavement exists in China. The bridge design program considers pavement as simply a structural layer. Recently, researchers have begun to examine pavement in

more detail due to frequently reported problems including cracking, rutting and fatigue of bridge pavement. Zhang Zhan-jun (2000) utilized FEM (Finite Element Method) to analyze the shear stress of concrete bridge pavement with and without a waterproofing layer. Wang Jing-yuan (2003) presented the law of shear stress with horizontal and vertical loading. Luo Li-feng (1999) touched on the design method of bridge pavement associated with thin plate theory. However, the upper structure was simplified in the literature, resulting in the analysis model and the boundary conditions differing from actual conditions. To solve such problems, related bridge structure theory and pavement design method were used to study the double-layered asphalt concrete of the 100 m-span tied arch concrete bridge of the second Huanghe bridge.

CALCULATION PARAMETERS AND MODEL

The second Huanghe bridge is an oversize concrete bridge in Jing-Zhu on the main state road. It is 9848.16m in length, 19.377m in unidirectional width and the design driving speed is 120km/h. The 100m-span tied arch bridge is composed of beams, arch ribs, suspenders, bridge deck, pavement and etc.

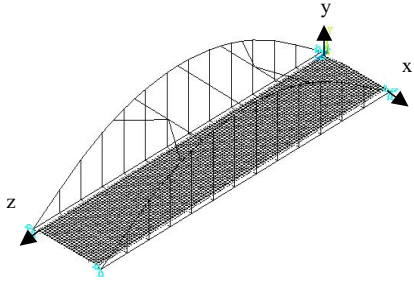

Fig.1. The second Huanghe bridge calculation model

Table 1. Basic Parameter of the Deck of Tied Arch Bridge

Layer	Material	Thickness (cm)	Modulus (MPa)	Poisson ratio (μ)
Surface	AC-13I modified asphalt concret	4	2200	0.25
Middle course	AC-16I modified asphalt concrete	5	2000	0.25
Bottom course	40# steel fibre cement concrete	8	35000	0.15
Bridge deck	50# plain cement concrete	12	35000	0.15

The analysis model (Fig. 1.) is the same size as the actual structure, the calculated span is 95.5m, the width is 19.377m, and the transverse slope is 2%. Because the upper structure is simply supported by the pier, displacement in three direction of one end in the model was limited, and the vertical and longitudinal displacement was limited on the other end. The basic parameter of the model is shown in Table 1.

MECHANICAL ANALYSIS

The model was first coarsely meshed to determine the weakest load location. Then the area nearby the weak load location was meshed again, and the bridge deck pavement system under the wheel path was analyzed, 1.4m in the transverse direction and 2m in the longitudinal direction.

According to the standard (2006), the standard axle load was used for analysis. To simplify the calculation, the tire/ground contact area of the wheel was turned from a circle (JTJ D50-2006) into a square, 200mm×200mm. The distance between wheels used was 300mm. The horizontal load produced as the vehicle brakes or starts to accelerate was used. The horizontal load was assumed to be proportional to the vertical load, with the proportional coefficient of *f*. Because the design load uses a double wheel, there are two loading modes: the first loading mode, midpoint between two wheels was added to the weakest location; the second loading mode, center of one wheel was added to the same location.

Weakest LOADING LOCATION

Because it is symmetric in longitudinal and transverse direction, the focus load was added uniformly on 104 positions in 1/4 bridge (Fig. 2), vertical component force, 50 kN, and horizontal force 0.2×50=10kN. The real lines in Fig. 2 represent ribs and beams, while ⊕ indicates loading location.

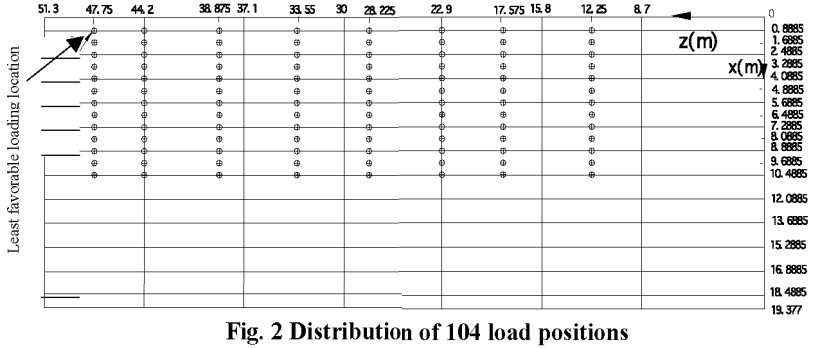

Fig. 2 Distribution of 104 load positions

According to the analysis results, the maximum principle stress, the maximum transverse tension stress, the maximum vertical tension stress, the maximum longitudinal tension stress, the maximum transverse shear stress, the maximum vertical shear stress, the maximum longitudinal shear stress and the maximum displacement of the bridge deck pavement resulted when the focus loading on the mid span was x＝0.8885m，y＝0，z＝47.75m (Fig. 2). So the mid span appears to be the weakest location.

CRACKING

Cracking is one of the most common failures in cement concrete bridge deck pavement, and the maximum tension stress is an important design index to control cracking. Analyzing the applicable laws of stress will help to determine failure characteristics and effective prevention measures. The calculations are shown in Table 2.

Table 2. Maximum Tension Stress in Bridge Deck Pavement

Index	First loading mode	Second loading mode
Maximum principle stress σ_{1max}(MPa)	0.1751	0.1746
Maximum transverse tension stress	0.1047	0.0798
Maximum longitudinal tension stress	0.0648	0.0671

According to Table 2, the maximum transverse tension stress is almost equal to the maximum principle stress under the two loading modes, but the maximum transverse tension stress is bigger than the longitudinal. Because of the complexity of the principle stress, the maximum transverse stress was used as the primary design index for the pavement controlling the cracking failure. Observations of the index under the first loading mode concluded it to be bigger than the second, thus determining the first mode to be the weakest loading mode. Also, σ_{xmax} occurred at the 0.05m-front of the midpoint between the two wheels.

Fig.3 presents the distribution of transverse positive stress on the horizon plane at the position of maximum value, indicating that: (1) the positive tension stress right under the wheel is compressive stress, but there is local tension stress in front of the two wheels. Notably, there is maximum tension stress at 0.05m in front of the wheel, of 0.1047MPa; (2) there are also two smaller tension stresses beside each wheel, of 0.015MPa; cumulatively leaving the pavement vulnerable to cracking in three locations.

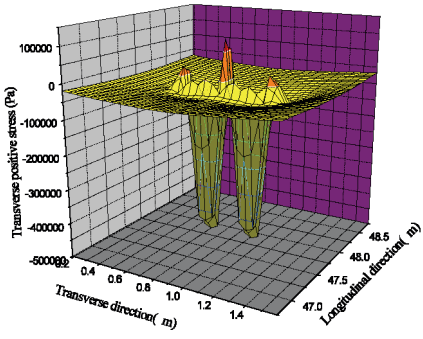

Fig. 3 Distribution of transverse positive stress on horizon plane at the position of maximum value

DELAMINATION

Because the pavement on the Huanghe Bridge is a two-layer system, binding layers leave the bridge susceptible to shearing failure. Therefore shear failure was examined.

Table 3. Maximum Shear Stress between Pavements

Index	First loading mode	Second loading mode
Maximum transverse shear stress τ_{xmax}(MPa)	0.1075	0.1096
Maximum longitudinal shear stress τ_{zmax}(MPa)	0.1617	0.1624

Table 4. Maximum Shear Stress between Pavement and Bridge Deck

Index	First loading mode	Second loading mode
Maximum transverse shear stress τ_{xmax}(MPa)	0.1331	0.1460
Maximum longitudinal shear stress τ_{zmax}(MPa)	0.1743	0.1790

Table 3 and 4 present the shear stress at binding layers. Shearing failure is more common between pavement and bridge deck, than between pavements, therefore it is important to guarantee the shearing capability between the pavement and bridge deck. The maximum longitudinal shear stress is greater than the transverse, so the maximum longitudinal stress is the main controlling index of the shearing failure between layers, similar to that of more simplistic bridges (Jing-yuan Wang, 2003); The second loading

mode is the least favorable loading mode for the shear stress, and τ_{zmax} occurs at the midpoint front of the right wheel path, which is shown in Fig.4.

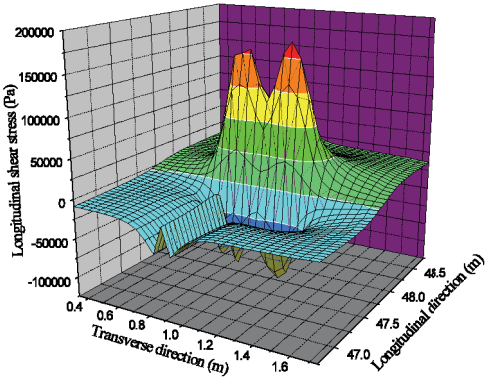

Fig. 4 Distribution of longitudinal tension stress on horizon plane at the position of maximum value

EFFECTS OF HORIZONTAL LOAD

The main controlling indexes were analyzed under different horizontal loads, where the friction coefficient was 0.2, 0.3, and 0.5. The results shown in table 5 indicate that: (1) both controlling indexes increased remarkably with increased horizontal load. The horizontal load had considerable influence on the shear stress between layers, confirming that shearing failure between pavement and bridge deck is a greater risk than between pavement layers.

Table 5. Influence of Horizontal Load on Control Index

Index	f=0.2	f=0.3	f=0.5
Maximum tension stress σ_{xmax}(MPa)	0.1047	0.1125	0.1282
Maximum shear stress between layers τ_{zmax}(MPa)	0.1790	0.2353	0.3864

STABILITY TESTS BETWEEN LAYERS

SHEAR TEST

Special waterprcof bonding material, a hybrid polymer, was used in the specimen. It was found that there is an optimum dose of the material, 0.85kg/m^2. With this dose,

the shear test was carried out at different temperatures with the vertical press and the shear speed held constant. The results are shown in Table 6.

Table 6. Shear Test Results at Different Temperature

Temperature(℃)	15	25	35	45	60
Horizontal shear load (kN)	6.2	5.3	5.0	4.3	3.9
	6.3	5.5	5.0	3.6	3.5
	6.2	5.5	4.3	4.2	4.1
Average horizontal shear stress (MPa)	0.794	0.692	0.607	0.514	0.488

Shear strength at 60℃ is 60.5% of that at 15℃, which means that the shear strength of the hybrid polymer material depreciated at higher temperatures. Because the hot bitumen at 60℃ always depreciated to 1/6～1/4 of that at 15℃ (Jian-zhong Pei, 2001), it was concluded that the hybrid polymer waterproof bonding material is more reliable at a range of temperatures than hot bitumen.

PULLOUT TEST

The pullout tests were carried out at different temperatures on a hydraulic testing machine, as shown in table 7. As shown, the bonding strength at 60℃ is 55.7% of that at 15℃, which indicates that bonding strength of the hybrid polymer material depreciated at high temperatures.

Table 7. Bonding Test Result under Different Temperature

Temperature (℃)	15	25	35	45	60
Pullout force (kN)	4.8	4.1	3.8	3.3	2.3
	4.5	4.2	3.8	3.1	2.8
	4.5	4.1	3.7	3.0	2.6
Average bonding strength f_v(MPa)	0.587	0.528	0.479	0.400	0.327

BONDING STRENGTH

The results of the shear test and pullout test were analyzed by multiple nonlinear regression methods. The model is as shown in Eq. (1).

$$\tau = 1.94 f_v + 0.0044t - 0.44 \quad (R^2 = 0.9463) \tag{1}$$

When t=15℃,

$$\tau = 1.94\ f_v + 0.0044t - 0.44 = 1.94\ f_v - 0.374 \quad (2)$$

where, τ is shear strength, MPa; f_v is bonding strength, MPa; t is temperature, ℃.

Because shearing failure on the bridge deck pavement usually occurs at fatigue shear load, the shear strength structure coefficient (Xue-jun Deng,1999), K_τ, was introduced. When K_τ is 1.2 in least favorable situations (friction coefficient, f=0.5), the allowable shear strength, τ_R, between layers is τ/1.2. Then the checking condition of shearing failure is shown in Eq. (3).

$$\tau_m \leqslant \tau_R \quad (3)$$

It is shown that the theoretical shear strength is as Eq. (4) when friction coefficient of 0.5 at standard tire press in table 5.

$$\tau_m = 0.3864 \text{ MPa} \quad (4)$$

The minimum allowable shear strength is 0.3864, calculated from Eq. (3). Then the allowable maximum shear strength is $1.2 \times 0.3864 = 0.4637$MPa and the corresponding allowable bonding strength is 0.4318 MPa, which is the allowable bonding strength at 15℃ between pavement and cement concrete bridge decks.

FIELD TESTS

The field test was carried out by the bridge deck pavement pullout system, QLP-1 (Fig. 5). The sensor technology, load sensor and displacement sensor, electronic controlling technology and mechanical driving technology were used to make the system automatic.

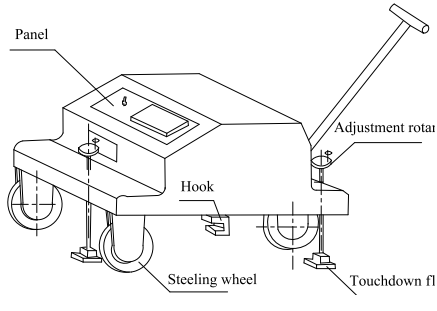

Fig. 5 QLP-1 pullout system

After the construction of the pavement, the pavement of test location was cut to be separated from the other part of pavement. Then the metal bonding head of QLP-1 was bonded with the test location by epoxy resin, and the pullout test was ready to start when the epoxy resin was dry. Pullout test procedure at 15℃ was as shown in Fig. 6, the speed of pullout was 10mm/min, and the results are shown in table 8.

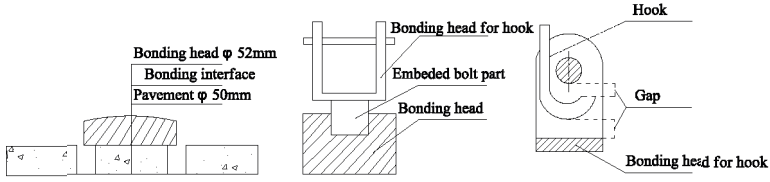

Fig. 6 Testing process

Table 8 presents the bonding strength between pavement and bridge deck from pullout test of 0.724MPa, which is greater than the allowable bonding strength, preventing shearing failure.

Table 8. Bonding Strength between Deck and Asphalt Pavement

Pullout force (kN)	Bonding strength (MPa)	Average bonding stress (MPa)
5.57	0.709	
5.88	0.749	
5.70	0.726	
5.76	0.733	0.724
5.40	0.688	
5.70	0.726	
5.80	0.738	

SUMMARY AND CONCLUSIONS

Based on the above results, the following conclusions can be drawn: (1) the weakest location in the wheel path is at the mid span; (2) local pavement in front of the two wheels is vulnerable to cracking; (3) shearing failure between pavement and bridge deck is more of a risk than between pavements, thus it is important to guarantee the shearing capability between pavement and bridge deck; (4) both controlling indexes increase remarkably with the increase of horizontal loading. Specifically, horizontal loading has much influence on shear stress between layers; (5) the relationship

between shear strength and bonding strength is built, and the allowable bonding strength at 15℃ is presented.

REFERENCE

JTJ D50-2006, "Design Specifications of Highway Asphalt Pavement." Beijing, *Peoper's Communication Press*.

Zhan-jun Zhang (2000). "Study on asphalt concrete pavement on cement concrete bridge." Changan: *Changan University*.

Wang Jing-yuan (2003). "Causes analysis of early distresses and design method of asphalt concrete pavement for concrete bridge deck." Dalian: *Dalian University of Technology*.

Luo Li-feng, and Zhong Ming (1999). "Discuss on design method of bridge deck pavement." Changsha: *Journal of central south highway engineering*. Vol. 24 (2):20-22.

Zhu Zhao-hong, and Xu Zhi-hong (1987). "Design theory and method of performance of flexible pavement." Shanghai: *Tongji University*.

Pei Jian-zhong (2001). "Study on the technical performance of flexible waterproof material on bridge deck." Changan: *Changan University*.

Deng Xue-jun (1999). "Subgrad-pavement construction." Beijing: *Peoper's Communication Press*.

Cullimore, M.S.G., Flett, I.D. and Smith, J.W. (1983). "Flexure of Steel Bridge Deck Plate with Asphalt Surfacing."*IABSE periodica1*.

Project Design and Mechanical Analysis for Sutong Bridge Deck Pavement

YANG Jian-jun[1] and ZHENG Jian-long[2]

[1]Ph.D. candidate, Key Lab of Road Structure and Material, Changsha University of Science & Technology, Changsha 410076, China. Tel.:+86-731-5219539; E-mail:yangjianjun01@126.com
[2]Professor, Department of Communication and Transportation Engineering, Changsha University of Science & Technology. Tel.:+86-731-2309080

ABSTRACT: The project design of epoxy asphalt concrete surfacing on the steel deck of Sutong Bridge is commended. The response of the layered pavement system under wheel load was analyzed by the Finite Element Method, and the key mechanics parameters of easily damaged layers were calculated and portrayed. The research showed that the notable draught stress in the surfacing layer and high shear stress in the binder layer are the cause of the deck pavement's poor performance. Reasonable structure and material design is the crucial factor for project success. The results can be a reference for paving design of steel decks.

KEYWORDS: Deck pavement; Mechanical analysis**;** Sutong Bridge

INTRODUCTION

Sutong Bridge, located in the southeast of China, is a key passage across Yangtze River. The bridge is designed by the Chinese Ministry of Communications, and sets a world record of 1088 meters main span in cable-stayed style bridge. Orthotropic decks offer a flexible, low thermal capacity dependence base for pavement(Figure1). Severe conditions challenge the pavement to perform well, so the paving project is also a critical and arduous task for Sutong Bridge construction.

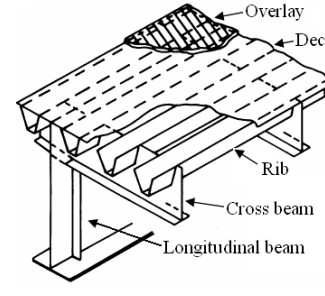

Fig 1: Orthotropic deck pavement

Surfacing on steel decks is a formidable challenge, since the stress and deformation of pavement on orthotropic deck are much more complex than those on highways. In the last three decades, failures of steel deck pavement have become very familiar to the whole world[1,2], so the subject has been a popular research topic in recent years. In China, with the rapid development of traffic infrastructure, the research

into deck pavement has soared since the 1990s, and there have been some important improvements made recently[3-6].

1. SERVICE CIRCUMSTANCES OF DECK PAVEMENT

According to the project feasibility report of Sutong Bridge, traffic will reach 46,850 vehicles per day in the first year the bridge is operational. Forecasts show the traffic average increase rate per year will be 3.9% until 2015, and 2.7% from 2015 to 2025[7]. The Standard Axial Loading(SAL) on the pavement will bring the cumulative total to 15.43 million applications in its design service span of 12 years, calculated by traffic makeup and vehicle types in the report. Also, the Sutong Bridge is located in a semitropical monsoon area, which is pluvial and moist all year. It is sweltering in summer and frigid in winter, with the monthly average air temperature high at 31.6° and low at -0.2°, highest recorded temperature in history is 42.2°, and lowest is -10.5°. In summer high temperature times, the surface temperature of the deck pavement will be nearly 70°. Therefore, the design service temperature scope of the deck pavement is -15° to 70°.

2. DECK PAVEMENT STRUCTURE

Epoxy asphalt concrete (EAC) is an excellent surfacing material for deck pavement, with solidity, heat stability and fatigue resistance. EAC was first adopted as deck pavement on the American Mateo-Hayward Bridge in 1967, subsequently extending its use in Canada, Holland, Australia, etc. In China, The Second Nanjing Yangtze River Bridge first selected EAC as deck pavement material in 2000. Later, the Runyang Bridge and other newly constructed and replacement steel bridge deck pavement programs have also used the material.

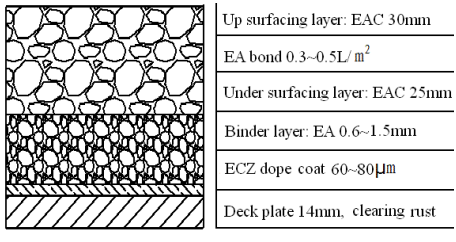

Fig. 2: Deck pavement structure

Tab.1:**Character of EAC**

Index (15t)	Value
Asphalt-aggregate ratio/%	6. 5
Stability/*kN*	25. 5
Flow value/0.1*mm*	31. 6
Percentage of void/%	1. 86
Split strength/*Mpa*	4. 73
Stiffness module/*Mpa*	1088. 3
Bend stiffness module/*Mpa*	2386. 7

Since EAC has been used successfully for deck pavement in China, and it has such a high performance, EAC deck pavement for Sutong Bridge is recommended here (Figure 2). The overlay is made up of two layers; the top surfacing layer is 30mm thickness EAC, the under layer is 25mm thickness EAC, the bond between two layers is epoxy asphalt (EA). The deck plate is coated with a mixture of epoxy

colophony and zinc lacquer. The binder layer between deck and overlay is EA, and this layer also has an isolation function.

EA is a polymer of bisphenol-A epoxide resin (component A) and asphalt mixed with solidification and dissolution aids (component B). The EA should be concocted of different components according to the function target. The aggregates should be carefully selected; they should be hard, wearable and alkaline. The exterior of the aggregates should be rough; thin components should be less than 5%; and limestone is the ideal choice for the powder material. The optimal asphalt-aggregate ration of EAC is determined by the Marshall Test, and the quality of the EAC is evaluated by using the splitting test and flexural test on beams (Table 1).

3. SIMULATION OF THE DECK PAVEMENT STRUCTURE

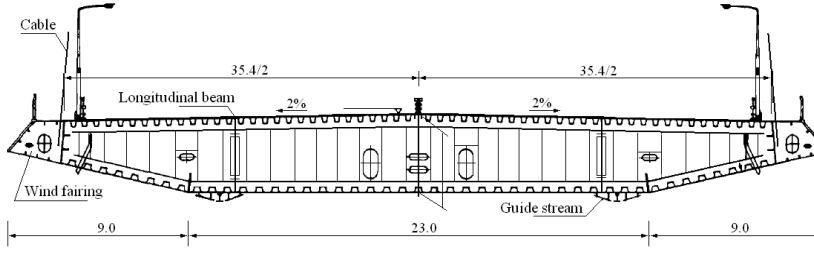

Fig. 3: Girder conformation of Sutong Bridge (*m*)

An orthotropic steel deck bridge is relatively lightweight, which makes it attractive where pre-fabrication or rapid erection is required. Orthotropic steel decks also lessen the mass and reduce wind loads. These are all important considerations for the long-span bridges. The figure dimension of the Sutong Bridge girder is indicated in Figure 3. Total width of the girder is 41.0*m*, the height at the symmetry line is 4.0*m*. In standard girder sections, space between neighboring cross beams is 4.0*m*, with the thickness of deck plate, cross beam, longitudinal beam all being 14*mm*. The thickness of the U rib wall, welded to the deck, is 8*mm*; it's mouth width is 300*mm*, bottom width 180*mm*, height 300*mm*, and the space between 600*mm*[8].

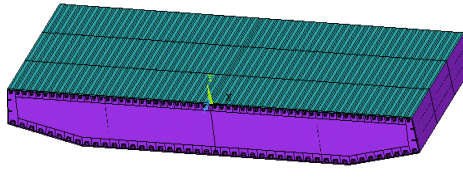

Fig. 4: Model of girder section

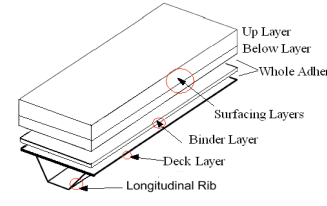

Fig. 5: Deck & pavement layers

FEM model of Sutong Bridge girder is showed in Figure 4, the model includes 3 spans which are mono-compartmentalized by cross beams. The combined layer structure is made up of a deck layer, binder layer, and surfacing layers(Figure 5), it is modeled by 3 dimensional shell element[10], and it's calculation precision is controlled by Mindlin-Reissner shell theory. Since pavement under traffic load is a minute distortion on its elasticity, it is credible for calculation results of pavement material to be assumed as liner elastic. The bend elastic module of the EAC is adopted 500~600*MPa*, which is back-calculated by FEM based on the composite beam test.

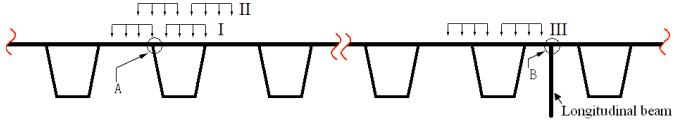

Fig. 6: Load locations on orthotropic deck

The SAL is the calculated load, and the weight of the twin wheels load is 100*KN*. The contact area of a single tire to pavement is $0.2 \times 0.2\ m^2$, and the distance between the two contact areas is 0.1*m*. The typical load locations are portrayed as in Figure 6: location I is twin tires riding on side wall of a rib, II is twin tires symmetrically pressing on a rib, III is tires near to the longitudinal beam.

4. PAVEMENT RESPONSE TO TRAFFIC LOAD

The deflections of paving layers reflect the rigidity of pavement and orthotropic decks. The calculation result of calculated paving distortion is shown in Figure 7. Most of the deflection occurred at the area near to the load location, and a centralization effect is distinct to the orthotropic character of the decking system.

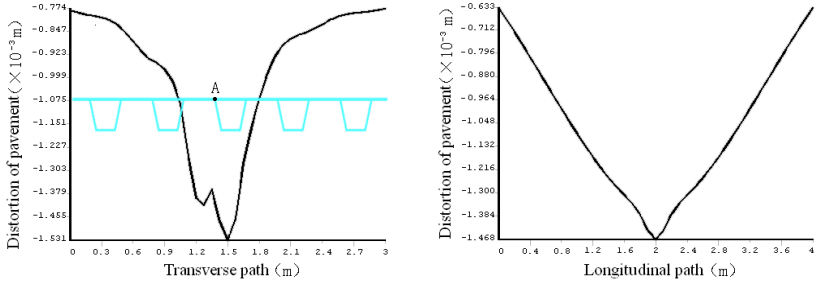

Fig. 7: Distortion of pavement (location I)

Fatigue cracking is the predominant source of pavement distress. The calculation of draught stress in the upper surface layer is described in Figure 8. The peak value of

draught stress is located at the top of the U rib wall sides on transverse paths, and at the top of cross beams on longitudinal paths. So longitudinal cracks usually appeared along U rib side wall in the pavement, and transverse cracks always occurred at the top of the cross beam.

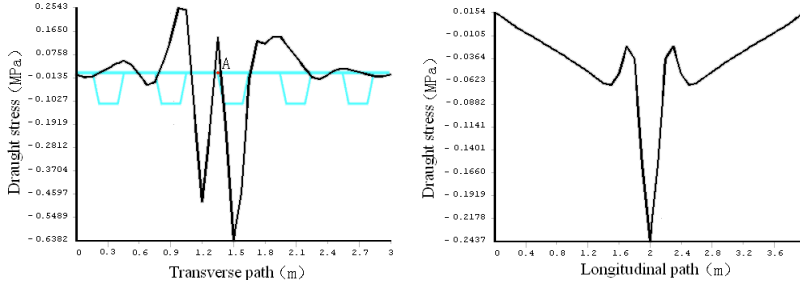

Fig. 8: Draught stress in up surfacing layer (location I)

Loss of bonding between the wearing course and the steel plate is another type of prominent distress for deck pavement. Shear stress in the binder layer is calculated here; the results are portrayed in Figure 9. Shear stress in the binder layer soars when pavement has uneven decline under load, and even worse, because the binder layer is located at the critical location between the different material layers of steel deck plate and EAC surfacing layers, it is more easily separated.

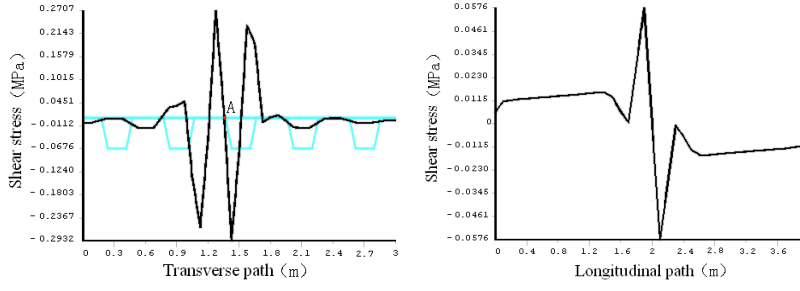

Fig. 9: Shear stress in binder layer (location I)

Tab.2: Contrast of key mechanical indexes for 3 traffic load locations

Load location	Distortion of pavement /*m*	Tension stress of SL /*MPa*		Shear stress of BL /*MPa*	
		T-Path	L-Path	T-Path	L-Path
I	1.531e-3	0.2542962	0.0154065	0.2931709	0.0576598
II	1.518e-3	0.2409690	0.0163405	0.1964628	0.0468398
III	0.632e-3	0.2914735	0.0111412	0.2024438	0.0729317

Pavement mechanical response varies when traffic load locations are changed to rib positions. In order to check the effect of pavement response to load location, the key mechanics indexes of pavement for the three typical load locations (Figure 6) were analyzed, and the results are listed in Table 2. We can see that the longitudinal beam can strengthen the rigidity of the deck system, but stress concentration in pavement is more distinct when traffic load is near the beam. The extremes of tension stress on load location III is about 21% more than that of load location II.

CONCLUSIONS

(1) The high draught stress in the upper surface layer and shear stress in the binder layer responding to traffic loads by mechanical analysis, can explain the common distress of cracking, loss bond in orthotropic steel bridge surfaces.

(2) Tensile strength of EAC is more than 1.2*MPa*, and breaking strength is also more than 1*MPa*. Material testing program indicates that EAC is sufficient resistance against fatigue cracking and rutting, so the surfacing material is an ideal choice for deck pavement.

(3) Static SAL is adopted in calculation here, so guaranteed factors should be considered for the calculation results. Dynamic load modification factor K_1 is advised to adopt 1.3, 50% over freight modification factor K_2 is advised to adopt 1.5.

(4) The deck pavement in service is influenced by repeated traffic loads. Therefore, fatigue resistance of surfacing material is the key issue for deck pavement design, so further empirical-analytical approach is recommended here.

ACKNOWLEDGMENTS

The authors appreciate the support of the Key Project of Hunan Natural Science Foundation and Hunan Science & Technology Plan Foundation.

REFERENCES

[1] Ali Touran and Alex Okereke(1991). “Performance of Orthotropic Bridge Decks.” *Journal of Performance of Constructed Facilities*, Vol. 5(2):134-148.

[2] YANG Jian-jun, ZHOU Zhi-gang, LIU Xiao-yan(2006). **“**Research evolvement of structure theory on pavement for orthotropic deck.” *Journal of China & Foreign Highway*, Vol. 26(4):179-184. (in Chinese)

[3] Hicks, R.G.; Dussek, I.J.; Seim, C.(2000). “Asphalt surfaces on steel bridge decks.” *Transportation Research Record*, n 1740:135-142.

[4] Huang Wei, Liu Zhen-qing(2005). “Research on Theory & Method of Long Span Steel Bridges Deck Surfacing Design.” *China Civil Engineering Journal,* Vol. 36(1):51-59. (in Chinese)

[5] QIAN Zhen-dong, LUO Jian, JING Miao-miao(2005). “Mechanical analysis of asphalt concrete paving projects on steel bridge deck.” *China Journal of Highway and Transport,* Vol.18(2):61-64. (in Chinese)

[6] ZHANG Qi-sen; LI Yu-shi, et al(2001). “Research on fatigue tests in the direct track for the asphalt deck pavement of Xiamen Haicang steel bridge.” *China Journal of Highway and Transport*, Vol.13 No.1:60-72. (in Chinese)

[7] FAN Dong-tao, HU Hou-bin(2003). “Analysis and Forecast of Available Traffic Volume on Su-Tong Changjiang Highway Bridge.” *East China Highway,* Vol.145(6):37-39. (in Chinese)

[8] PEI Min-shan, ZHANG Xi-gang, YUAN Hong, et al(2004). “Design of Superstructure for Main Bridge, Sutong Bridge.” *Disquisitions Collection on Sutong Bridge(1st Volume)*. Beijing: China Science and Technology Press, pp26-34. (in Chinese)

Study on the Interface Treatment of Concrete Deck Pavement

PAN Youqiang[1] GUO Zhongyin[2] LING Chen[3]

[1] Doctor Candidate, Key Laboratory of Road and Traffic Engineering of the Ministry of Education, Tongji University, Shanghai, 20009, Jiangsu Transportation research institute, Nanjing, 211112,pyq@ti.js.cn
[2]Professor, Key Laboratory of Road and Traffic Engineering of the Ministry of Education, Tongji University, Shanghai, 20009,zhongyin@mail.tongji.edu.cn
[3] Vice-director, Jiangsu Transportation research institute, Nanjing, 211112,lingchen@ti.js.cn

ABSTRACT: Today, serious deterioration has occurred on concrete deck pavement in China. One reason for the problem is the interface slippage between the concrete deck and the pavement. An efficient interface treatment can solve the problem. The interface treatment contains two aspects: the concrete deck treatment and the adhesion layer. Concrete deck treatment can change the physical form of the concrete deck and is more reliable in improving the shear performance of the concrete deck pavement. This paper summarizes and presents a comparison through physical form analysis and indoor tests of three kinds of concrete deck treatment: manual work treatment, milling treatment and sandblast treatment. The test results show that milling treatment can improve shear performance more than sandblast treatment. This paper suggests a more reliable way to improve the shear performance of concrete deck pavement.

INTRODUCTION

In China, most of the concrete decks were paved with asphalt materials. Shear performance is a key design parameter in deck pavement design. There are two ways to improve the shear performance: concrete deck treatment and improved adhesion layer performance. Today, adhesion layer is considered more frequently than the concrete deck treatment. People want to solve the shear problem by improving the properties of the adhesion materials. The adhesion materials becomes more and more expensive as the cost of emulsion asphalt, modified emulsion asphalt, special adhesion asphalt and epoxy asphalt increases. Based on the adhesion theories, the destruction of the adhesion layer may occur in three positions: between the upper layer and the adhesion layer, in the interior of the adhesion layer and between the adhesion layer and the lower layer(see FIG.1). The shear performance of the deck pavement relies on the minimum shear strength between the three positions. Epoxy asphalt is a super adhesion material, but it

does not improve the shear performance a lot due to this affect. The destruction position of epoxy asphalt adhesion layer is between deck pavement and epoxy asphalt layer.

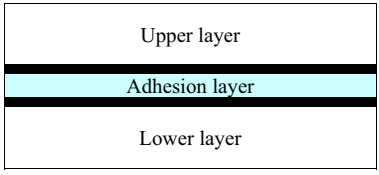

FIG.1 Adhesion model

Improving the shear performance of deck pavement by concrete deck treatment is more effective than improving the adhesive capacity of adhesion layer materials. No matter what type of adhesion layer is used, the shear performance for the adhesion layer is less reliable than the physical form of the concrete deck. The reason for this is very simple. If the concrete deck was broken, the adhesion layer would become useless and the pavement could have problems too. The shear strength from the physical form of the concrete deck does not change as the temperature changes. Therefore more attention should be paid to the physical form of concrete deck than to the adhesion materials in concrete deck pavement.

PHYSICAL FORM ANALYSIS

Many people think that concrete deck treatment is only a way to improve the cohesional strength of the adhesion layer by cleaning up the dust, the smeary part and the weak concrete layer. In fact, appropriate concrete deck treatment can improve the shear strength effectively.

To the complete concrete bridge deck which is smooth and slick, there are three kinds of concrete deck treatment: manual work treatment (see FIG.2), sandblast treatment (see FIG.3) and milling treatment (see FIG.4).

FIG.2 Manual work treatment

In the past, manual work treatment was used a lot in China because it does not need special equipments. Manual work treatment can improve the shear strength, but can not clean up the dust, smeary part or weak concrete layer. It also requires significant man power and is inefficient.

FIG.3 Sandblast treatment

Sandblast treatment is efficient and can clean up the dust, smeary part and weak concrete layer effectively. After the treatment, the concrete deck becomes very clean. The treatment is helpful to improve the cohesional strength of the adhesion layer. To our disappointment, sandblast can not change the physical form of the deck and can not improve the shear strength effectively.

FIG.4 Milling treatment

Milling treatment can change the physical form of the deck and clean up the dust, the smeary part and the weak concrete layer. Milling treatment is efficient and can improve the shear strength effectively too.

FIG.5 is the sketch map of concrete deck physical form after treatment. Based on FIG.4, we will know the difference between the three kinds of concrete deck treatment. There are small shear pins on the deck surface after milling treatment. The manual work treatment and sandblast treatment can not get the same effect.

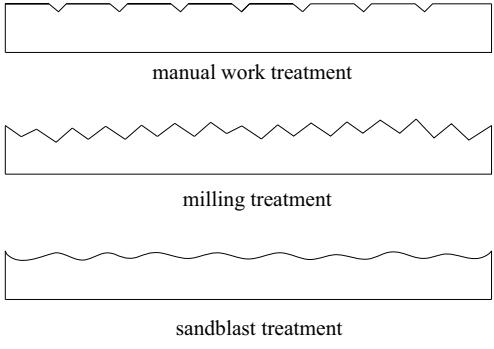

FIG.5 Concrete deck physical form analysis

INDOOR TEST RESULTS ANALYSIS

In order to evaluate the shear strength achevied by concrete deck treatment, 45º shear tests and 0º shear tests were performed. Hot-coated modified bitumen adhesion material was used in the test because it is popular in deck pavement today.
The specimens used in the tests were precisely prepared under the construction procedure. The concrete deck was treated like in the spot and then was coated with the adhesion layer.

45ºshear test results

The 45ºshear test is a better way to evaluate the stress in the interface. It can simulate the mechanics of the deck pavement under the traffic load. FIG.6 is the sketch map of the 45ºshear test. In the test, the horizontal force was eliminated by the roller. Tab1 and FIG.7 give the test results.

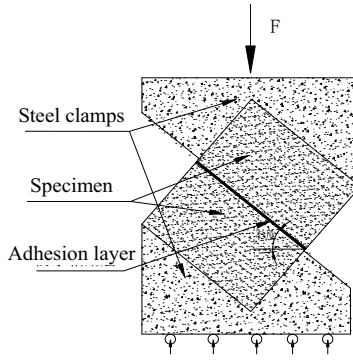

FIG.6 45°shear test

Tab.1 Hot-coated modified bitumen 45°shear test results(MPa)

Treatment / Temperature	Manual work treatment	Sandblast treatment	Milling treatment
20 °C	1.262	1.106	1.313
60 °C	0.075	0.048	0.125

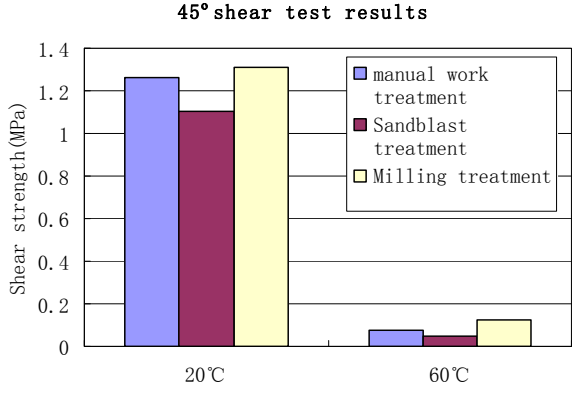

FIG.7 Hot-coated modified bitumen 45°shear test results(MPa)

The test results showed that the shear strength of the deck pavement with milling treatment is larger than the deck pavement with sandblast treatment or manual work treatment both at normal or high temperature. Manual work treatment is also better in improving the shear performance than the sandblast treatment.

The strength of the deck pavement with milling treatment increases about 18.7 percent to the sandblast one at 20 . But the value is 160 percent at 60 .At high temperature, the cohesional strength of the asphalt becomes small and the physical form is the main cause of the shear performance. The difference between the different kinds of the concrete treatment is obvious.

0ºshear test results

The 0º shear test is an easy way to evaluate the shear performance of the deck pavement. The stress is clear but can not simulate the traffic load on the deck pavement.FIG.8 is the sketch map of the 0º shear test. Tab.2 shows the results of deck pavement with different kinds of concrete deck treatment and the same hot-coated modified bitumen adhesion layer at 20 .

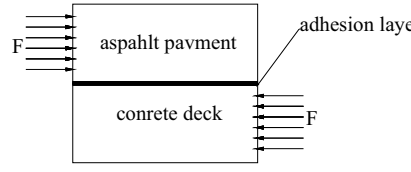

FIG.8 0ºshear test

Tab.2 Hot-coated modified bitumen 0ºshear test results(MPa)

Treatment / Temperature	Manual work treatment	Sandblast treatment	Milling treatment
20 °C	0.672	0.770	1.019

The test results showed that the shear strength of the deck pavement with milling treatment is larger than the deck pavement with sandblast treatment or manual work treatment. Making the concrete deck rough is a better way to improve the shear performance of the deck pavement.

Adhesion test

The cohesion strength of the deck pavement relies on the adhesion materials and the cleanness of the interface. The milling and sandblast treatment can clean up the dust and weak part and improve the cleanness of the deck. The adhesion test was carried out to compare the treatment effect .Tab.3 is the test results of deck pavement with hot-coated modified bitumen adhesion layer.

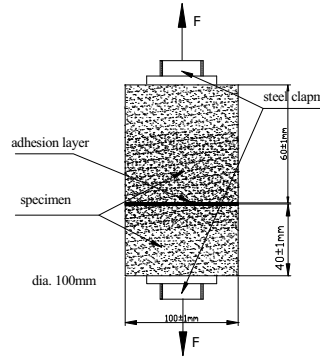

FIG.9 Adhesion test

Tab.3 Hot-coated modified bitumen adhesion test results(MPa)

Treatment / Temperature	Manual work treatment	Sandblast treatment	Milling treatment
20°C	0.431	0.588	0.589

The deck pavement treated with sandblast has same cohesional strength as the one with milling treatment. Manual work treatment can not achieve the same effect.

SPOT TEST RESULTS

In order to evaluate the effective of the deck treatment, one trial was carried out in the spot. After the deck treatment, the same adhesion layer and the asphalt pavement were constructed. And then, two groups of specimens with Dia.100mm were drilled which were composed of concrete deck, adhesion layer and asphalt pavement(See FIG.10).

FIG.10 Specimens drilled in the spot

The specimens were used to do shear test to compare the shear strength. The test was carried out at 20°C .Tab.4 shows the results.

Tab.4 20 Shear test results(MPa)

Treatment / Test method	Sandblast treatment	Milling treatment	Milling /Sandblast
45ºshear test	0.803	1.282	1.60
0ºshear test	0.414	0.651	1.57

The spot test gave the same results as the indoor tests. The results in the table show that the shear strength achieved by deck milling treatment is 60 percent more than the one achieved by the deck sandblast treatment in 45ºshear test. An increase of 57 percent was found in 0ºshear test. It is sure that the milling treatment can improve the shear strength effectively.

CONCLUSION

Interface treatment is the key point in the concrete deck pavement. The adhesion materials do not mater as much. The concrete deck treatment is the better way to improve the shear performance, especially in high temperature conditions. This paper presents the physical form analysis, indoor test results analysis and spot test results analysis on three kinds of concrete deck treatment.

1) Physical form analysis showed that the shear pin produced by milling treatment can improve the shear strength.

2) The indoor shear test results showed that the shear strength of the deck pavement with milling treatment is bigger than the deck pavement with sandblast treatment or manual work treatment.

3) The indoor adhesion test results told us that both milling and sandblast treatment can clean up the dust, smeary part and weak concrete layer effectively.

4) The spot test results gave the same results.

The concrete deck treatment is only suited for the finish on concrete bridge. The best way to improve the shear strength is to produce the shear pin in the construction of the concrete deck.

ACKNOWLEDGMENTS

The authors thank Mr. Zhang Zhihong for his assistance in the Research on the deck pavement for Hangzhou Bay Bridge. The authors also appreciate the support of the International Engineering Foundation.

REFERENCES

[1]Ministry of transport of People's Republic of China, Technical specifications for construction of highway asphalt pavement[S], Beijing, 2004

[2] Third Highway Construction Bureau CO.LTD, Jiangsu Transportation research institute, Study of dual-layer SMA deck pavement of the Hangzhou Bay bridge[R], Nanjing, 2007

[3] Jiangsu Transportation research institute, Study of adhesion layer of concrete deck pavement [R], Nanjing, 2007

[4]YU Liangming, Research on waterproof and cohesive layer of porous asphalt pavement[D], Southeast University, Nanjing,2006

Effects of Material Design Parameters on Mechanical States of Bridge Deck Pavement

Xu Tao[1] and Huang Xiaoming[2]
[1]Graduate Research Assistant, Southeast University, 2 Sipailou, Nanjing 210096, China; seuxt@163.com
[2]Professor, PhD, Southeast University, 2 Sipailou, Nanjing 210096, China; huangxm@seu.edu.cn

Abstract: Bridge deck pavement suffers from more complicated stresses than ordinary pavement, and mechanical states of the paving layers are influenced by material design parameters. After mechanical computation, the effects of material design parameters on the mechanical state and the variation law of pavement are analyzed. Analytical results indicate that following the traditional HAM design method can not adapt to actual mechanical states, and easily result in usual distress types on the asphalt concrete paving. Economical and reasonable paving materials should be designed or developed according to mechanical paving characteristics, such as multilevel dense built-in modified HMA, fiber-reinforced asphalt concrete and modified SMA, which can harmonize paving layers as a whole, adapt to the deformations of bridge decks, improve the mechanical states of the paving layers, increase the service years, and offer some helpful references for similar bridge deck pavement design.

Keywords: bridge deck pavement; material design parameters; FEM; structure compages

Introduction

In about the past 30 years, many long-span bridges have been built, and bridge structures are constantly innovated within the rapidly developed highway system in China. Bridge deck pavement, as an important part of bridge deck system, disperses vehicle loads and suffers from more complicated stresses than ordinary pavement. The paving layers are not only protecting layers, but also stress carrying layers. The mechanical states of long-span bridge deck pavement are influenced directly by the deformation, displacement, vibration and so on. Therefore, the high quality paving materials are sought to meet the requirement of bridge deck pavement by researchers (1).

It is well known that material is the most active factor among in structures, because many kinds of materials can be selected for bridge deck pavement, which influence the mechanical characteristics of paving layers. On the other hand, modulus values of paving layers which is one of structure character indices to decide mechanical characteristics of the pavement, rest with material composition design (2～4). Of course, material design is related to structural design, and mechanical state of the paving layers relies on the feedback characteristics of modulus compages and thickness compages. Therefore, design parameters of paving material should be studied according to the mechanical characteristic requirements of different structure

layers, and structure compages design should be based on material type selection and new material development. The mechanical state of the paving layers is influenced by its material modulus which is an important design parameter because different material modulus cause stress redistributing in paving layers(5).
This paper is based on a double layer HMA paving on a long-span cable-stayed concrete bridge. A full scale three-dimensional finite element model was built to explore the influence of different material modulus and modulus compages on the mechanical state of the paving layers, and to provide theoretical bases for bridge deck pavement design and material selection. This is quite necessary to improve mechanical state, to enhance using performances and to prolong service life of the paving layers.

Research Actuality

The current specifications do not include detailed design theory or method for bridge deck pavement design. The specifications only provide direct recommendations for materials, designs, construction, etc. Moreover, the HMA design for bridge decks is the same as ordinary highway pavement, and the paving is usually constructed together with adjacent highway pavement to reduce construction gaps. Therefore the bridge deck pavements are regarded as accessorial structures to bridge, and spend little time is spent on it. This causes hidden troubles to remain, and distress becomes severe with the increase in traffic and heavy vehicles.
In recent years, some new paving materials have been used to pave bridge decks in China, such as gusasphalt concrete, epoxy asphalt concrete, SMA, modified SMA, fiber-reinforced asphalt concrete and others. Previous researches mainly focus on material design and its high-temperature stability, low-temperature cracking resistance, fatigue behavior, and aged behavior, but few researches have carried out testing concerning material design parameters, modulus compages and their influence on mechanical characteristic of paving layers. However, under the comprehensive effects of vehicle loads, deformation and environmental factors, the working state of paving layers on a concrete bridge deck is different from that of ordinary highway pavement and steel deck pavement. These differences put higher demands on the paving materials. Therefore, the inherent relation between material property and mechanical state of paving layers needs to be analyzed in relation to the mechanical characteristics of whole bridge deck system. This can solve the problems in bridge deck pavements, provide theoretical bases for selecting economical and reasonable paving materials, harmonize paving layer design as a whole, improve mechanical states of the paving layers and prolong the service life.

Finite Element Model of Paving Layer

Engineering Background

The bridge deck pavement studied in this paper is on a long-span cable-stayed concrete bridge, which is 32.18m in width, and 42m + 42m +300m + 300m + 42m + 42m in length. The girder is 3m in height and made of prestressed concrete with a triangle box on both sides. Diaphragm plates are laid out at intervals of 6.5m in side span and 7.5m in middle span.

Computing Parameters of Paving Layer

Double-layer asphalt concrete is laid on the bridge deck to make full use of the paving material potentials in order to meet requirements of high-temperature salability and low-temperature cracking resistance for HMA. In the computational model, the material properties of different paving layers are created separately with different parameters which form different modulus compages. A Poisson ratio of 0.3 is used thouroughout.

In this research, it is hypothesized that a complete continuum includes the bridge deck and paving layers and that the materials are isotropic and elastic. Because the stress from live loads is small and local in paving layers when the bridge is in service, the influence of supporting conditions on stresses of paving layers is ignored according to Saint-Venant principle (7). Both ends of the girder are fixed in computing model. This has little effect on the mechanical state of paving layers. The computing parameters of bridge deck pavement system are shown in Table.1.

Table.1 Computing parameters of bridge deck pavement system

Top layer thickness (mm)	Under layer thickness (mm)	Bridge deck (cm)	Direct web thickness (cm)	Diaphragm plate thickness (cm)	Concrete modulus (GPa)	Concrete Poisson ratio
50	60	30	30	30	36	0.18

A uniform load of .707MPa was applied over a rectangular area 0.6m×0.2m in size. The space between load centers was 1.8m as described in the Specifications(6)(8), when mechanical characteristics of the paving layers are analyzed.

Mechanical Model and Loading Position

Because stiffening effects due to longitudinal direct webs and diaphragm plates cause local stress concentration in the paving layers, general beam plate theory can not exactly analyze their mechanical characteristics. So, in this paper, the bridge deck, direct webs, diaphragm plates and asphalt concrete paving layers are regarded as a unified mechanical analysis model to compute the maximal tension stress and shear stress using three-dimensional FEM. The mechanical analysis model is shown in FIG.1.

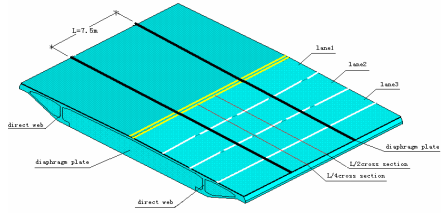

FIG.1 mechanical analysis model of FEM

Based on the computed results in the reference(9), the variation law of stress is discussed by changing the modulus and modulus compages (E_{top}/E_{under}) to select

reasonable paving materials, and improve mechanical states.

Computing Results of FEM

Recent researches indicate that cracking and shear distress are the most destructive types of distress on bridge deck pavement. The variation law of maximal tension stress and shear stress was treated as a design control indices for paving layers. The variation law was analyzed to determine distress characters, so that preventive measures can be adopted in design.

The Specifications (6), in general, require a modulus value of under layer of 1800MPa and a modulus value of the top layer of 2000MPa. Then stresses in paving layers were computed by changing modulus and modulus compages, such as transverse maximal tension stress, σ_{xmax}, longitudinal maximal tension stress, σ_{ymax}, transverse maximal shear stress between paving layers, τ_{1xmax}, longitudinal maximal shear stress between paving layers τ_{1ymax}, transverse maximal shear stress between bridge deck and under paving layer, $\tau_{2xmax,}$ longitudinal maximal shear stress between bridge deck and under paving layer, $\tau_{2ymax,}$ and maximal shear stress in paving layers, τ_{max}.

Computing Stress under E_{under} Changed and E_{top} Fixed

It is assumed that top paving modulus value, $E_{top,}$ was unchangeable, and assigned 2000MPa, but the modulus value of under paving layer, $E_{under,}$ was assigned 1000, 1400, 1800 and 2200 MPa to compute stresses in the paving layers. The computed results are shown in Table.2.

Table.2 Computing Results of Stress under E_{under} Changed and E_{top} Fixed

E_{under} (MPa)	Stresses of top layer/MPa					Stresses of under layer/MPa				
	σ_{xmax}	σ_{ymax}	τ_{1xmax}	τ_{1ymax}	τ_{max}	σ_{xmax}	σ_{ymax}	τ_{2xmax}	τ_{2ymax}	τ_{max}
1000	0.274	0.119	0.489	0.245	0.200	0.019	0.016	0.504	0.262	0.217
1400	0.226	0.090	0.471	0.232	0.166	0.025	0.019	0.524	0.275	0.232
1800	0.196	0.081	0.448	0.217	0.144	0.029	0.021	0.537	0.285	0.244
2200	0.176	0.070	0.429	0.207	0.128	0.032	0.023	0.545	0.294	0.254

Computed results indicate that stresses in the paving layers are influenced obviously by the modulus variety of under layer. The main reasons follow.

(1) When the modulus of the under layer increases, the influence of bridge deck deformation on the stresses of top layer is weakened, which makes the top layer adapt better to the deformation of the under layer. Therefore, the maximum tension stresses gradually decrease. On the other hand, when the modulus of under layer increases, the rigidity ratio of the under layer of the paving system becomes higher, which causes the under layer to share more loading under the same deformation. Therefore, the maximum tension stresses gradually increase.

(2) Because the modulus of top layer is unchangeable, stronger support is provided for the top layer when the modulus of the under layer increases. This makes the relative slippage between paving layers decrease in horizontal direction. Therefore, maximum shear stresses between the paving layers gradually decrease. Otherwise, when the rigidity ratio of under layer increases in the paving system, the under layer deformation associated with the bridge deck causes the relative slippage between the

deck and the under layer becomes significantly larger. Therefore maximum shear stresses increase.

(3) When the rigidity ratio increase for the under layer of the paving system, the supporting function of the under layer becomes stronger, and the under layer shares more loading. Therefore the maximum shear stress in the under layer increases, but the maximum shear stress in the top layer decreases.

Computing Stress under E_{top} Changed and E_{under} Fixed

It was assumed that the under paving modulus value, $E_{under,}$ is unchangeable and set to 1800 MPa, but the modulus value of the top paving layer, $E_{top,}$ was assigned 1200, 1600, 2000 and 2400MPa to compute the stresses in the layers. The computed results are shown in Table.3.

Table.3 Computing results of stress under E_{top} changed and E_{under} fixed

E_{top}(MPa)	Stresses of top layer/MPa					Stresses of under layer/MPa				
	σ_{xmax}	σ_{ymax}	τ_{1xmax}	τ_{1ymax}	τ_{max}	σ_{xmax}	σ_{ymax}	τ_{2xmax}	τ_{2ymax}	τ_{max}
1200	0.148	0.059	0.397	0.190	0.106	0.037	0.026	0.555	0.306	0.270
1600	0.174	0.070	0.426	0.205	0.126	0.033	0.024	0.546	0.294	0.255
2000	0.196	0.081	0.448	0.217	0.144	0.029	0.021	0.537	0.285	0.244
2400	0.218	0.090	0.465	0.236	0.160	0.026	0.019	0.528	0.278	0.236

Table.3 shows that the rigidity ratio of the top layer of the paving system becomes higher when the modulus of the under layer increases, which makes maximal tension stresses of top layer to increase monotonously. Conversely, when the rigidity ratio of the under layer of the paving system decreases, the maximum tension stresses in the under layer decrease gradually.

Computing Stress under E_{top}/E_{under} Descending

In order to comprehensively analyze the influence of different modulus compages on stresses in the pavement layers, stresses were computed with the value of E_{top}/E_{under} descending. The computed results are shown in FIG.2 and FIG.3.

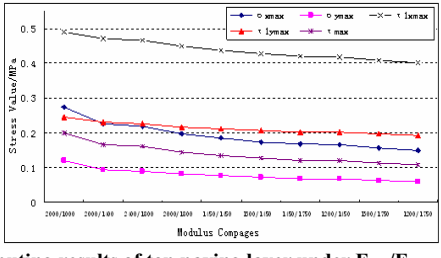

FIG.2 Computing results of top paving layer under E_{top}/E_{under} descending

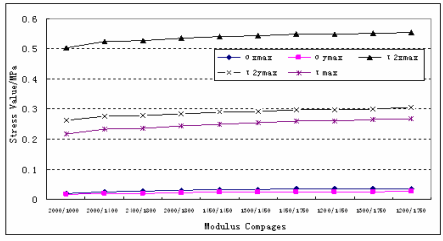

FIG.3 Computing results of under paving layer under E_{top}/E_{under} descending

Results from FIG.2 and FIG.3 are three fold:

(1) When the value of E_{top}/E_{under} descends, the maximum tension stresses in the top layer increases, but maximum tension stresses in the under layer slowly decrease. Considering that the fatigue cracking distress in bridge deck pavement often occurs on the top of ribbed stiffeners in bridge deck system, the maximum tension stress on the top layer surface should be limited.

In addition, when the E_{top}/E_{under} value of modulus compages is between 1450/1750 and 1200/1450MPA, the maximum tension stress in the top layer is reduced. It is necessary to design new-style HMA or develop new material to meet the requirements of modulus compages of the paving layers, which can harmonize paving layers as a whole to adapt to deformations in the bridge deck and improve the mechanical states of the paving layers. Whether or not the conventional HMA design method is followed, the E_{top}/E_{under} value of modulus compages is often 2000/1800. Computed results indicate that the maximum tension stresses in the paving layers are largest under the value of 2000/1800, which is the main reason for fatigue cracking distress in bridge deck pavement.

(2) The variation trend of the maximum shear stresses between the top layer and the under layer is opposite to the maximum shear stresses between the under layer and bridge deck. The maximum shear stresses between the under layer and the bridge deck is larger. The cohesive layer is laid between paving layers to enhanced compound effect and improve the mechanical state of the paving layers, however, the difference of material property, between cement concrete deck and asphalt concrete paving layer, is great enough to cause horizontal shear stress concentration(10). Therefore shear distress between the deck and the under paving layer should considered more closely when bridge deck pavement is designed.

(3) The variation trend of the maximum shear stresses in the top layer is opposite to the under layer, and the latter is much larger. Therefore, the paving layer should be separately designed to meet its mechanical requirements.

Conclusions

(1) The influence of material design parameters on the mechanical states of paving layers is obvious when the paving thickness is unchangeable.
(2) When the modulus of the under layer increases, stresses in the top layer become gradually smaller; however, stresses in the under layer gradually increase.
(3) When the modulus of the top layer increases, stresses in the top layer gradually

increase, but stresses in the under layer gradually decrease.

(4) When the value of E_{top}/E_{under} descends, the stresses in the top layer gradually decrease; however, stresses in the under layer gradually increase. Therefore, paving materials should be separately chosen to meet mechanical requirements.

(5) Whether or not the traditional design method is followed, material design parameters can not adapt to the actual mechanical states of paving layers. Therefore, multilevel dense built-in modified HMA, fiber- reinforced asphalt concrete and modified SMA can be selected to meet requirements of mechanical characteristics and water-proofing.

References

(1) DING Jian-ming, QIAN Zhen-dong, DU Xin, et al. Mechanical Specific Character of Long-span Cable-stayed Bridge Pavement under Live Loading [J]. Journal of Highway and Transportation Research and Development, 2005.22(9):91～93.

(2) XIN De-gang, WANG Zhe-ren, ZHOU Xiao-long. Material and Structure of Highway Asphalt Pavement [M].BEI JING: China Communication Press,2001.

(3) WANG Li-yong, ZHONG Yuan, LI Jun. BinZhou Yellow River Highway Bridge Deck Pavement Design and Construction [J]. Journal of Highway and Transportation Research and Development, 2005.22（8）:74～78.

(4) GAO Xue-chi, HUANG Xiao-ming, XUTao. Mechanical Analysis of Long-span Concrete Bridge Asphalt Concrete Deck [J]. Journal of Highway and Transportation Research and Development, 2005.22（1）:70～73.

(5) DENG Xue-jun, HUANG Xiao-ming. Principles and design Method of Pavement[m]. BEI JING: China Communication Press, 2001.

(6) Ministry of Communications of the People's Republic of China. Specifications for Design of Highway Asphalt Pavement（JTG D50-2006）[S]. BEI JING: China Communication Press, 2006.

(7) FAN Li-chu. Bridge Engineering[M]. BEI JING: China Communication Press, 2003.

(8) Ministry of Communications of the People's Republic of China. Highway Engineering Standard（JTG B01-2003）[S]. BEI JING: China Communication Press, 2004.

(9) Xu Tao. RESEARCH ON PAVEMENT STRUCTURE OF LARGE SPAN CONCRETE BRIDGE DECK [D].NANJING: Southeast University, 2004.

(10) WANG Zhen-ming. Mechanics of Composite Materials and Structural Mechanics of Composite Materials [M]. BEIJING: China Machine Press, 1999.

Mechanic analysis of bridge reinforcement with mesh and steel fiber reinforced concrete and Experimental construction technology

ZHANG Wen-xian[1] , LUO Bing[1], Jin Shu-yang[1]

[1]College of Resources & Civil Engineering, Northeastern University, Shenyang 110004, China, zwx239@163.com

ABSTRACT: The context of this paper is the research on reinforcement of Dongguan Northern Bridge of the Guangzhou-Shenzhen highway in China by using mesh and steel fiber reinforced concrete (SFRC). Numerical program MIDAS has been utilized to model the mechanical response of the bridge. The interaction between the new and old concrete bridge structures is simulated. Mechanic analysis has been performed on the most unfavorable load positions. The overloads and shrinkage creep of concrete are considered. The anchor bar's distance and the optimal thickness of the concrete bridge deck have been discussed. Finally, a real life application of the construction technology for treating the flaws of the bridge deck paving overlay with mesh and steel fiber reinforced concrete is given.

Keywords: Mesh and steel fiber reinforced concrete; Bridge reinforcement; Mechanic analysis; Construction technology

INTRODUCTION

Mechanical properties of SFRC such as compression, tensile, anti-fatigue, anti-cracking are better than the ordinary concrete. The concrete reinforced both by steel bars and SFRC are called mesh and steel fiber reinforced concrete. This method

strengthening bridge deck can enhance the integrity of the bridge structure and reduce crack propagation in the bridge deck.

Engineering Background

In the project of Dongguan North Bridge on Guang-Shen highway of China, the mesh and SFRC method had been utilized to reinforce the bridge deck. The bridge was designed originally on the base of British specification. The simple T-beam is used in the bridge structure. The conventional long-span of the bridge is 32.5 m and the horizontal half-width is built up with five T-beams. The distance between the main beams is 3.45 m and the height of main beams is 2.3 m. The width of the prefabricated roof is 1.6 m and the width of the cast-in-place plate is 1.85 m. The thickness of the bridge deck is 0.2 m (Figure 1). The full length of the bridge is 19638 m. The most substructures are constructed with reinforced concrete covered beams and reinforced concrete bored piles.

The main flaws of this bridge are the lower quality of the material in the wetland joints, the leakages at the joint between the flange plates of the prefabricated T-beam and cast-in-place plates, localized corrosion of steel bars, localized scaling on concrete surface and perforations. The original bridge deck is constructed with poor waterproof asphalt concrete.

In order to maintain the bridge deck, a new concrete overlay is placed. The concrete overlay should be generally 15 cm thick. The procedure is first to remove all old original cast-in-place plates and pour in situ plate and concrete overlay at the same time. However, there are many limitations during the project construction such as many separate engineering tasks, heavy traffic flow, limited construction time and other factors. Especially, this may increase the dead load of the bridge greatly. Finally, it is decided to remove the damaged cast-in-place plates merely and use mesh and steel fiber reinforced concrete as the overlay material. Then, the modified asphalt adhesive overlay solves waterproof problem and modified asphalt concrete is used as pavement. The bridge deck structure after strengthening is shown in Figure 1.

NUMERICAL EXAMPLE

Numerical model and material characteristic

In this study, the MIDAS software has been used for the numerical analyses. The element mesh consists of 3374 space beam elements with total 3149 nodes. The Cartesian xyz coordinate system is shown in Figure 2. Table 1 shows the main material elasticity parameters. The prestressing tendons used in the bridge were made in the United Kingdom, each of which is composed by 6 tendons, and each tendon is made by super strand (two relaxation) whose radius is 15.7 mm.

The original design of the bridge is based on the British standard BS5400. The bridge after the reinforcement should meet to the Chinese standard JTJ001–97 in

which the traffic load grade is the car- super-20. The type of steel fiber utilized in the numerical analyses is milling AMi04-32-600 with amount to 40 kg/m^3. The tensile strength of the steel fiber is about 800 MPa.

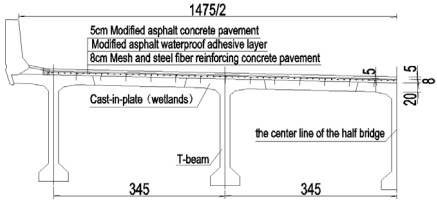

Fig. 1 The drawing of typical bridge section (Unit: cm)

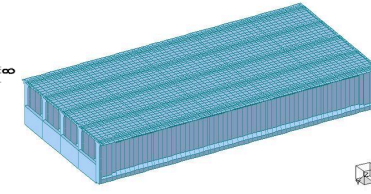

Fig. 2 Schematic of the element mesh

Tab. 1 Structure model parameters value

Project	Strength grade	Bulk density (kN/m^3)	Elastic modulus (MPa)	Poisson ratio
T-beam	C45	26	3.45×10^4	0.1667
Bridge deck cast-in-place	C30	26	3.00×10^4	0.1667
Mesh and SFRC pavement	C40	26	3.91×10^4	0.1667

According to the construction procedure, in this numerical simulation, two stages are simulated:

(1) Construction stage: the weight of mesh and steel fiber reinforcing concrete is considered as secondary load applied on the original bridge structure;

(2) Service stage: the mesh and steel fiber reinforcing concrete and original bridge are treated as a whole integrated body.

Mechanical response of the bridge at construction stage

Because the new 8 cm thick mesh and SFRC overlay replaces the original 8 cm thick asphalt paving, the change in secondary loading on the bridge is negligible. Thus, the construction stage is safe.

Mechanical response of the bridge at service stage

(a) The overall mechanical analysis of the bridge at service stage

At service stage, the concrete shrinkage and creep are computed directly by using the Chinese standard JTJ023-85. In this investigation, it is assumed that the concrete shrinkage and creep in the mesh and SFRC layer is same as in the original concrete

bridge. The equivalent load caused by temperature gradient can be computed by equations (1), (2).

For beam element: $$M = \alpha EI \frac{\Delta T}{h} \quad (1)$$

For plate element: $$M = \frac{\alpha E t^3 \Delta T}{6(1-\nu)} \quad (2)$$

in which α is linear thermal expansion coefficient of concrete, E is the elastic modulus of concrete, I is the inertia moment of the beam, ΔT is temperature difference , h is the distance between the edges of one unit section, t is the plate thickness, v is the Poisson's ratio.

There are three types possible load combination during the service stage. The first type is dead load +the most disadvantageous position in vehicle load+ steel beam prestressed+ shrinkage and creep; the second is temperature gradient warming; the third is cooling down the temperature gradient. The stress of the strengthening bridge in the service stage and the original bridge are shown in Tab. 2. It should be noted that the original bridge deck is assumed to be loaded at same time as the mesh and SFRC overlay and it is treated as a general prestressed concrete component（Zhang 2006）.

Through Table 2, it can be observed that, during the service stage, all stresses in both beam and plate elements meet (JTJ023-85), and some stresses are less than the one in the original bridge. The numbers in bracket of table 2 are the stresses in the original bridge. The vertical deformation (1.00 cm) is also smaller than the one in the original bridge (1.28 cm). Thus it can be concluded that the reinforced bridge is safe at service stage.

Tab. 2 Stress summary of bridge in the service stage and the original bridge

Load combination	Beam element stress (MPa)			Plate element (MPa)		
	Maximum principal stress	Minimum principal stress	Shear force	maximum principal stress	Minimum principal stress	Shear force
1	-0.261 (-0.188)	-9.665 (-9.787)	0.045 (0.053)	1.943 (2.088)	-7.332 (-7.573)	1.504 (1.631)
2	-0.126 (-0.118)	-2.189 (-1.705)	0.049 (0.038)	2.909 (3.036)	-2.490 (-2.525)	0.868 (0.878)
3	1.098 (0.858)	0.061 (0.061)	0.025 (0.025)	1.220 (1.249)	-1.371 (-0.973)	0.450 (0.439)

(b) The Local mechanical analysis of the bridge at service stage

During construction of the mesh and SFRC overlay, the heavily damaged cast-in-place plate should be removed first. But there are still some micro-cracks

between the connection of cast-in-place plate and the flange. It is difficult to determine whether the cracks go through the whole component or not. Following, two states have to be assumed. The top and bottom joins are assumed to be articulated, see Figure 3 and micro-cracks are assumed to propagate throughout the body, see Figure 4.

The most critical wheel loading layout is shown in Figure 3(l.) for the first state while in Figure 4(l.) for the second state, The weight of original cast-in-place plate is considered as the secondary equivalent load q as shown in Figure 4(l.). And The moment in the plate is calculated by Eq. (3)(JTJ023－85).

$$\gamma_0 M_{ud}=1.2M_g+1.4M_q \tag{3}$$

where: γ_0 is the important factor of structure, M_g is the moment produced by dead load, M_q is the moment produced by live load.

The results of maximum moment in the plate are shown in Table 3 according to numerical analysis in figure 3(r.) and figure 4(r.). It should be noted that the maximum negative moment occurs at the root of the flange and the maximum positive moment occurs in the middle of the two adjacent flange roots.

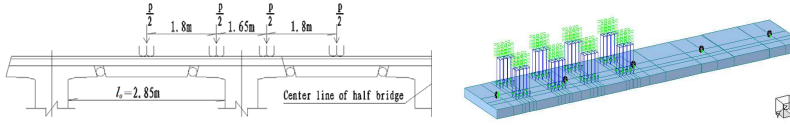

Fig. 3 schematic diagram and analysis model of state one

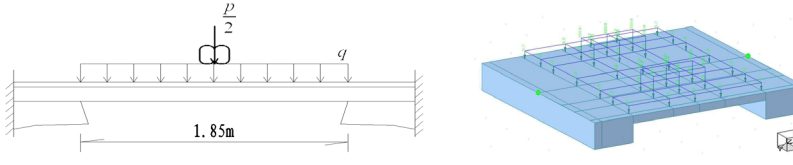

Fig. 4 schematic diagram and analysis model of state two

Tab. 3 Maximum moment of longitudinally plate per meter (M_d)

bridge state		maximum negative moment(kN·m)	maximum positive moment(kN·m)
original bridge		-22.222	19.578
service stage	State one	-26.657	15.094
	State two	-31.618	7.034

(c) Normal section's bending bearing capacity

In the reinforced overlay, the rod spacing is 12.5×12.5 cm. The diameters of steels along transverse and vertical direction are Φ16 and Φ12 respectively. The original bridge deck is assumed to be loaded at same time as the mesh and SFRC overlay.

However, there are differences between JTJ023－85 and BS5400. C45 in JTJ023－85 f_{cd}=20.5 MPa while in BS5400 f_{cd}=20.1 MPa. In JTJ023－85 HRB335(f_{sd}'=280 MPa, f_{sd}=280 MPa) is equal to G460(f_{sd}'=400 MPa, f_{sd}=331 MPa) in BS5400.

1) The checking of the maximum negative moment section

Because of the anchor bars' depth is 10 cm, it will cause damages of some N2 steels in drilling, N2 steels are considered as failure. On the base of double reinforced rectangular section assumption, Figure 5, the design value of moment M_{du}= 82.94 kN·m is bigger than $\gamma_0 M_d$=31.618 kN·m by using the inter force balance equations. It should be noted that the safety factor 1.0 is utilized in this calculation. It can meet the demand.

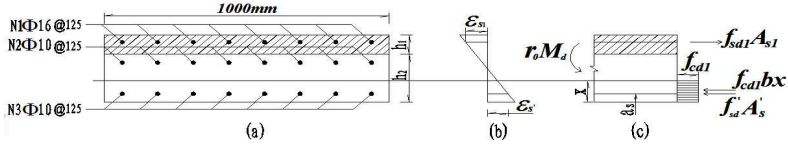

Fig. 5 the calculating diagram of the normal section's bearing capacity at the maximum negative moment point
(a) sectional drawing；(b) strain distribution；(c) stress distribution

2) The checking of the maximum positive moment section

As shown in Table 3, M_d at state one is 15.094 kN·m which is smaller than 19.578 kN·m in the original bridge. Therefore it is not necessary to check the maximum positive moment section. For state two, because M_d occurs between the positive middle of the two girder ribs, and the section's height here is just the thickness of the mesh and SFRC overlay, which is 80 mm, N3 steel bar is failure, so it must be checked.

On the base of single reinforced rectangular section assumption, Figure 5, the design value of moment M_{du}= 17.987 kN·m is bigger than $\gamma_0 M_d$=7.03 kN·m by using the inter force balance equations (Zhang 2006). It meets the demand.

Calculating the anchor bars distance

There is 12-year age difference between the old and new concrete, so the larger shrinkage tensile stress will appear. In order to improve the combination of reinforced overlay and the original bridge deck, the anchored steel bars are placed between the two layers（Wang 2007）.

The diameter of the anchored steel bar is Φ=16 mm. The Shear Strength of per anchor bar T is: T=62.6kN, according to the formula $T = 0.43A_s\sqrt{E_c f_c} \le 0.7A_s f_{sk}$. And the shear between the old and the new F=253.44kN/m^2，which based on the formula $F = bh_1E_1(150 - \varepsilon)$. Thus, the number of anchor bar per square meter is:

n=253.44/62.6=4.05≈4, so 6 roots /m^2 meets the demand. It should be noted that the safety factor 1.5 is utilized in this calculation. They are arranged in quincunx shape and the transverse and vertical distance of the steel bars are 50 cm.

The above calculations show that the bridge strengthening method by using mesh and SFRC is safe and feasible. It can meet the demand（JTJ001–97） of the minimum bridge paving thickness.

CONSTRUCTION PROCESS DISCUSSION

The construction process of bridge reinforcement with mesh and SFRC paving overlay is divided into four steps: asphalt concrete milling-planning, planting reinforcing bar, laying steel mesh reinforcement and pouring steel fiber reinforcing concrete.

The original bridge's asphalt surface should be milled carefully by using Wirtgen milling machine. After the asphalt concrete milling, the dust should be cleaned by using air compressor and high-pressure water. The retained asphalt oil film should be cleaned by using a milling-planning machine (0.5 m). After that, the retained asphalt oil film should be washed again by the high-pressure water and cleaned manually. The local retained asphalt oil film should be cleaned manually by electric angle-milling until the fresh concrete appears. It should be noted that during the surface cleaning the bridge structure should not be damaged. This construction process is very important to prevent appearance of the sandwich effect between the new and old concrete.

The steps of planting anchor bar and laying steel mesh are mainly drilling, cleaning the borehole, automatic glues pouring, inserting the steels and lashing the mesh. In case of the bar's diameter extension due to the machining process and the colloid extrusion extension, the diameter of the drill bit should be bigger than the diameter of the anchor bar, which is 4 mm. The drilling should not interfere with the constructional steel bar (N2) in the original bridge.

The channel should keep straight. The dust and fragment on the bottom of the drilling hole should be blown away by using high-pressure dry air. The reinforcing glue is injected until two-thirds of the height of the hole. The steel bar is inserted to the bottom of the hole and rotated 360 degrees. The extra glue should be cleaned up with acetone. After the pull out force reaches 21 kN, the steel mesh can be laid with distance of 12.5×12.5 cm and the anchored bar can be bent 90 degrees.

The advised mix proportion of the steel fiber reinforced concrete: the cement-water- steel fiber-sand-coarse aggregate ratio is 1: 0.40: 0.10: 1.87: 2.69. The high performance retarded (FST-2) is added by 2.5%. In order to reach the concrete's ideal compactness, the speed of pouring generally be between 0.6 and 1.0 m/min.

CONCLUSIONS

1. The bridge strengthening method by using 8 cm mesh and SFRC and 6 roots anchored bars per square meter can enhance the integrity of the old bridge structure and reduce crack propagation in the bridge deck. It also has the advantage of increasing bearing capacity of the bridge structure. In addition, the construction time of this method is relatively short. It can also improve the durability of bridge structure, result to prolong the service life of the bridge.
2. In the local checking, it's assumed that the micro-cracks between the connection of cast-in-place plate and the flange are articulated or propagated throughout the body. The method is convenient accords with actual.
3. On the bridge completion with superior quality, it's proved that the construction process of bridge reinforcement with mesh and SFRC paving overlay is feasible, and it's worth to use the construction experience of the similar bridge reinforcement for reference.

REFERENCES

Completion Data of Dongguan North Bridge on Guang-Shen highway, unpublished internal report, February 1994.

Su Wu. (2008). "Comparison of BS5400 and Chinese highway standards on reinforced concrete design" *Journal of Railway Engineering,* Vol. 3: 24-32.

Wang Zhen-ling. (2007). "Study on bond theory and test of new and old concrete and its application in bridge strengthening engineering" doctoral dissertation. Southwest JIAOTONG University, Chengdu, China.

Zhang Shu-ren, Wang Zong-lin. (2006). "Bridge diseases treatment and Strengthening Design" *People's Communications Publishing House*, Beijing, China: 134-135.

New Composite Pavement System For Orthotropic Steel Bridge Decks

Li Xue-lian[1], Chen Yu-liang[2]

[1]Lecturer and PhD, School of Communication and Transportation Engineering, Changsha University of Science and Technology, Chiling Road 45#, Changsha, Hunan, China, 410076. E-mail: lixuelianfj@yahoo.com.cn

[2]Lecturer, School of Engineering & Architecture, East China Jiaotong University, Nanchang, Jiangxi, China, 330013. E-mail: chenyuliangjx@yahoo.com.cn

ABSTRACT: Orthotropic steel bridge decks are widely used for large and medium span bridges, however early failure in traditional asphalt concrete surfaces has proved to be a problem on high traffic routes. Consequently, a demand exists to find a durable overlay for such bridges. In this paper, four kinds of design indices are explored, based on the primary types of pavement distress. In addition, the mechanics of surface wear on orthotropic steel bridges was analyzed by the Finite Element Method (FEM), which shows that the higher elastic modulus of the intermediate layer and/or the thicker the wearing surface, the less stress there is in the critical fatigue parts of the surface and the more favorable the wearing surface is. A new composite wearing surface system was presented, with a cement-based intermediate layer, shear stud connector, and SMA13 surface. Also, a number of small-scale tests were conducted to investigate the performance of bonding the new composite overlay to a steel plate, such as the thermal compatibility, rutting test under high temperature, and fatigue durability of the new composite wearing surface system. These were then compared to the traditional double-layer asphalt concrete surface. It was concluded that the performance of the new composite system is more durable than the traditional one.

KEYWORDS: orthotropic steel bridge; mechanical behavior; bridge deck composite pavement; cement mortar; stability; fatigue; design index

INTRODUCTION

Pavement on orthotropic steel bridge decks is a complex problem. Due to the great flexibility and large local deformation of orthotropic steel bridges, particular when dealing with traffic, temperature, wind, earthquakes and other natural factors, the stress and deformation of bridge decks is very complicated. In addition, the tensile, compressive and shear strength of asphalt concrete are relatively small, compared to the steel bridge deck it resides on. Fatigue cracking, rutting, delaminating and other early damage are common.

MECHANICS ANALYSIS

DESIGN INDEX

In addition to fatigue cracking, shear layer destruction, rutting and folding also must be controlled in steel bridge deck pavement. Four main design indexes were put forward: surface tension stress, shear stress between layers, vertical compressive strain and shear stress in pavement. These indexes are the focus of the following mechanics analysis of orthotropic steel bridge pavement.

CALCULATION PARAMETERS AND MODEL

Monolayer and double-layer are the typical structure of the orthotropic steel bridge deck pavement. There are a variety of combinations for different pavement materials and thickness. The best combination for the structure can be selected by comparing the pavement response under the vehicle load. Theoretical research and engineering practice shows that the double-layer steel bridge deck pavement with a clear distribution of functions is better. The double-layer structures are more effective than monolayer structures, and double-layer structures are in mainstream use. Therefore, only the double-layer pavement structure was calculated and analyzed in this paper, in addition to the design indexes.

According to the vehicle load indicators of Universal Norms Highway Bridge Design (JTG D60-2004), a single-axis, 140 kN load was used 200 mm along the bridge and 600mm in width, which is shown in Table 1. The horizontal load is equivalent to the vertical load multiplied by the load factor. The horizontal load factor is 0.3.

Table 1. Calculation Load

Load type	Tire pressure (MPa)	Horizontal load (MPa)	Width (mm)	Length (mm)
Single wheel	0.758	0.228	200	600

EFFECTS OF TRANSITION LAYER MODULUS

The modulus of the transition layer ranged from 2000MPa to 12000MPa, while the other parameters remained unchanged. As shown in Fig.1, when the modulus of the transition layer increases, all main design indexes except for the stress between pavement and bridge deck decrease. When the modulus of the transition layer changed from 2000MPa to 12000MPa, the maximum tension stress of the surface, the maximum shear stress of the bridge deck pavement and the maximum vertical compressive strain of the bridge deck pavement decreased by 47.0% percent, 38.6 % and 17.8%, respectively.

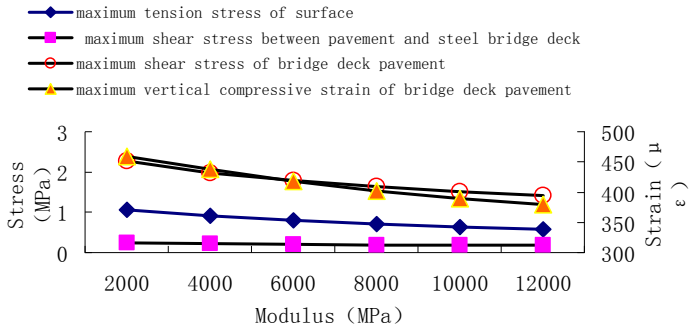

FIG.1. Change law of index under various modulus of the transition layer

Because the compounded properties of pavement and steel bridge decks result in a proportional relationship between the modulus of the transition layer and other layers, the compound rigidity is larger when the modulus of the transition layer is greater, and the stress and strain in orthotropic steel bridge decks are less. At the same time, the deformation of local steel bridge decks under the same conditions is less, too. The direct layer of pavement applied to an orthotropic steel bridge deck is preferable.

EFFECTS OF PAVEMENT THICKNESS

The thickness of the bridge deck pavement is an important design index. Generally, the thickness of pavement is between 38mm and 120mm. There are two kinds of designs for pavement thickness, thin and thick. Thin pavement is very common in Europe and the United States, the thinnest is 38mm; while in Japan thick pavement, 60mm-80 mm, is widely used. In China, typical pavement thickness of long-span steel bridges is between 50mm-80mm, therefore only the 35mm-95mm-thick pavements were analyzed here. The calculated results are shown in Fig 2.

(1) When the pavement thickness increases, the main design indexes decrease. However the reducing rate is different; the specific order is: the maximum tension stress of surface > the maximum shear stress of bridge deck pavement > the maximum vertical compressive strain of bridge deck pavement > the maximum shear stress between pavement and steel bridge deck. When the thickness increased from 35mm to 95mm, the maximum tension stress of the surface, the maximum shear stress of bridge deck pavement, the maximum vertical compressive strain of bridge deck pavement and the maximum shear stress between layers decreased by 75.2%, 61.5%, 56.1% and 45.8%, respectively.

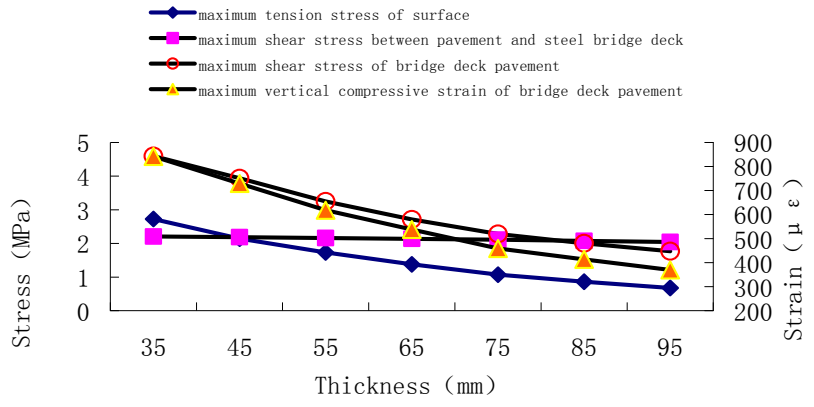

FIG.2. Change law of every index under various thickness

(2) Appropriately increasing thickness of pavement can effectively improve the force state of pavement. However, the reducing rate of the main indexes is very limited when the thickness increases to a certain extent. The effect of increasing thickness may not be so obviously. For example, when the thickness increased from 35 to 45 mm, 45mm to 55 mm, 55mm to 65 mm, 65mm to 75 mm, 75mm to 85 mm and 85 mm to 95 mm,, then the maximum tension stress of the surface decreased by 0.587MPa, 0.409MPa, 0.354MPa, 0.284MPa, 0.234MPa and 0.184MPa, respectively. Thus, 75mm is a more ideal pavement thickness.

NEW COMPOSITE PAVEMENT SYSTEM

From the above analysis, we can see that the pavement is in a more favorable condition when the modulus of the transition layer increases and that appropriately increasing thickness of pavement can improve the force state of pavement. In view of the unique advantages of the composite structure of steel and concrete, a new composite wearing surface system was used, with light polymer concrete mortar (LPCM) transition layer, shear stud connector, and SMA13 surface, as shown in Fig 3.

The main advantages of new composite structure:

(1) An asphalt concrete pavement surface can improve driving comfort and greatly alleviate traffic impact on the bridge deck.

(2) Pertaining to the deformation of coordination, the modulus of LPCM in the composite pavement structure is placed between asphalt concrete and the steel bridge deck, which can ease the rigidity of the structure and improve the force state of the

structure.

(3) Regarding permanent deformation, LPCM has minimal local permanent deformation, and although the top layer of asphalt concrete does experience deformation., the thickness of the asphalt concrete in a composite pavement structure is less than that of the traditional asphalt concrete pavement, thus the new structure has a reduced amount of rutting.

(4) Pertaining to the bonding capability between layers, the groove on the surface of LPCM has a bigger horizontal shear strength than simple binder.

(5) In view of heat transfer, the temperature sensitivity of LPCM is less than that of asphalt concrete.

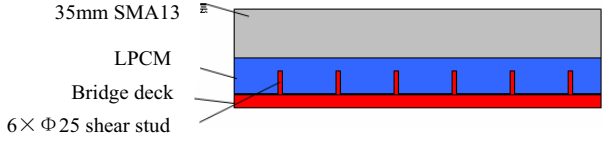

FIG3. New Composite Structure

STUDY ON COMPOSITE PAVEMENT

To inspect the overall stability of the composite pavement structure, the thermal compatibility, rutting under high temperature, and fatigue durability tests were carried out.

THERMAL COMPATIBILITY TEST

Sample Design

Length × width × height of the sample is 400mm × 100mm × 90mm, effectively. The span of the beam is 350 mm; pavement thickness is 76 mm; the steel bridge deck is 16Mn and the thickness is 14 mm (specimen span is longer than cross-section, about three times).

Pavement structure

Option 1: 35mm SMA13 +0.5 L/m^2 modified asphalt +40mm LPCM; Option 2: 35mm SMA13 +0.65 L/m^2 modified asphalt +40 mm SMA13.

Test Procedure

The plane size of the specimen is 400 mm × 100mm, including four kinds of samples: (1) LPCM + steel bridge deck; (2) single-layer SMA13 + steel bridge deck; (3) SMA13 + LPCM + steel bridge deck; (4) double-layer SMA13 + steel bridge deck.

The first test, according to ASTM C884(ASTM 2005), consisted of five cycles of temperature changes: 25°C and -10°C. Specimens were kept 24 h at every

temperature level during each cycle. Specimens that passed the first test were brought into the second test. The second test, named freeze-thaw-heat nonstandard test consisted of five cycles of temperature change: -10°C, 25°C, and 60°C. For the second test, the specimens were kept for 24 h at every temperature level during each cycle. The specimens that passed the second test were brought into the third test. The third test, called submerge-freeze nonstandard test, consisted of five cycles of condition changes where the specimens were submerged in the water for 24 h at room temperature, and then kept in a freezer for 24 h at -10°C.

Cracks at the interface were monitored at every cycle. Magnified close-up photographs of the sides of the panels were taken using a high resolution camera. The close-up images focused on the interface between the pavement and the steel bridge deck. Debonding of the pavement from the bridge deck was considered a failure state for the system.

Results and Discussion

The results show that the new composite pavement and the traditional pavement both passed three thermal compatibility tests. No cracks or delamination occur during these tests. Accordingly, based on the thermal compatibility test results presented, it can be concluded that the new composite pavement structure has good adhesion between layers and each layers are thermally compatible.

COMPOSITE RUTTING TEST

Table 2. Results of Composite Rutting at 70℃

Project Number / Index	Transition layer	surface	Dynamic stability (times/mm)	Rutting depth (mm)
Ⅰ	40mmLPCM	35mmSMA13	5800	0.62
Ⅱ	25mm epoxy asphalt concrete	25mm epoxy asphalt concrete	9000	0.32
Ⅲ	20-25mm Gussasphalt concrete	35-40mm epoxy asphalt concrete	7000	0.34
Ⅳ	25mm epoxy asphalt concrete	35-40mmSMA10	5214	0.74
Ⅴ	20-30mm Gussasphalt concrete	35-40mmSMA13	1218	1.74
Ⅵ	30 mmSMA10	35mmSMA13	4469	1.05
Ⅷ	30 mm Gussasphalt concrete	40mm Gussasphalt concrete	415	3.58

A composite rutting test was carried out at 70 °C. Dynamic stability and rutting depth were used to study the stability of the composite pavement structure at high temperature. Rutting specimens consisted of transition layer, bonding layer, and

surface, in turn: pouring LPCM and then grooving the surface; applying coating modified asphalt; profiling SMA13 in 2-4 h. The rutting test results and some related results of Hongtao Li (2005) are listed in table 2.

The high temperature stability or anti-rutting capability of varied structures shows a significant difference. LPCM + SMA, double-layer epoxy asphalt concrete, gussasphalt + epoxy asphalt concrete and epoxy asphalt concrete + double-layer SMA have dynamic stability, and their rutting depth was less than 2 mm. Therefore, the new composite structure and the other four kinds of structures have better high-temperature stability and stronger anti-rutting capability than those of the traditional double-layer SMA structure.

FATIGUE TEST OF COMPOSITE BEAM

Specimen and load

(1) Specimen design is the same as that of thermal compatibility;

(2) Loading position: medium span of the beam (Fig 4);

(3) Loading frequency: 10 Hz;

(4) Loaded waveform: half-sine.

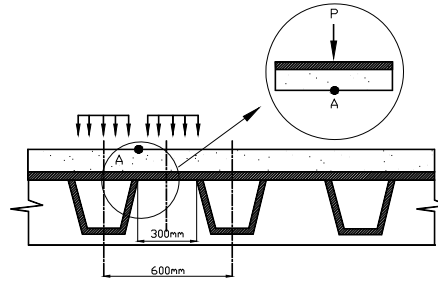

FIG.4. Loading position

Fatigue damage standard

Once one of the following circumstance results, the test should cease:

(1) Cracks occur on the surface;

(2) Delamination appears;

(3) Total deflection (deflection at the peak load) or difference of deflection (the difference of peak and valley deflection) significantly deviates from the initial value.

Four-point fatigue test

Before the fatigue test, bending tests were conducted, which showed the maximum bending load of the composite beam to be 2485 N, greater than that of traditional beams at 1400 N. To the new composite structure, SMA13 + LPCM, two levels of

load amplitudes were applied in the fatigue test that had a total of 840,000 load cycles and 8940 load cycles. For the first 840,000 cycles, the amplitude of the load was 500N. For the remaining 8940 load cycles, the amplitude of the load was 1000N, as shown in table 3. For the traditional structure, double-layer SMA13, the same levels of load amplitude were applied on the beam, but the load cycle of second level was only 635 times. Thus, when the same load is applied, the fatigue performance of SMA13 + LPCM is far better than that of double-layer SMA13.

Table 3. Fatigue Test Results of Composite Beam

Project	Total thickness of bridge deck pavement(mm)	Load cycles (times)
SMA+13LPCM+Steel panel	40+35	8940
Double-layer SMA13+ Steel panel	40+35	635

CONCLUSIONS

Characteristics and requirements of the orthotropic steel bridge deck pavement were investigated and analyzed, based on technical exploration, theoretical analysis and laboratory tests. Given the unique advantage and great achievements of the steel-concrete composite structure in civil engineering, a new composite wearing surface system consisting of SMA13 wearing course and lightweight polymer cement mortar (LPCM) transition layer were studied. Based on the results of this study, the following conclusions can be drawn: (1) By considering an orthotropic steel bridge with stiffening ribs and vertical/cross slabs, and wearing surface on beam segment as calculation target, the typical wearing surface response was analyzed and determined. The relation between main design index and the modulus of transition layer or between main design index and the thickness of pavement was analyzed. Given the great achievements of the steel-concrete composite structure, a new composite wearing surface system was presented, with a cement-based intermediate layer, shear stud connector, and SMA13 surface. (2)The stability between pavement and steel deck, and the thermal compatibility and durability of the new wearing surface system under high temperature were used to investigate the temperature and intensity of the new system. The four-point bending fatigue test results show the fatigue performance of the new composite structure system to have a greater tolerance than the traditional structure.

REFERENCE

Chen Xian-hua (2003). “Test study on Runyang bridge deck pavement structure.” Nanjing: *Southeast University*.

Pan Shi-jian., Sheng-fu, Yang. “Construction series of Xiamen Haicang bridge.”

Beijing: *Peoper's Communication Press*.

Li Hong-tao(2006). “Research on new structure of long span suspension bridge steel deck surfacing”. Nanjing: *Southeast University*.

JTG B01-2003 (2003). “Highway engineering and technical standards.” Beijing: *People's republic of China Ministry of transportation*.

JTG D60-2004 (2004). “General design specification of highway bridge”. Beijing: *People's republic of China Ministry of transportation*.

Deng Xue-jun, (2002). “Pavement structure stress under horizontal load.” Nanjing: *Journal of Geotechnical Engineering*. Vol.24（4）：427 -431.

Gu Xing-yu. “Impact of various loadings toward asphalt paving on steel deck bridge.” Beijing: *Journal of Highway and Transportation Research and Development*. Vol.19（2）：56-59.

Zhang Qi-sen (2005). “Design theory and method higher pavement structure.” Beijing: *Peoper's Communication Press*.

Stress Analysis of Portland Cement Concrete Pavement Slab Under Various Supporting Conditions

Hongyuan Fu, Yang Zhang, Bo Kuang

Professor, School of Traffic and Transportation Engineering, Changsha University of Science & Technology, Hunan Changsha, 410076, P. R. China; fuhy1@163.com

ABSTRACT： Rigid concrete pavement slab under various supporting conditions was analyzed by elasto-plastic nonlinear three-dimensional finite element technique. The influences of void size on the stress, and deflection of concrete pavement slabs were investigated and are presented in this study. This research shows that the stress peak value of a loaded slab is approximately two times higher than at the across corner slab. Due to stress concentration, the void area boundary of PCC slabs becomes a fracture boundary, because it eventually ends up as a corner crack. The deflections of loaded slabs grow rapidly when the tire load approaches the center of the slab. As expected, the highest deflection occurred at the location directly below where the tire load was applied. In addition, the deflections increase directly with increases in the void size.

KEYWORDS: Void shape; Void boundary; Stress peak; Deflection of road slab; Simple supporting conditions

INTRODUCTION

Although Portland Cement Concrete (PCC) pavement has many advantages over the flexible asphalt pavement, there are some inherent weaknesses. For instance, common symptoms found in China include faulting that result in poor ride, cracks near the joints, excessive post settlements after construction on soft roadbeds, differential settlements owing to differential compactions. In China, voids under the PCC slabs are common. Voids not only lead to premature failures but also are very difficult to repair properly. The stress concentrations are extremely high at the localized void areas and under cyclic traffic loading they can easily crack the PCC slabs. Voids under PCC slabs are one of the main factors that contribute to poor pavement performance. Therefore, it is very important to characterize the stress-strain relationships of PCC slabs with localized voids for different supporting conditions.

As early as 1939, an empirical formula for calculations of slab corner and edge stresses with localized voids between pavement and roadbed was proposed by Kelly (Kelly, 1939). Further refinement was done by Pickett (Pickett, 1946) to incorporate the influences of corner load transfer and warping stresses. With the advancements of finite element modeling techniques, the stress and strain relationships of PCC slabs have been investigated by many researchers under various supporting conditions at different load levels (Zhou, 2007; Yang, 2007). Although those research results are very helpful for better understanding of the fracture mechanisms of PCC slabs, there is no complete and systematic study to explain the influences of voids on stress and

strain distributions at both sides of a joint. The complexity increases when it couples with various supporting conditions. This is mainly due to the uncertainty of boundary conditions and the imperfection of thin plate theory. Thus, analytical solution based on elastic foundation theory is rarely reported. Although analytical solutions are presented by Zhang (2003), Zhou (Zhou, 1996), Huang (1992), there are significant limitations for those studies. To analyze this complex problem, elasto-plastic nonlinear three-dimensional finite element technique was utilized in this study.

FINITE ELEMENT ANALYSIS

Finite Element Model

Based on the values suggested by the Chinese design code (JTG D40-2002), the length, diameter, and spacing of tie bar at longitudinal joints are 800mm, 16mm, and 700mm, respectively. A PCC slab size of 3.75m×5m was selected and analyzed in this study. The length, diameter, and spacing of dowel bars at transverse contraction joints are 450mm, 32mm and 300mm, respectively. The widths of longitudinal and transverse contraction joints are 8mm. The thicknesses of slabs range from 220mm to 320mm. A brick element with 8 nodes was adopted in this study. The typical pavement structure consists of slabs, steel bar, base (with void area), sub-base, underlayer, cushion, and soil matrix.

Boundary Conditions and Input Material Parameters

Because of infinite widths and lengths of pavements, several faces were fixed that included the four lateral surfaces of base, the displacement in the y-direction on the surface perpendicular to x-direction, the displacement in x-direction on the surface perpendicular to y-direction. In addition, three-directional constraints were applied to the subsurface. Structure joint constraints were regarded as rigid where the steels dowel or tie bars are located. Good bonding conditions were assumed, and a buried steel model was adopted. The “tie-touch model” was utilized for the simulation of interface between base (with void area), sub-base, cushion, and soil matrix. The input material parameters utilized in this study are shown in Table 1. Based on the recommendation by Zhao (2004), a frictional factor of 1.5 for between concrete and base was employed in this study.

Table 1. Material parameters

Levels	Material	Bulk density (t/mm^3)	E(MPa)	Poiss-on´s ratio
Surface (260mm)	Concrete(C35)	2.4e-09	3.15e+04	0.167
Construction joint	Steel	7.8e-09	2.0e+05	0.3

Base(160 mm)	Cementation sand gravel	2.2e-09	2093	0.3
Sub-base(180 mm)	Cementation limestone soil	2.0e-09	1000	0.3
Cushion (150 mm)	Gradation gravel or limestone soil	2.0e-09	800	0.3
Soil base	Soil	1.8e-09	100	0.35

Loading and Void Condition

A single axle with dual tires at the standard axle load was utilized in this study. The tire pressure, tire shape, and tire distance was selected according to the recommendations by Himeno (1997). The void area proposed by Zeng (2005) and Zhao (2004) that considers symmetry distribution was adopted in the analyses. The shape of the void area is approximately a triangular wedge. The void height is smaller when it closer to the slab center. The void area was assumed to be quadrangle when the transverse edge of void area was connected with the longitudinal edge of the void area. At the joint of the PCC slab, the shear and moment were transferred through the surrounding concrete material and dowel bars, and the influences of the bending rigidity of dowel bars was taken into account. The void under PCC slab is predominately due to pumping. Therefore, the void areas were assumed to occur at the corners of the four slabs intersected. In order to stimulate voids in the analyses, the elastic moduli of affected elements in void areas were set to zero. The eight different void areas were increased in sequence and were called void area-1 to void area-8.

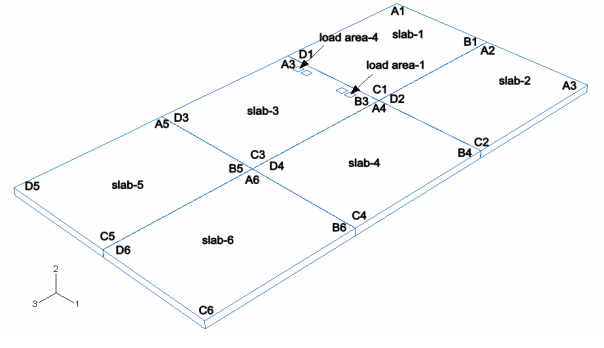

FIG. 1. The finite element model of cement concrete pavement

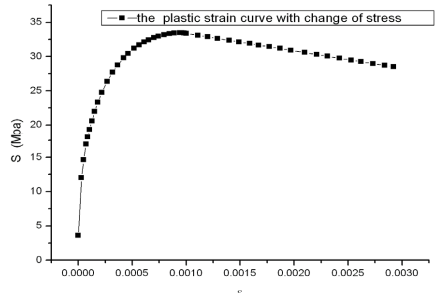

FIG. 2. The elasto-plastic strain curve of concrete with varying stress

Analysis Steps

The first step was used to analyze the stress distribution under gravity action. The second step was to exert standard axial load. The third step through the tenth step simulated the stress state of each slab as the void areas increased in sequence of 0.2m×0.2m (void area-1), 0.4m×0.4m(void area-2), …, 1.6m×1.6m(void area-8).

STRESS AND DEFLECTION ANALYSIS OF PCC SLAB UNDER VARIOUS VOID SIZE

Stress Analysis

Because the pavement was considered as an infinite structure in length, six parallel slabs were used to simulate this condition. They were numbered in sequence as slab-1, slab-2, …, slab-6, from top to bottom. The four corners of each slab were marked clockwise as A, B, C and D. Loads were applied on load area-1 to load area-4 of slab-3, as shown in FIG. 1. FIG. 2 is the constitutive model utilized in this study that illustrates elasto-plastic strain curve of concrete with varying of stress.

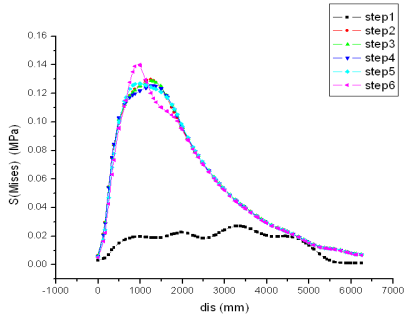

FIG. 3. The stress curve of D_2B_2 at Step1~Step6

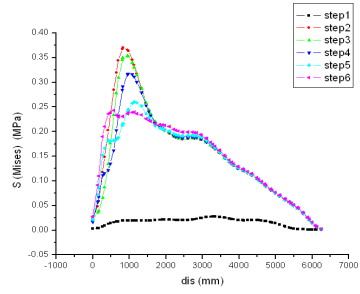

FIG. 4. The stress curve of D_3B_3 at Step1~Step6

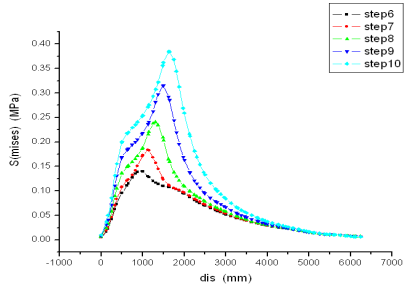

FIG. 5. The stress curve of D_2B_2 at Step6~Step10

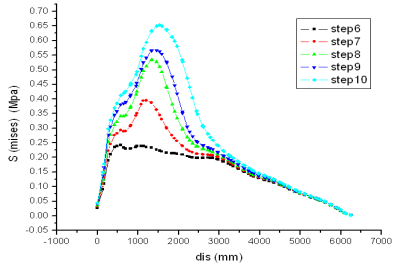

FIG. 6. The stress curve of D_3B_3 at Step6~Step10

FIG.3 to FIG.6 show that stress peak exists in all the stress curves. In particular, the values of stress peak increased significantly from step 6 to step 10, as the void areas increase in size. The highest peak was found when the tire load was located directly

above the void area, as expected. There is considerable difference between peak value of loaded slab and that of across corner slab (away from the tire load). The stress peak value of the loaded slab is approximately two times higher than the across corner slab. Because of void under PCC slabs, stress peak values occurred in all the stress curves. Due to stress concentration, the void area boundary of PCC slab becomes a fracture boundary, as it eventually ends up as a corner crack.

Deflection Analysis

The deflection of PCC slabs not only influences the load transferring capacity but also impacts the driving comfort. Thus, it is critical to study the impacts of voids on deflection. The analysis results are presented in FIG.7 to FIG.10. For step 6 to step10, the deflections of the loaded slab grow rapidly at the center of the tire load. As expected, the highest deflection occurred at the location directly below where the tire load was applied. In addition, the deflections increase with void size.

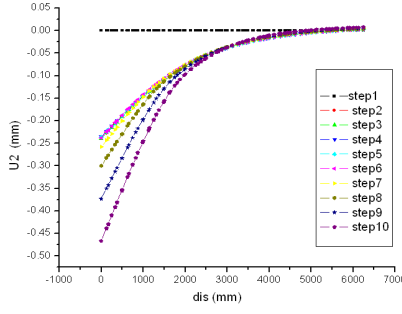

FIG. 7. The deflection curve of D_2B_2 at Step1~Step10

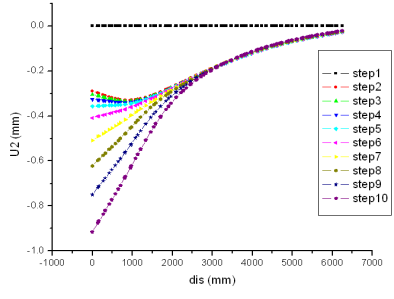

FIG. 8. The deflection curve of D_3B_3 at Step1~Step10

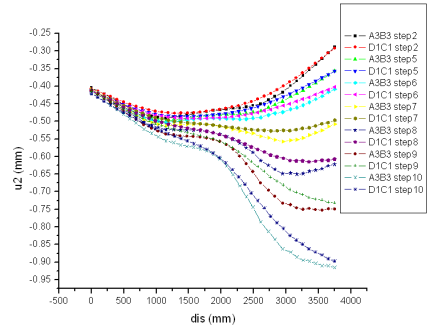

FIG. 9. The deflection curve of A_3B_3 and D_1C_1 at Step2 and Step1~Step10

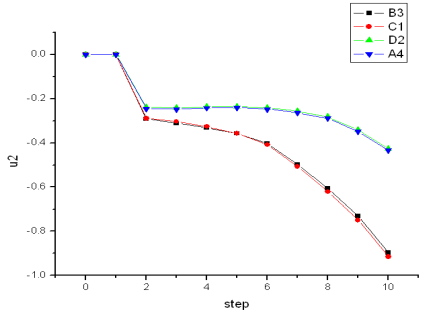

FIG. 10. The deflection contrast curve of different node

CONCLUSIONS

1) It was observed that the stress peak value of the loaded slab is approximately two times higher than at the opposite corner slab. Because of void under the PCC slab, stress peak value occurred in all the stress curves. Due to stress concentration, the void area boundary of PCC slab becomes a fracture boundary, as it eventually ends up as corner crack.

2) The deflection of loaded slab grows rapidly near the center of the tire load. As expected, the highest deflection occurred at the location directly below where the tire load was applied. In addition, the deflections increase with void size.

REFERENCES

Kelly, E. F. (1939). "Application of the results of research to the structural design of concrete pavements". *Public Roads*. 20(5): 83. 20(6): 107.

Pickett, G. (1946). "Concrete pavement design". Skorkie: Portland Cement Association.

Chen, Wen. Liao, Weidong. Zhu, Jidong. Ma, Guangyue. And Wu, Shaopeng. (2003). "Finite element analysis of separation under cement concrete pavement". *Journal of Wuhan University of Technology*. 25(12).

Guan, Hongxin. Zhang, Qisen. and Zheng, Jianlong. (2004). "Stress analysis on asphalt overlay on cracked concrete with cavity underneath repaired with bridging slab". *Journal of Highway and Transportation Research and Development*. (6).

Zhou, Yumin. Tan, Zhiming. and Liu, Boying. (2007). "Loading stresses in cement concrete pavement slab with void underneath". *Journal of Tongji University (Natural Science)*. 35(3).

Yang, Qun. Guo, Zhongyin. and Chen, Liping. (2007). "Structure design method of composite pavement in road tunnel". *Journal of Harbin Institute of Technology*. 39(6).

Zhang, Jiafan. and Zhang Huimei. (2003). "Additional stress in pavement structure due to asymmetrical settlement of soft subgrade". *Journal of Chang'an University (Natural Science Edition)*. 23(3).

Zhou, Ding. (1996). "An exact method of bending of elastic thin plates with arbitrary shape". *Applied Mathematics and Mechanics*. 17(12).

Huang, Yan. (1992). "The theory of elastic sheet". National University of Defense Technology Press.

JTG D40-2002. (2002). "Specifications of cement concrete pavement design for highway". Beijing: People Communications Publishing House.

Yao, Zukang. (2003). "The design theroy and method for cement concrete pavement". Beijing: People Communications Publishing House.

Himeno, K. Kamijima, T. Ikeda, T. et a1. (1997). "Distribution of tire contract pressure of vehicles and its influence on pavement distress". *Proceedings of 8th International Conference on Asphalt Pavement*. Washington: the International Society for Asphalt Pavements. 129-139.

Zeng, Sheng. and Cheng, Mingxian. (2005). "Research on the concrete pavement void and load transfer mechanism". *Journal of Railway Science and Engineering*. 2(1): 68-72.

Zhao, Maocai. (2004). "Analysis of the effect of the cavity beneath cement concrete pavement slabs on life span". *Journal of Highway and Transportation Research and Development*.21(2).

The Reliability Calculation Program and the Parameter Sensitivity Analysis of Airfield Cement Concrete Pavement

LI Le[1] and CEN Guo-ping[2]

[1]The 15th Team of Postgraduates of the Engineering College, Air Force Engineering University, Xi′an, Shaanxi, China, Postcode: 710038, Simoslee@gmail.com

[2]The Airfield Architecture Department of the Engineering College, Air Force Engineering University, Xi′an, Shaanxi, China, Postcode: 710038, Cenguoping@163.com

ABSTRACT: The fatigue destructive model which considers the temperature fatigue stress in airfield cement concrete pavement was introduced. The distribution rules for four main parameters were developed by measurement and analysis. The Reliability Calculation Program for Airfield Cement Pavement (RCPACP) was compiled based on Monte Carlo Method. The ranges of variability coefficients of parameters were described and the sensitivity of the parameters was qualitatively and quantitatively analyzed based on the program. The results show that the sensitivity of flexural flexibility modulus of concrete is largest and the flexibility modulus on top of the base is smallest.

1 INTRODUCTION

The fatigue destructive model of airfield cement pavement in which the temperature fatigue stress was considered was recently redesigned (National Standard, 2008). The distribution rules of five main parameters were put forward based on the model. The distribution rules of parameters and Monte Carlo method, the Reliability Calculation Program for Airfield Cement Pavement (RCPACP) was compiled using Matlab 7.0 language.

The sensitivity of a parameter is defined as the change of the reliability when the parameter is at different values or different variability coefficients. It reflects the effect of the value or variability of the parameter on pavement reliability (Ove Ditlevsen, 2006). Based on the RCPACP, the qualitative and quantitative analyses of the sensitivity of four main parameters were given.

2 THE RELIABILITY CALCULATION PROGRAM FOR AIRFIELD CEMENT PAVEMENT (RCPACP)

2.1 THE FATIGUE DESTRUCTIVE MODEL

The reliability-based airfield cement concrete pavement design method is based on

the fatigue destructive model. The fatigue destructive model compares compares functioning times. When the functioning times which the pavement could support (N) is larger than design functioning times (n), the pavement is reliable, otherwise the pavement is disabled. The relationship between N and n is independent, so they were chosen for reliability performance function. The performance function of airfield cement concrete pavement is $Z = N - n$, When Z<0, the pavement is disabled, when Z>0, the pavement is reliable, when Z=0, the pavement is at a critical state.

The invalidation probability of pavement (P_f) can be expressed as: P_f=P(Z<0), the reliability of the pavement can be expressed as: R=1-P_f.

The N can be calculated by formula 1(National Standard, 2008).

$$\lg\frac{\sigma_p}{f_r-\sigma_t} = 0.097 - 0.024\lg N \tag{1}$$

In the formula, σ_p is flexural stress of pavement; σ_t is temperature fatigue stress; f_r is the standard value of flexural strength of pavement cement.

The σ_p can be calculated by formula 2 (for single wheel load) and formula 3 (for double wheel load) (National Standard, 2008).

$$\sigma_p = (5.2059 - 2.0984T_w)\left(\frac{E_c}{E_t}\right)^{0.0715} r^{1.7114} qh^{-1.3692} \tag{2}$$

$$\begin{cases} \sigma_p = (5.2059 - 2.0984T_w)\left(\dfrac{E_c}{E_t}\right)^{0.0715} (K\cdot r)^{1.7114} qh^{-1.3692} \\ K = 1 + 0.1236\left(\dfrac{E_c}{E_t}\right)^{-0.0235} h^{0.2664} R^{-1.1291} r^{-0.0454} \end{cases} \tag{3}$$

In formula 2 and formula 3, T_w is the load transfer coefficient at concrete pavement joints; E_c is the flexural flexibility modulus of concrete; E_t is the flexibility modulus on top of the base; r is the radius of wheel trace which can be calculated by formula 4; q is the wheel pressure; h is the pavement thickness; R is the distance between double wheel.

$$r = \sqrt{P/q\pi} \tag{4}$$

In formula 4, P is dynamic load of wheel; the other parameters are as mentioned above.

The σ_t can be calculated by formula 5.

$$\begin{cases} \sigma_t = f_r\left[a\left(\dfrac{\sigma_{tqm}}{f_r}\right)^c - b\right] \\ \sigma_{tqm} = 0.5\times10^{-5} E_c h T_g B_x \end{cases} \tag{5}$$

In formula 5, σ_{tqm} is the warping stress of pavement at the maximum temperature gradient; T_g is the maximum temperature gradient; B_x is the coefficient of temperature stress; a, b, c are the regression coefficients; the other parameters are as mentioned above.

2.2 THE DISTRIBUTION RULES OF PARAMETERS

According to the fatigue destructive model, four parameters (E_c, E_t, h and P) were considered as random variables, the others were considered as constants. The splitting strength of pavement concrete was tested 522 times in order to calculate E_c; the E_t was obtained by 106 plate-bearing tests; the h was tested 382 times by drill pavement method; the P was tested 420 times. Because the parameters vary at different airfields, the relative E_c, E_t, h and P which can be expressed by formula 6 were used for the RCPACP programming.

$$E_c^r = E_c / E_c^d,\ E_t^r = E_t / E_t^d,\ h^r = h / h^d,\ P^r = P / P^d \tag{6}$$

In formula 6, E_c^r, E_t^r, h^r and P^r are respectively relative E_c, relative E_t, relative h and relative P; E_c^d, E_t^d, h^d and P^d are respectively the design values of E_c, E_t, h and P.

The Kolmogorov–Smirnov test was used for distributions rules test of parameters (Keith Ord, 1999), the results were list in Table 1.

Table 1 The distribution rules of parameters

Parameters	E_c^r	E_t^r	h^r	P^r
Distribution Rules	Lognormal	Lognormal	Normal	Normal
μ	1.020	1.033	0.983	1.021
σ	0.095	0.337	0.029	0.103
δ	0.093	0.326	0.029	0.101

In the table, μ is the mean value of the parameters; σ is the standard deviation of the parameters; δ is the coefficient of variability of the parameters.

2.3 THE DESIGN THOUGHT OF RCPACP

The design thought of RCPACP was shown in Figure 1. For calculation precision, the program simulates 10^6 runs. The invalidation probability of pavement is usually between 1% and 10%, so the relative error of the program is between 0.25% and 1%(Zhao Guofan, 2000).

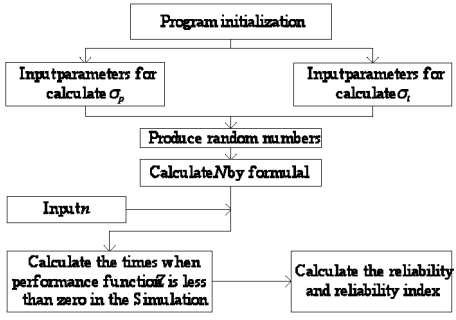

FIG.1 Design thought of RCPACP

3 THE SENSITIVITY ANALYSIS OF PARAMETERS

To study the effect of the parameters' values and variability coefficients on pavement reliability, the parameters' "value sensitivity"(*VS*) and "variability coefficient sensitivity"(*VCS*) were analyzed. The *VS* and *VCS* of E_c, E_t and h were analyzed; however, only the *VCS* of P was analyzed because the airplane for pavement design would not change.

3.1 THE CLASSIFICATION OF PARAMETERS' COEFFICIENT OF VARIATION

With the measurement results in Table 1 and the former studies (LI Le, 2003), the ranges of variability coefficients were listed in Table 2.

Table 2. Ranges of coefficient of variation of parameters

Parameters	Ranges of variability coefficients (%)		
	low	medium	high
E_c	5	10	15
E_t	15	30	45
h	3	5	8
P	5	10	15

3.2 THE QUANTITATIVE ANALYSIS OF *VS*

The design values of a certain parameter were changed and the others were kept unchanged to calculate the reliabilities by the RCPACP in order to study the *VS* of the parameter. The results were shown in Figure 2.

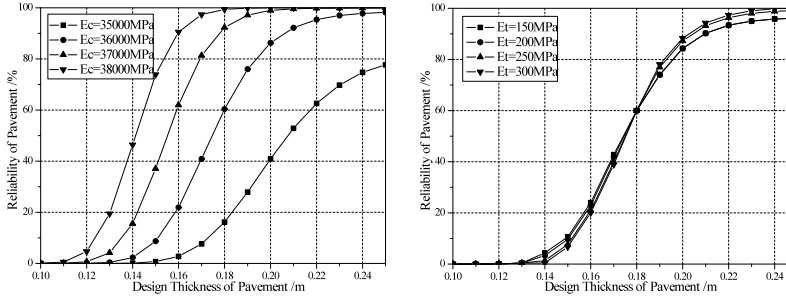

(a) (b)

FIG.2 The *VS* of E_c (a) and E_t (b)

Figure 2 shows several things First, the reliability increases as the design thickness (*h*) increases. When *h* is less than 0.13 m, the reliability increases slowly. When *h* is between 0.13 m and 0.20 m, the reliability increases sharply. When *h* is larger than 0.20 m and the reliability is near objective reliability (usually 95%) (National Standard, 2008), the reliability increases slowly. Second, the figures also show the *VS* of *h* because all the figures are the relationship of reliability and thickness. Finally, the *VS* of E_c is larger than the VS of E_t and the relationship between the *VS* of E_c and the *VS* of *h* is not obvious and need to be further studied (See part 3.4).

3.3 THE QUANTITATIVE ANALYSIS OF *VCS*

The variability coefficient of a certain parameter (choose 'low', 'medium' and 'high' respectively in Table 2) were changed and the others were kept unchanged to calculate the reliabilities by the RCPACP in order to study the *VCS* of the parameter (David W. Pittman, 1996). The results were shown in Figure 3.

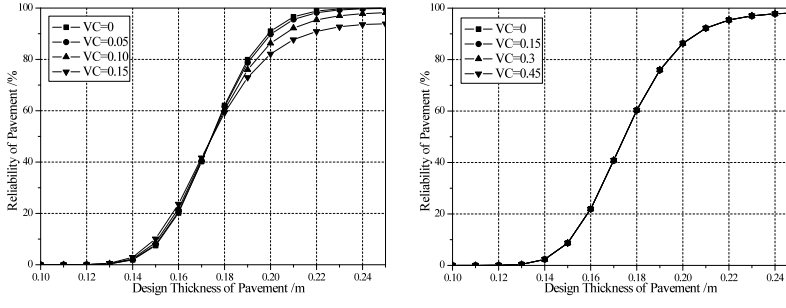

(a) (b)

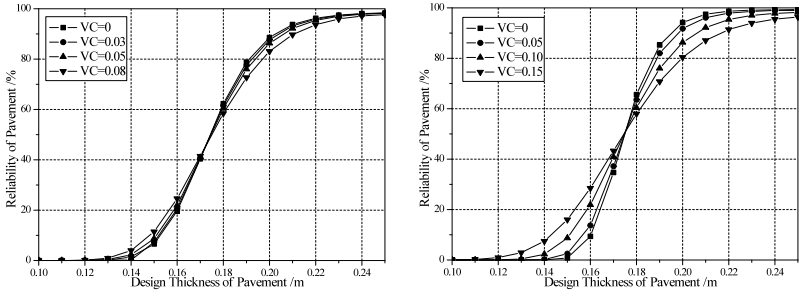

(c) (d)

FIG.3 The *VCS* of E_c (a), E_t (b), h (c) and P(d)

In Figure 3, "VC" expresses variability coefficient.

Figure 3 shows several things. First, when the variability coefficient of a parameter increases, the reliability decreases. Secondl, when h is larger than 0.18 and the reliability is close to objective reliability (usually 95%), the effect of variability of parameters on reliability is obviously. Finally, the *VCS* of P is largest, the *VCS* of h is as much as the *VCS* of E_c and need to be further studied (See part 3.4), the *VCS* of E_t is almost zero.

3.4 THE QUANTITATIVE ANALYSIS OF VS AND VCS OF THE PARAMETERS

The "sensitivity degree" (*SD*) is defined as the difference of the largest reliability and the smallest reliability at a certain design thickness of pavement. See formula 7:

$$SD = R_{\max,h} - R_{\min,h} \tag{7}$$

In the formula: $R_{max,h}$ is the largest reliability when the pavement thickness is h, $R_{min,h}$ is the smallest one. The *SD* of *VS* and *VCS* at different design thickness (0.18m~0.25m) of pavement were listed in Table 3.

Table 3 *SD* of *VS* and *VCS* at different design thickness of pavement

h(m)		0.18	0.19	0.20	0.21	0.22	0.23	0.24	0.25
SD of *VS* (%)	E_c	83.1	71.9	59.1	47.1	37.4	30.2	25.2	22.3
	E_t	3.9	3.9	4.0	4.0	4.1	4.1	4.0	3.8
	h	19.5	15.6	10.3	5.9	3.2	1.6	0.8	0.4
SD of *VCS* (%)	E_c	2.8	6.9	8.9	8.9	8.0	7.0	6.3	6.1
	E_t	<0.1	<0.1	<0.1	<0.1	<0.1	<0.1	<0.1	<0.1
	h	3.9	6.1	5.6	4.0	2.6	1.5	0.9	0.6
	P	7.6	14.6	13.8	10.4	7.3	5.1	3.7	2.9

The figure 4 shows *SD* of *VS* and *SD* of *VCS*.

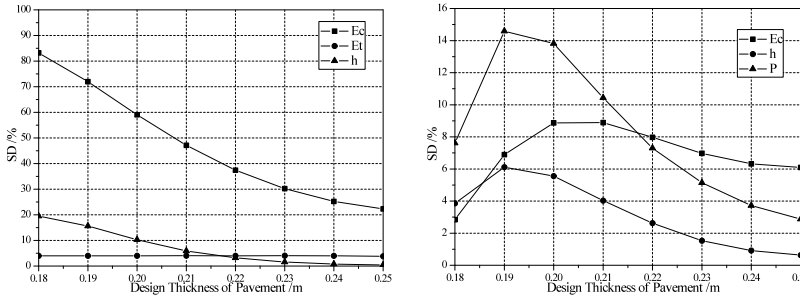

(a) (b)

FIG.4 The *SD* of *VS*(a) *and VCS*(b)

Figure 4 shows that when the reliability is close to objective reliability. The order of *SD* of *VS* is: E_c>E_t>h. The order of *SD* of *VCS* is E_c>P>h>E_t. Because the *SD* of *VCS* of E_t is less than 0.1%, it was not shown in Figure 4(b).

The conclusion is that the *SD* of *h* is smaller because the changes of values and the range of variability coefficient is small.

4 CONCLUSIONS

The RCPACP program was compiled based on the fatigue destructive model of the airfield cement concrete pavement and Monte Carlo Method for calculating the reliability of pavement. The distribution rules and ranges of variability coefficients of four main parameters were given based on a mass data obtained from measurement and test. The qualitative and quantitative analyses of value sensitivity and variability coefficient sensitivity of parameters were done. The conclusions provide referenced basis for the design method based on the reliability theory for the airfields' cement concrete pavement.

ACKNOWLEDGMENTS

The authors appreciate the support of the Doctorate Foundation of the Engineering College, Air Force Engineering University (BC07008).

REFERENCES

David W. Pittman. (1996). "Development of a Reliability-Based Design Procedure

for Rigid and Flexible Airfield Pavements". *U.S. Army Corps of Engineers*.47-66

Keith Ord and Steven Arnold (1999). "Kendall's Advanced Theory of Statistics". 2A. London: *Arnold, a member of the Hodder Headline Group*. pp. 25.37–25.43.

LI Le. (2003). "Study of Reliability Design Method for Military Airfield Cement Concrete Pavement". *Postgraduate Dissertation of Airforce Engineering University*, 19-59 (*in Chineses*)

National Standard.(2008). "Design Specification for Airfield Cement Pavement". 18-19 (*in Chineses*)

Ove Ditlevsen and Henrik O. Madsen(2005). "Structural Reliability Methods." *Wiley Press Inc*. 135-137.

Zhao Guofan, Jin Weiliang and Gong Jinxin.(2000). "Structure Reliability Theory". Beijing: *China Architecture Industry Press*, 79-80 (*in Chineses*)

Initial Behavior of Thin-Bonded Continuously Reinforced Concrete Overlay (CRCO) on Aged Jointed Concrete Pavement.

Sung Woo Ryu[1], Min -Young Park[1], Jung-Hee Nam[2], ZuOg An[3], Jong-Oh Bae[4], Yoon-Ho Cho[5], Seung Woo Lee[6]

[1]Graduate student, Department of Civil and Environmental Engineering, Chung-Ang University
[2]Senior Researcher, Korea Institute of Construction Technology
[3]Professor, Department of Civil Engineering, Kyunghee University
[4]Executive Director, Sam-Woo IMC
[5]Professor, Department of Civil and Environmental Engineering, Chung-Ang University
[6]Professor, Department of Civil and Environmental Engineering, Kangnung National University

ABSTRACT: A thin-bonded CRCO (Continuously Reinforced Concrete Overlay) on a JCO (Jointed Concrete Overlay) was constructed at Seo Hae Ahn Express Highway in Korea. This project includes two experimental sections: 1) a JCO with saw-cut joints over existing transverse joints, and 2) a CRCO, which employs transverse and longitudinal steel reinforcing rods, that is placed on top of an existing JCO. After milling 5 cm off the top of the JCO, an overlay thickness of 10 cm remains. Several VWSGs (Vibrating Wire Strain Gauges) were installed to evaluate curling, delamination behavior, and crack propagation of the thin-bonded CRCO. This paper describes the early behavior of this overlay and compares the current and new rehabilitation methods available in Korea.

INTRODUCTION

The need for the expansion of roads due to the development of Korea's national industry and economy has nearly doubled the road extension projects over the past twenty years. Starting in the 1980s, concrete pavement, which has a relatively longer service life than asphalt pavement, has been preferred for highways and national roads with heavy traffic volumes. However, the number of vehicles on the roadways has increased explosively, along with a significant increase in the volume of heavy load traffic due to increased industrial development. Consequently, it is expected that the service life of road pavements will be shortened and that extensive road repair and maintenance will be needed over the next ten years. Accordingly, appropriate road rehabilitation methods are needed very soon to protect the economy and increase the durability of the roadways.

Various asphalt and concrete overlay methods have been developed for the restoration and rehabilitation of roads to extend the service life of aged concrete pavements. However, problems such as reflection cracking, which is propagated from the damaged area and joint area of the existing concrete pavement sections to the overlay, have been found to decrease the service life and performance of the pavement. Various research studies have been carried out internationally to determine ways to overcome this problem using new forms and material. To further this research direction, this paper reports the research carried out on a thin-bonded overlay that is applicable to continuously reinforced concrete pavements in Korea.

Concrete Overlay Method and Case Study

Concrete overlays are currently used for the structural and functional rehabilitation of aged concrete pavements, and various overlay methods have been used in field construction. Because Korea has few deteriorated concrete pavements, local repair work and maintenance of the slab joint or crack repair of the damaged slab is much more prevalent than an overall overlay of an extensive concrete pavement section. Korea has only two reported cases of the use of overlay.

In the United States, however, extensive research into concrete overlay methods has been undertaken. Concrete overlay construction was initiated and employed extensively between 1913 and 1960, and has continuously increased since that period. In 1970, SFRC began to be used as the primary overlay material. Green County, Iowa used SFRC overlay to extend the service life of its road sections for about ten to fifteen years. In another project on I-80, BCO was used to extend the service life of the pavement. In the 1980s, many studies were conducted to improve the material used for bonding between the existing pavement and the overlay pavement. South Loop IH-610 in Texas was constructed using various materials and interface treatments, and it was found that the bonding between the layers was not a significant problem; the overlay was not seriously affected if the damaged area of the existing pavement was properly treated. Various studies on overlays also were conducted in the 1990s. Virginia employed a "Fast Track" thin-bonded concrete overlay method in order to allow the JCO to open for traffic within 48 hours. The results of a follow-up study after six years revealed that its performance had been satisfactory after all, and the interface problem had occurred within about 0.5 m of the jointed area. Recently, Texas has investigated the applicability of CRCO based on previous research by the State of Mississippi into applying CRCO over a continuously reinforced concrete pavement.

Field Test Construction

The field test construction site is the construction site of the Maesong rest area between the Maesong interchange and the Bibong interchange of the Northbound Seohaean (West Coast) Highway. The existing pavement section is 15 cm of lean concrete with a surface concrete course of 30 cm. The width and length of the slab are 3.8 m and 6.0 m, respectively. An inspection of the pavement condition revealed that although no serious cracking or damage was evident, hairline cracks were observed at the pavement surface.

Demec Gauge Measurements

Demec measurements were taken at 34 joints to measure the width of the spaces between the specimens. These measurements were used to determine the effect of the movement of the existing JCO on the overlay prior to the field pilot construction. The air temperature was also measured at the same time. The results indicate that the seventh joint (i.e., the joint between the seventh and eighth slabs) in the test construction section showed the most evidence of movement. The lowest degree of movement was observed at the ninth joint. Based on this finding, the Demec gauges were installed at the second, seventh, and ninth joints to investigate the changes in joint spacing and movement of the test slabs.

Test Construction

The test construction employed both CRCO and existing JCO. The method used for the CRCO removes the damaged area by milling the existing pavement by 5 cm and then installing reinforcing steel over it to create a 10 cm overlay. The quantity of the reinforcing steel is 0.6% of the pavement section with the 10 cm overlay. The JCO method likewise involves 10 cm of overlay after milling, but the overlay is aligned with the joints such that the depth of the saw cut is about 12 cm, i.e., deeper than the thickness of the overlay.

Although the CRCO method can exclude the effect of the boundary condition at both ends because the number of slabs is larger than the JCO method, only eight slabs were chosen for the test due to the construction costs and other field conditions. JCO sections were constructed on six slabs, and two of these slabs were evaluated for the bond strength between the layers.

First, micro-cracks or damage in the existing aged pavement were removed, and milling was performed to about a 5 cm depth to enhance the bond strength between the new and old concrete pavement. However, the actual depth of the milling was measured at 4.4 cm on average. After milling, the impurities remaining on the road surface were removed by air spraying. VWSGs (vibrating wire strain gauges), to measure the movement by depth, were installed at the selected locations (i.e., the 2nd, 7th, and 9th joints) in accordance with the aforementioned Demec measurements. VWSGs were installed so that the joints in the JCO and CRCO sections would be spaced evenly from the widest joint area to the vertical end in order to measure the interface behavior of the new-old concrete pavement. A non-stress device and a VWSG were installed at the joint where the most movement takes place to measure the strain by temperature change and dry shrinkage.

Deformed reinforcing steel rods of a nominal 19 mm diameter were used for the longitudinal and transverse steel. The quantity and spacing of the transverse steel rods were set at 0.6% of the overlay pavement thickness and 1 @ 29 cm + 15@ 23 cm + 1 @ 29 cm, respectively. The splicing of the steel caused a 50 cm overlap. Also, because problems can occur in the splicing if the rods are aligned in a straight line, they were assembled in an oblique pattern. Transverse steel rods were laid out in about 1 m intervals to affix the location of the longitudinal steel.

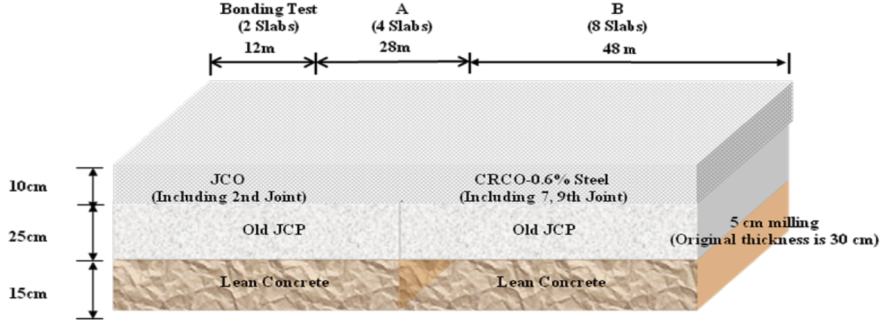

Fig. 1. Plan for the field test construction section

Table 1. Materials used for Field Test Construction

W/C (%)	S/a (%)	Unit material quantity (Kg/m^3)				Admixture (%)	
		W	C (Type 3)	S	G (19mm)	SP	Accelerator
30	45	160	412	766	969	1.5	2

Analysis of Gauge Measurement Results

Coefficient of Thermal Expansion and Dry Shrinkage Change

VWSG data obtained from the non-stress device were analyzed in order to classify the strain of the concrete pavement specimen according to the effects of temperature and dry shrinkage. As the strength began to manifest, the heat expansion coefficient increased gradually, regardless of the computation method. The results from the analyzed data after 43 days of concrete pavement construction, as illustrated in Figure 2 , indicate that the stabilized coefficient of thermal expansion was about 7.142×10^{-6}/℃.

The analysis of the dry shrinkage change by the hour indicates that the dry shrinkage changed in a given day in response to the change of the humidity in the air. The time that exhibited the most dry shrinkage was between 7 PM and 8 PM, and the time between 11 AM and 12 AM restored the dry shrinkage to the minimum.

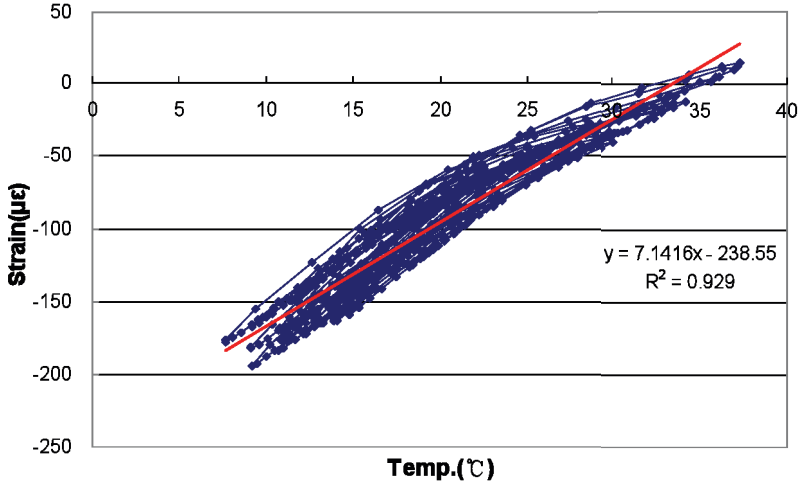

Fig. 2. Heat expansion coefficient after 43 days of concrete pavement construction

Horizontal Movement Behavior Evaluation

The researchers of this study anticipated that reflection cracking would occur at the upper part of the concrete pavement due to the movement of the existing concrete

pavement at the joint areas, and due to the fact that a crack inducer was not inserted in the CRCO. However, contrary to expectations, cracking occurred about 38 cm away from the existing joints at a location where not much movement took place. Thus, the data from the VWSGs, which were installed at locations of significant movement in the existing CRCO and JCO regions, were used for the analysis.

Figure 3 shows the data at about a 1.5 cm depth from the surface during the early stages (days) of construction. Upon examination of the early behavior of the upper part of the concrete pavement, the temperature of the slab in the days immediately following construction was about 20℃, and the temperature fluctuated repeatedly. Using the Demec gauge to measure the movement of the old pavement at the joint, the movement before CRCO application was more than twice the movement at the joint prior to the application of the existing JCO. Nevertheless, the movement in the joint area after the application of the CRCO was only about half of that of the JCO. The reinforcing steels of the CRCO mitigate the expansion of the crack width (joint spaces).

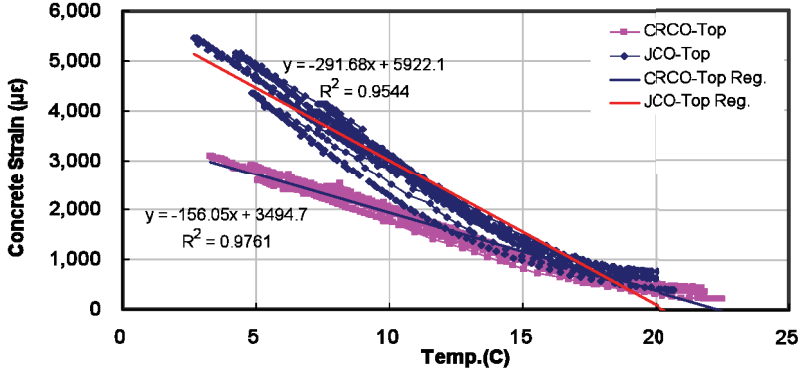

Fig. 3. Comparison of strain data at the upper part of the concrete pavement

Vertical Movement Behavior Evaluation

Of the vertical movement gauges, the gauges at the corners, which were installed to evaluate the bonding behavior of the pavement specimens at the interface of the new-old concrete pavement in response to curling and warping, were damaged by the vibrator of the slip form paver. Thus, only the measurements taken by the vertical gauges installed at about 20 cm and 30 cm from the corners were used for the movement behavior analysis. The results show that both pavement specimens constructed by the aforementioned two engineering methods did not exhibit fracture at the interfaces, and that the strain change by temperature fluctuation was almost the same regardless of the location and methods.

Conclusions

The following conclusions are drawn from the literature review of both Korean and international research into thin-bonded concrete overlay engineering methods that are

applicable to Korean roadways and test pavement construction.

- The CRCO engineering method, which uses transverse reinforcing bars, and the current JCO method were applied to aged concrete pavements on the Seo Hae Ahn Express (West Coast) Highway (I-15).
- The movement of the concrete pavement specimens early in the construction process was analyzed using measurements taken from embedded VWSGs and a non-stress device. The early coefficient of thermal expansion did not stay constant but continued to increase, reaching the level of $7.142 \times 10^{-6}/℃$ about 43 days after construction had begun. Dry shrinkage changes were observed, and fluctuated daily.
- The horizontal movement of the test specimens constructed by the aforementioned two engineering methods, i.e., CRCO and JCO, was analyzed. The movement of the specimens in the joint areas was about three times greater than the movement before the overlay construction. After the application of the CRCO, the strain change was about 50% of the strain change as compared to the JCO method. The vertical movement analysis revealed that the interface of the two layers of the new-old concrete pavement did not detach or fracture and exhibited the same trend regardless of the location and the overlay method.

The researchers are working towards the confirmation of CRCO as the choice of pavement rehabilitation method for aged domestic (Korean) concrete pavements by carrying out follow-up studies and investigations in the future that make up for any shortcomings of the current study.

References

1.Seo Young Chan(1997). “Investigation of Pavement Rehabilitation Method by Concrete Overlay *(3)”*. Korea Highway Corporation, Road Research Center

2. Yoo, S. G. and J. W. Choi(2001. 6). "Special Issue: Concrete Pavement Overlay and Re-pavement] Concrete Overlay for Air Field Pavement." *Journal of Korea Society of Pavement Engineers*, Vol. 3, No. 2: 3-10.

3. Felt, Earl J.(1956). “Resurfacing and Patching Concrete Pavements with Bonded Concrete.” *TRB Proceedings*, Vol. 35, Washington D. C.

4. Delatte, N. J. and J. T. Laird, II.(1998). "Performance of Bonded Concrete Overlays." *TRB*. 1998.

5. Temple, W. H. and S. L. Cumbaa(1985). “Thin Bonded PCC Resurfacing.” Louisiana DOT, Report No. FHQA/LA-85/181. July,.

6. German Claros, Moon Won. “Project Summary, O-4893: Performance of Old Concrete under Thin Overlays.” Texas DOT.

7. Jeong-Hee, Nam(2006). “Measurement and Analysis of Early-Age Concrete Strains and Stresses in Continuously Reinforced Concrete Pavement under Environmental Loading.” Center for Transportation Research, The University of Texas at Austin.

Physical Properties of Rapid-Setting Concrete Using Ultra Fine Fly Ash

Sungil Jeon[1], Jeong-Hee Nam[2], Ji-Hwan An[3], and Soo-Ahn Kwon[4]

[1]Researcher, Korea Institute of Construction Technology, Republic of Korea, jeonsi@kict.re.kr
[2]Senior Researcher, Korea Institute of Construction Technology, Republic of Korea, archnam@kict.re.kr
[3]Researcher, Korea Institute of Construction Technology, Republic of Korea, jenix@kict.re.kr
[4]Researcher Fellow, Korea Institute of Construction Technology, Republic of Korea, sakwon@kict.re.kr

ABSTRACT: Generally, Ultra Fine Fly Ash (UFFA) has the advantage that it advances greater concrete workability and that it activates a greater pozzolanic reaction than common fly ash due to its ultra fine particle size. These properties enhance concrete durability by reducing permeability and increasing resistance to alkali silica reaction (ASR) and sulfate attack, etc. For these reasons, UFFA can be used in rapid setting concrete. The purpose of this study is to develop and evaluate the rapid setting concrete with UFFA as a repair material for early-opening-to-traffic. In previous studies, if only UFFA is added to the rapid setting concrete mixture, the pozzolanic reaction does not happen actively. In this study, the chemical and physical tests were performed for rapid setting concrete with a combination of UFFA and calcium hydroxide. This enabled the activity of pozzolanic reaction to be evaluated as well as the effectiveness of this mixture on enhancing concrete durability was investigated. This study found that adding UFFA decreased the water/cement ratio of concrete and compensated the reduced portion of the early strength of concrete. Additionally, rapid setting concrete with UFFA and calcium hydroxide activated a greater pozzolanic reaction than normal-UFFA concrete. As the calcium hydroxide increased, the electrical indication of the concrete's ability to resist chloride ion penetration was promoted significantly.

INTRODUCTION

Currently, rapid-setting cement, heating-type polyurethane, and polymer concrete are used as repair materials for concrete pavement. However, those materials are frequently damaged due to the heterogeneity of the repair materials with the original materials. For this reason, the necessity of developing repair materials that can enhance the durability of cement is growing. In order to enhance the long-term durability of concrete, pozzolanic materials are widely used at home and abroad. In particular, the use of pozzolanic materials is very important in terms of recycling industrial byproducts.

In addition, reducing the use of cement by using pozzolanic materials is suggested as a way to protect the environment, given that 7% of the CO_2 that is created globally arises from the process of producing cement (Metha, 1998).

In this respect, the trend of recycling fly ash, an industrial byproduct, is on the rise. However, since fly ash leads to a decline in the early strength of concrete, the material is currently not used as a repair material for concrete pavement, which requires early-opening-to-traffic.

Recent studies from home and abroad show that the water-cement ratio can be lowered more when the particle size of fly ash is smaller, suggesting that it may be possible to use fly ash as a material for early-opening -to-traffic.

Moreover, the pozzolanic reaction was not activated much in rapid-setting concrete with fly ash in the previous study, showing that there was no effect in enhancing the long-term durability of concrete (Jeon et al, 2007). The amount of calcium hydroxide, which is created in the process of hydration reaction, was small since little, if any, C_3S and C_2S were contained in the rapid-setting cement.

Thus, this study was performed to see whether the pozzolanic reaction occurs when calcium hydroxide is added to rapid setting cement and Ultra Fine Fly Ash (UFFA), and to analyze which effect is brought onto the physical properties of cement.

LITERATURE REVIEW

Fly ash is coal ash produced in a combustion boiler such as a thermal power plant. The term refers to a material of a particular particle size that is retrieved from waste gas by a precipitator, and it is one of the admixtures that represent the pozzolan type (KCI, 1992). Fly ash contains a smaller amount of CaO compared with slag, and fly ash is abundant with SiO_2 and Al_2O_3. Fly ash itself has no hydration. However, the soluble components such as SiO_2 and Al_2O_3 contained in the fly ash slowly react under normal temperatures with $Ca(OH)_2$, which is created when C_3S and C_2S (the cement components) hydrate, and produce Calcium Silicate Hydrates (C-S-H) or Calcium Aluminate Hydrates (C-A-H) that are insoluble and stable. This is called the pozzolanic reaction.

In general, fly ash has great effects on improving durability of concrete as it has such positive effects in: the improvement of workability, the reduction of water content, the decrease of bleeding, the enhancement of long-term strength, the restraint of alkali-aggregate reaction, the improvement of permeability resistance, the reduction of the heat of hydration, and the enhancement of resistance to sulfate attach.

Of the recent studies performed overseas, the list below includes those that detail the effects made according to the degree of fineness of the fly ash, and on the permeability resistance of fly ash concrete.

Haque and Kayali (1998) reported that the workability of concrete can be enhanced when a particle size of fly ash is below 45㎛.

Li Yijin et al (2004) reported that the smaller the particle size, the less the water requirement, and that UFFA remarkably improves the workability of concrete remarkably.

Slanicka (1991) and Liu et al (2000) reported that the smaller the particle size, the greater the strength of concrete.

Davis (1954) reported that concrete with the ASTM Class F(low-lime) fly ash had larger permeability until 28th day compared with normal concrete. However, the concrete had lower permeability after 6 months.

Malhortra (1989) carried out the chloride ion permeability test on concrete to which 54%~58% of fly ash is replaced. According to the test results, the chloride ion permeability of the fly ash concrete was 197~973 coulombs at day 91, suggesting that the permeability was very low to the point that it could be ignored.

Armaghani et al (1991) reported that the permeability of concrete, to which 10%~50% of fly ash is added at day 91, dropped by 50% compared with normal concrete.

Obla et al (2000) reported that concrete with over 8% of UFFA at day 28 reduced the chloride ion permeability rate and chloride diffusivity by more than 50% compared with normal concrete.

EXPERIMENTAL TEST SCHEME

Outline

In this study, the mixture was made by applying 0%~15% of UFFA and 0~15% of calcium hydroxide in order to analyze the physical properties of UFFA rapid-setting concrete based on the changes in the amount of calcium hydroxide.

For each concrete mixture, the slump, air content, compressive strength, and chloride ion permeability resistance were tested. An X-ray diffraction analysis was also performed on the hardened cement paste at various ages to determine some variables.

UFFA and Cement

Figure 1 indicates the particles of UFFA photographed by the SEM equipment. Table 1 shows the properties of chemical components of UFFA and cement. The UFFA used in this study met the requirement of a class F fly ash per ASTM C 618, and the typical mean particle diameter was 3㎛. The cement used in this study is the hauyne type rapid-setting cement made by the company "S."

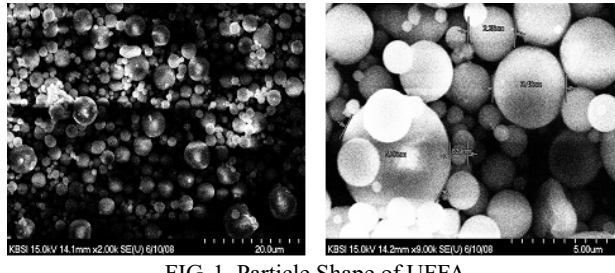

FIG. 1. Particle Shape of UFFA

Table 1. Chemical Components of UFFA and Cement

Type	Chemical Composition (%)						Fineness		Specific Gravity (g/cm^3)	Loss on Ignition (%)
	SiO_2	Al_2O_3	Fe_2O_3	CaO	MgO	SO_3	Blain Method (cm2/g)	Sieve Method (%)		
UFFA	54.2	23.7	4.85	8.51	1.97	1.19	6,710	0.34	2.49	1.76
Rapid-Setting Cement	23.5	16.8	1.7	50.7	1.8	6.7	5,627	-	2.91	-

Aggregate

The fine aggregate used in this study is a wash aggregate in which sea sand from Haeju of North Korea and sea sand from the Uechung Island of South Korea are mixed, and crushed rock of 19mm was used as a coarse aggregate. Figure 2 shows the gradation of fine aggregate and coarse aggregate.

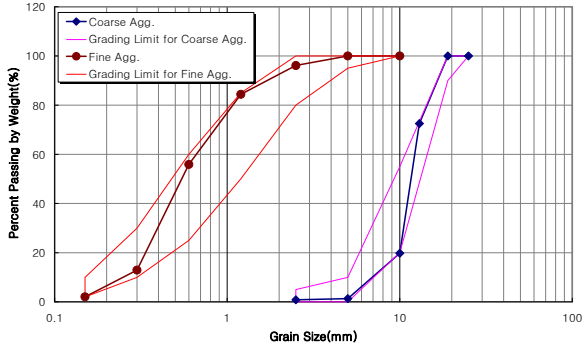

FIG. 2. Gradation of Fine and Coarse Aggregate

Test Method

- X-Ray Diffraction Analysis (XRD)

Hardened cement paste was pulverized to be made thin, and measured with the velocity of 4°/min within 5°~85° using the diffraction analyzer. The X-ray diffraction analysis was performed on the day 1, day 7 and day 28. The X'Pert MPD from Philips was used for the X-ray diffraction analysis.

- Slump Test / Air Content Test

As for the slump test which is one of the measurement methods for fluidity of fresh cement, a sample was taken in accordance with KS F 2401 (a method for taking samples of fresh cement), and the test was carried out according to KS F 2402 (a slump test method of concrete).

The air content test, which affects the compressive strength and durability of cement, was performed using the Washington Type Concrete Air Meter based on KS F 2421 (air content test method based on the pressure method of fresh concrete).

The air content test was made two times for each mixture in order to have better accuracy, and two average values were used to get the results.

- Compressive Strength Test

A specimen was made as stipulated in the standard-size specimen [KS F 2403 (a method used at a lab for manufacturing and curing specimen used in testing compression, flexural and splitting tensile strength)], and the compressive strength test was performed in accordance with KS F 2405 (test method for concrete compressive strength test) at 3 hours, 7 days and 28 days.

The average compressive strength was calculated using three samples for each variable using an Instron 8150 for the compressive strength test.

- Rapid Chloride Penetration Resistance Test

The rapid chloride penetration resistance test was carried out at day 7 and day 28 based on KS F 2711, and the average charge passed was calculated using two samples for each variable. The rapid chloride penetration resistance test makes it possible to figure out the penetration resistance of concrete in a relatively short period of time compared with the general permeability test.

Mixture Ratio

As for the mixture ratio of hardened cement paste, the W/B(C+F) was fixed to 0.35, UFFA of 0~15% (against the whole weight) was applied, and calcium hydroxide and high-range water reducer were fixed to 10% (against the weight of UFFA) and 0.5% (against the binder weight) respectively.

Table 2. Mixture Proportions

Name	UFFA replacement ratio (%)	$CaOH_2$ replacement ratio (%)	G_{max} (mm)	W/C (%)	S/a (%)	Unit Weight (kg/cm^3)						HRWR (%)	AE (%)	Retarder (%)
						W	Binder			S	G			
							C	UFFA	$Ca(OH)_2$					
U0C0	-			46		180	390	-	-	837	841		4	
U10C0	10			43		168	351	39	-	849	854			
U10C5	10	5		43		168	351	39	1.9	848	853			
U10C10	10	10		43		168	351	39	3.9	847	852			
U10C15	10	15	19	43	50	168	351	39	5.8	846	850	0.5	6	0.3 ~ 0.5
U15C0	15	-		42		164	331	58		853	858			
U15C5	15	5		42		164	331	58	2.9	851	856			
U15C10	15	10		42		164	331	58	5.8	849	854			
U15C15	15	15		42		164	331	58	8.8	848	853			

Table 2 shows the mixture proportions. In the table, the replacement ratio of UFFA refers to the percentage of the cement weight, and the replacement ratio of calcium hydroxide means the percentage of the weight of UFFA. Incremental volume based on

the weight differences is set by adjusting the amount of fine aggregate and coarse aggregate. The mixture table was made to have the same workability via a basic preliminary test. The mixture ratio was adjusted to W/C 46%, 43%, 42% for the replacement ratio of UFFA 0%, 10%, 15%, respectively. Under this process, the workability of mixtures was improved when UFFA was added, resulting in the decreased W/C.

In addition, an air-entrainer (against the weight of water-reducing agent) and a retarding agent (against the weight of binder) were added in the mixture ratio in order to secure the air content and work time.

EXPERIMENTAL RESULT & ANALYSIS

Results of X-Ray Diffraction Analysis

Figures 3 through 7 indicate the results of the X-ray diffraction analysis. In the case of U0C0 mixture, the diffraction peak of calcium hydroxide based on ages is consistent, and the diffraction peak show very little increase at day 28. In the event of U10C0 and U15C0, the diffraction peak of calcium hydroxide is shown to have a very small decrease as days passed. However, the intensity of the diffraction peak is low in general. This means that the amount of calcium hydroxide created through the hydration reaction is small as the amount of C_3S and C_2S is small in rapid setting cement. This leads to the reduced activity of pozzolanic reaction.

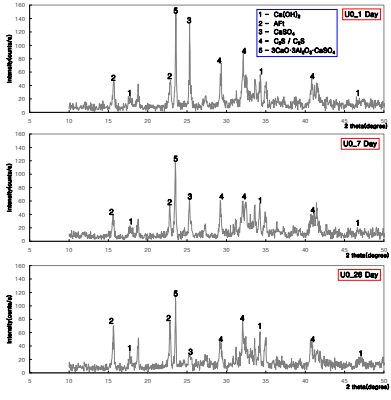

FIG. 3. XRD Pattern of U0C0 Mixture

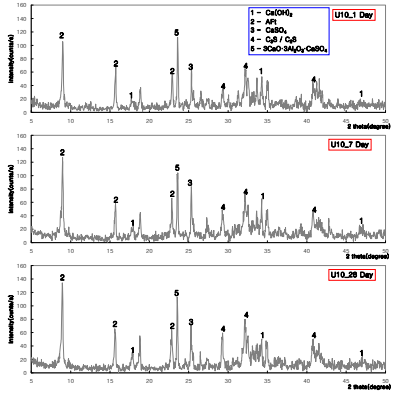

FIG. 4. XRD Pattern of U10C0 Mixture

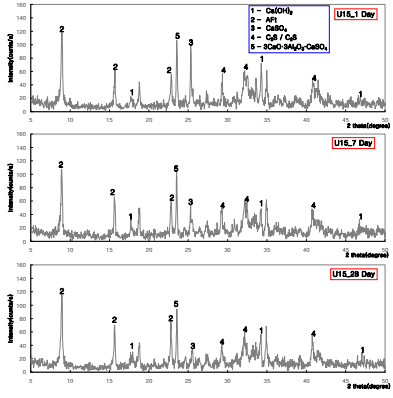

FIG. 5. XRD Pattern of U15C0 Mixture

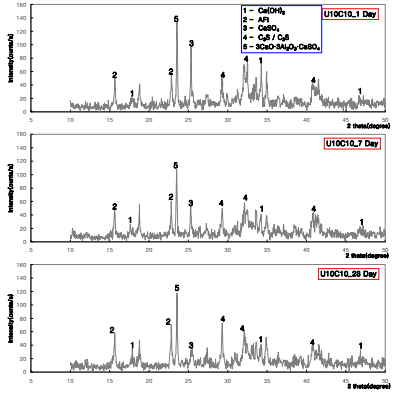

FIG. 6. XRD Pattern of U10C10 Mixture

On the other hand, the intensity of the diffraction peak for the mixture of U10C10 and U15C10, to which calcium hydroxide is added, is relatively higher, and the diffraction peak of calcium hydroxide decreased as the days passed. This resulted from the fact that the amount of calcium hydroxide decreased with the pozzolanic reaction which occurred after the first day. However, the overall intensity of the diffraction peak is not high since the amount of calcium hydroxide is small with the small amount of C_3S and C_2S in rapid setting cement, and the fly ash and calcium hydroxide are in limited quantities. Along with this, the reduction degree of the diffraction peak is also not high.

In addition, the diffraction peak of ettringite was very high at day 1, and it showed a small increase at day 28. This results from the creation of ettringite, which occurs as hauyne type ingredients ($3CaO.3Al_2O_3.CaSO_4$) in the rapid setting concrete react with water, which happens mostly in the early days.

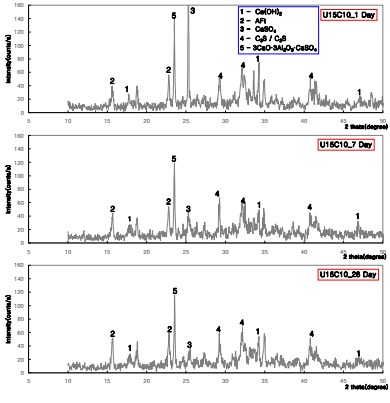

FIG. 7. XRD Pattern of U15C10 Mixture

Result of Slump Test / Air Content Test

The results of the slump test based on the UFFA replacement ratio are shown in the Figure 8. The slump loss with time in accordance with changes in the addition of calcium hydroxide is omitted from the graphs since there is no difference. Generally, if the water-cement ratio is the same, the workability of cement is improved with the addition of fly ash. Thus, the time of slump value '0' increases as the initial slump gets bigger and the setting is also delayed. However, the mixture ratio was adjusted to have the same workability through the preliminary test, and the slump loss with time has the same figure regardless of UFFA replacement ratios as indicated by the graph.

The result of the air content test based on the UFFA replacement ratio is shown in the Figure 9. The air content in accordance with changes in the addition of calcium hydroxide is omitted since again there is no difference. In order to have the consistent air content, a different amount of air-entrainer was used for each replacement ratio of UFFA. As a result, the differences in the air content for each mixture are small as shown (Fig. 9). 4% of air-entrainer was added to concrete without UFFA, and 6% of air-entrainer was added to concrete with UFFA.

In the case that the same air-entrainer is added, the air content of the concrete mixture is reduced when the amount of fly ash increases. This is because the concentration of air-entrainer in the cement paste decreases as the air-entrainer is absorbed into the uncombusted carbon of fly ash.

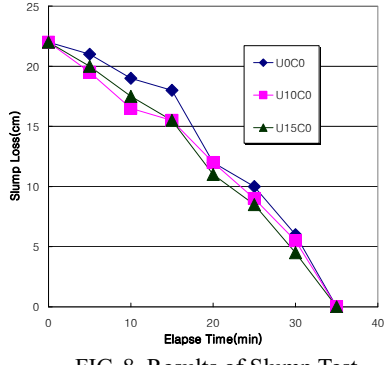

FIG. 8. Results of Slump Test

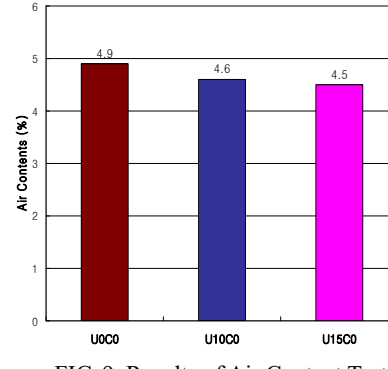

FIG. 9. Results of Air Content Test

Results of Compressive Strength Test

Figures 10 and 11 show the results of the compressive strength test on concrete mixtures for each day based on the mixture temperatures. As shown in the figures, the compressive strengths have a difference of around 10 MPa depending on the mixture temperatures. The reason for this difference is that the early heating temperature of rapid-setting concrete has a great effect on its strength. In particular, the decline in strength is shown in a greater manner as the addition of UFFA increases when the mixture is performed under low temperature.

In the case that the water-cement ratio is the same, the early strength weakened as the addition of UFFA increases. In this study, however, the W/C was lowered as the addition of UFFA increased, resulting in small differences in compressive strengths of all mixtures at 3 hours. In particular, all mixtures turned out to pass the reference strength of 21 MPa as required for traffic-opening, suggesting that they can be fully utilized as repair materials for the early-opening-to-traffic.

In addition, there is no significant difference in the compressive strength between the UFFA concrete with calcium hydroxide and the UFFA concrete without calcium hydroxide at 3 hour. At day 7 and day 28, the compressive strengths between the two mixtures also have no significant difference. Though some test results show that the compressive strength increased as the addition amount was increased, the difference was so small to the point that the results could be ignored. The results have been produced with the values measured until day 28. Thus, it is believed that additional long-term age analyses are required.

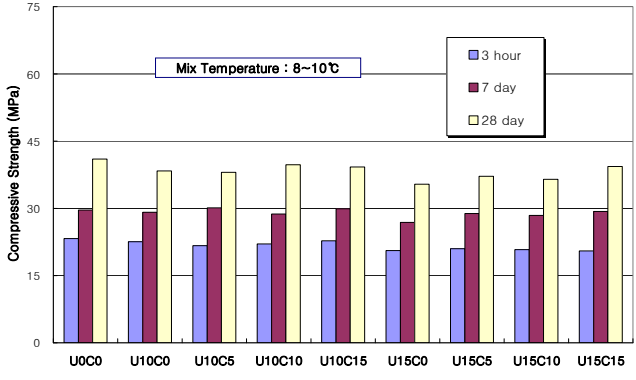

FIG. 10. Results of Compressive Strength Test (1)

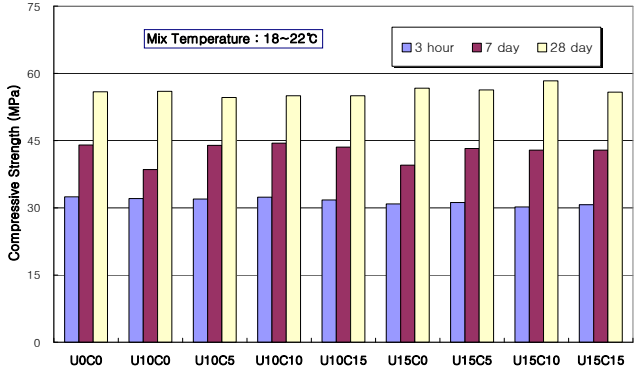

FIG. 11. Results of Compressive Strength Test (2)

Results of Chloride Ion Penetration Resistance Test

Figures 12 and 13 show the results of the chloride ion penetration resistance test for concrete mixtures at various ages based on mixture temperatures. As shown in the figures, the charges passed of concrete mixtures according to the mixture temperatures have no significant difference.

In addition, the passed charge of UFFA rapid-setting concrete without calcium hydroxide at day 28 does not show a big difference compared with the passed charge of normal rapid-setting concrete. This means that a small amount of calcium hydroxide is created in the first hydration reaction because the rapid setting cement contains a smaller amount of C_3S and C_2S compared with the general Portland cement. This causes the second pozzolanic reaction of SiO_2, and Al_2O_3 in fly ash and calcium hydroxide to be less activated than the general Portland cement.

However, when calcium hydroxide was added to UFFA rapid-setting concrete at day 28, the charge passed was around 500~1,000 coulombs. Thus, the charge passed was evaluated as 'very low' in accordance with KS F 2711, and the charge passed was shown to be reduced generally when the addition of calcium hydroxide was increased, suggesting that the permeability resistance was enhanced. This means that the Pozzolanic reaction of UFFA rapid-setting concrete was activated greatly with the addition of calcium hydroxide.

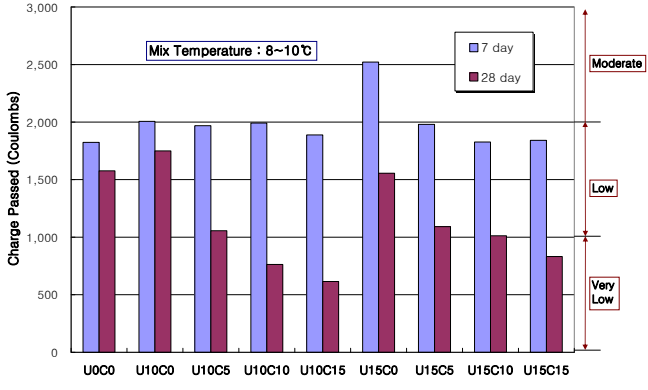

FIG. 12. Result of Rapid Chloride Penetration Resistance Test (1)

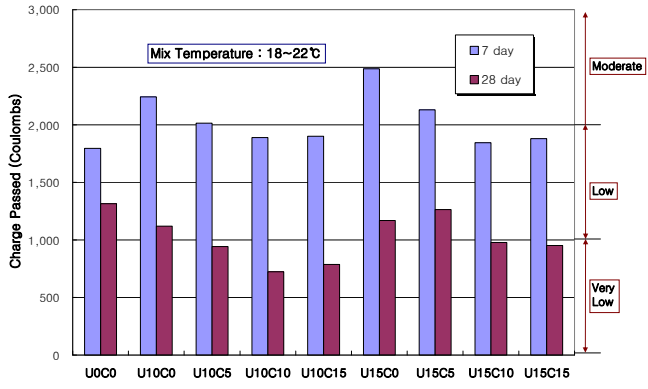

FIG. 13. Result of Rapid Chloride Penetration Resistance Test (2)

CONCLUSION

In this study, the physical properties of UFFA rapid-setting concrete have been analyzed based on the changes in the amount of calcium hydroxide. The following conclusions have been drawn:

1. In the case that UFFA is added to rapid-setting cement, the early reduction of concrete strength could be mitigated as the W/C ratio could be highly reduced. In particular, the UFFA rapid-setting concrete has turned to fully satisfy the strength of over 21MPa, which is the standard strength required for the early-opening-to-traffic.
2. As is shown in the X-Ray Diffraction Analysis and the results of the Chloride Ion Penetration Resistance test, the pozzolanic reaction of UFFA rapid-setting concrete with calcium hydroxide is activated more than that of UFFA rapid-setting cement without calcium hydroxide.
3. It was confirmed that the permeability resistance of UFFA rapid-setting concrete enhanced as a whole as the addition of calcium hydroxide was increased.
4. A study on the physical properties of UFFA rapid-setting concrete based on longer periods of time and on the calculation of proper amounts of calcium hydroxide is scheduled to be performed.

ACKNOWLEDGEMENTS

This work was part of the project “Development of Long-Lasting and Environmental-Friendly Materials and Design-Build Technologies for the Pavement” supported by Korea MLTM. Their financial support is gratefully acknowledged.

REFERENCE

KCI (1992), “Recent Concrete Engineering”, pp 150

Jeon et al (2007), “Strength and Permeability Property of Fast-Setting Concrete Using Ultra Fine Fly Ash”, Proceedings of KSRE Conference 2007, pp 413~416

Armaghani, J. M., Romano, D. C., and Larsen, T. J. (1991), "Strength and Durability of Concrete in Florida", Proc., 2nd CANMET/ACI Int. Conf. on Durability of Concrete: Supplementary Papers, Am. Concrete Inst., Detroit, Mich., 723-748

Davis, R. E. (1954), "Pozolanic Materials with Special Reference to Their Use in Concrete Pipe", Tech, Memo, Am. Concrete Pipe Assoc., Vienna, Va.

Federal Highway Administration (2003), "Full-Depth Repairs", U.S Department of Transportation, Washington, D.C. www.fhwa.dot.gov/pave ment/full.htm

Haque, M. n., and Kayali, O. (1998), "Properties of High-Strength Concrete Using a Fine Fly Ash", Cem. Concr. Res., 28(10), 1445-1452

Haque, M. n., and Kayali, O. (1992), "Fly Ash Reduces Harmful Choride ions in Concrete", ACI Mater: J., 89(3), 238-241

Horn, M. W., Stewart, C. F., and Boulware, R. L.(1972), "Factors Affecting the Durability of Concrete Bridge Decks : Normal vs Thickened Deck-Interim Report No. 3.", Bridge Department, California Division of Highways, CA-HY-4101-37211.

Karthik, Obla (2000), "Durability of Concrete Containing Fine Pozzolan", International HPC Symposium in Orlando, Florida

Li Yijin et al. (2004), "The Effect of Fly Ash on the Fludity of Cement Paste, Mortar, and Concrete", International Workshop on Sustainable Development and Concrete Technology

Liu, B., Xie, Y., Zhou, S., and Yuan, Q., and Aitcin, P. C. (2002). "Influence of ultrafine fly ash composite on the fluidity and compressive strength of concrete", Cem. Concr. Res., 30(9), 1489-1493.

Mehta, P. K. (1998), "In cement, Fly Ash Emerges as a Cure to Limit Greenhouse Gases", ENR, pp13.

Malhortra, V. M. (1989), "Durability of Concrete Incorporating High-Volumes of Low-Calcium(ASTM Class F) Fly Ash", Proc., 2ndInt. Seminar on Some Aspects of Admixtures and Industrial By-Products on the Durability of Concrete, Gothenburg, Sweden, 1-15.

Karthik Obla et al. (2000), "Durability of Concrete Contatining Fine Pozzolan", International HPC Symposium in Orlando, Florida.

Slanicka, S. (1991). "Influence of fly ash fineness on the strength of concrete", Cem. Concr. Res., 21(4), 285-296.

Repair of Longitudinal Joints and Cracks

Dar Hao Chen[1], Taylor Crawford[2], David W. Fowler[2], James Jirsa[2],
Megan Stringer[2], David Whitney[2], and Moon Won[3]

[1]School of Communication and Transportation Engineering, Changsha University of Science and Technology, Chiling Road 45#, Changsha, Hunan, China, 410076.
Dchen@dot.state.tx.us
[2]University of Texas at Austin
[3]Texas Tech University

ABSTRACT: Longitudinal cracking and longitudinal joint separations are commonly observed distresses in concrete pavements. The Texas Department of Transportation instituted a research project to determine the causes and to recommend repair methods. Repair methods that are generally recommended to repair cracks and joints are (1) cross stitching; (2) slot stitching; and (3) stapling. Finite element modeling was performed to determine the stress distribution in the concrete for each method when a truck tire load was placed on one side of the joint. Assuming no interlock between joint faces, the slot stitching model produced the lowest stress and cross stitching produced the highest stress, when the load was placed on the upper end of the diagonal bar. Cross stitching is recommended for repairing narrow cracks and slot stitching is recommended for wider cracks and joints.

INTRODUCTION

The Texas Department of Transportation (TxDOT) has observed longitudinal cracking and longitudinal joint separations on its concrete pavements statewide since the 1970s. This uncontrolled cracking and joint separation at the longitudinal construction joint has often led to further structural deterioration of the pavement. Additional cracking, spalling, and slab faulting has often occurred as well as corrosion of the steel reinforcement and the erosion and pumping of the base layer due to moisture penetration through the cracks and joints. These problems typically reduce the ride quality of the pavement and in severe cases can present safety hazards to motorists. TxDOT has typically used slot-stitching, cross-stitching, and routing and sealing for the repairs, but no research had been done to determine the effectiveness of these repairs. This paper addresses finite element model analysis of repair procedures for the existing distressed pavements. Considerable field work was performed to investigate the types of repairs previously made in Texas; however, due to space limitations only the analytical studies will be presented.

Description of Repair Methods

Three primary repair methods are considered in this paper: (1) cross stitching, (2)

slot stitching, and (3) stapling. Other concrete pavement restoration (CPR) techniques exist, such as full depth repair (FDR), but are generally more expensive and intrusive into the pavement. The focus of this paper is on less expensive alternative methods. Each of these is described below.

Cross Stitching

Cross stitching is the most common and easily installed repair method considered in this paper. TxDOT has implemented this method on several sections of concrete pavement for longitudinal crack and longitudinal joint repair.

Alternating diagonal holes are drilled into the pavement using an impact drill, with the angle of drilling and distance from the hole to the crack or joint varying by job. Holes are typically cleaned out with compressed air and partially filled with epoxy using a pneumatic injection gun. Three-quarter-inch-diameter (#6) deformed bars are then inserted into the holes. Bars are typically spaced 12 to 24 in. apart along the length of the crack or joint (Figures 1 and 2). Cross stitching is generally recommended for repairing cracks with relatively narrow widths, where interfacial interlock can assist in load transfer.

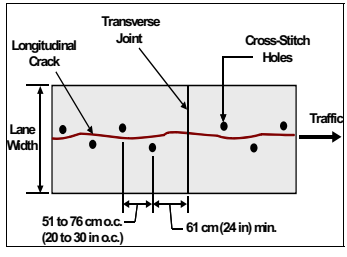

FIG. 1. Plan View of Cross Stitching Layout

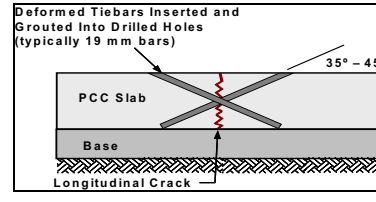

FIG. 2. Elevation View of Cross Stitching

Slot Stitching

Slot stitching is similar to the dowel bar retrofit technique commonly used to restore load transfer across transverse joints. In slot stitching, slots are saw-cut perpendicular to the joint or crack and chiseled out with a jackhammer to produce a rectangular cavity with a depth approximately equal to one half the thickness of the pavement slab. Deformed bars are then inserted into the slot and the slots are filled with repair material, (typically a rigid, fast-setting portland cement-based material). Slot stitching provides both load transfer and horizontal anchorage because deformed bars are installed. The goal of slot stitching is to restore the pavement to a pre-distress condition; stitch bar size, spacing, and location within the slab are selected to match the original tie bar design. The American Concrete Paving Association (ACPA) gives recommended design details for slot stitching, which are shown in Figure 3. Bars are placed approximately mid-depth in the slab and are at least 1 in. in diameter. This method is recommended for wider cracks and for joints, where no other load transfer mechanism remains.

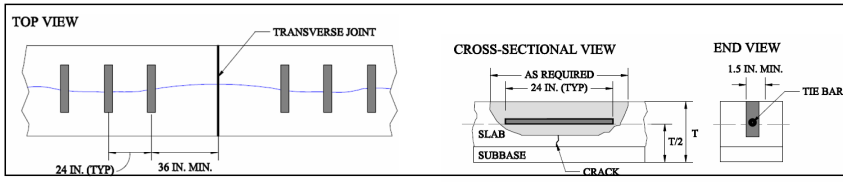

FIG. 3. Slot Stitching Details

Stapling

Staple slots consist of horizontal slots cut by sawing (much the same technique as described for slot stitching) and vertical holes drilled at the ends of the slots. U-shaped bars ("staples") are inserted into the slots, and the legs anchored into the vertical holes with high-modulus epoxy. The slots and the joint itself are then filled with a low-modulus elastomeric concrete. High-modulus material is used for the staple legs to provide positive mechanical anchorage, and low-modulus material is used in the slots and the joint to allow the pavement to flex without cracking and spalling the repair material, and to prevent "locking up" the joint so that cracks form elsewhere in the slabs. Bars are typically 1 in. diameter and are spaced 36 in. on center (Figures 4 and 5). The stapling repair method was developed to provide positive mechanical anchorage between the separated slabs, where load transfer is still provided by good base support.

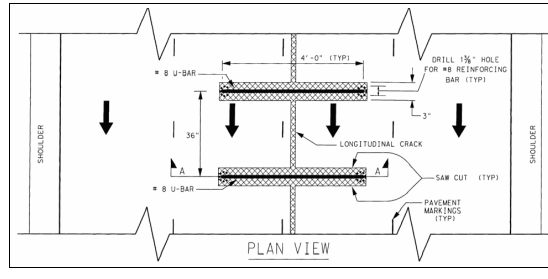

FIG. 4. Plan View of Stapling Repair

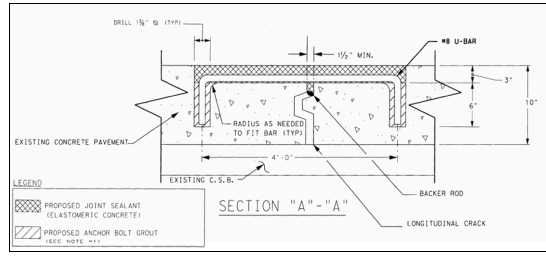

FIG. 5. Elevation View of Stapling Repair

Finite Element Modeling

Analytical finite element modeling (FEM) was conducted by Dr. Seongcheol Choi of the Center for Transportation Research (CTR) under the supervision of Dr. Moon Won to determine the elastic distribution of stress in concrete for three repair methods: (1) cross stitching, (2) slot stitching, and (3) stapling. For the finite element modeling the loading condition was limited to the most severe condition a repair might experience in the field. Each repair model was subjected to shear-type loading by a truck wheel next to the joint. The maximum principle tensile stress in the concrete was calculated for each model. The FEM software used was DIANA.

The following assumptions were inherent to the FEM analysis: 2-D elastic analysis (assumed a unit depth in the direction of traffic), 12-ft.-wide slabs with 0.5 in. longitudinal joint separation, no aggregate interlock across the joint, wheel loading only (no environmental effects), load: 9-k single wheel at edge of joint; 90-psi tire pressure, concrete pavement: 12 in. thick, modulus of elasticity = 5 x 10^6 psi, Poisson's ratio = 0.15, steel areas were taken from TxDOT specifications and adjusted to account for different bar spacing for each method in order to obtain the same bar area per unit length of repair (0.33 sq. in. per ft. of joint), steel reinforcement: modulus of elasticity = 29 x 10^6 psi, Poisson's ratio = 0.3, uniform subgrade support (no voids underneath the slabs), and subgrade reaction modulus = 200 psi/in.

The demand on the repair methods under the assumed loading condition is dominated by shear, although some flexural demand is present due to the gap between the slabs.

Results

Cross Stitch

Since cross stitch bars are oriented in an alternating fashion in the field two models were created: one in which the load is applied on the same slab in which the cross stitch bar is inserted (Case "R") and one in which the load is applied on the slab opposite the inserted bar (Case "L").

Cross stitching Case "L" gave a maximum principle tensile stress in the concrete of 300 psi (Figure 6). Cross stitching Case "R" yielded a maximum principle stress in the concrete of approximately 140 psi (Figure 7).

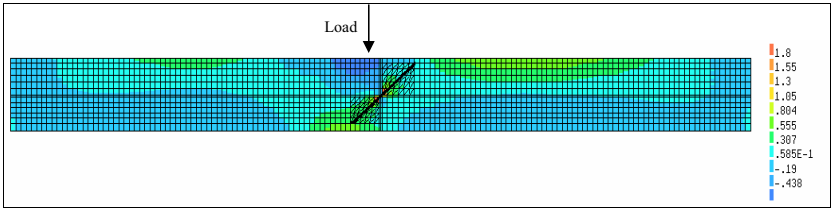

FIG. 6. Stress Contours for Cross Stitching Model (Case "L")

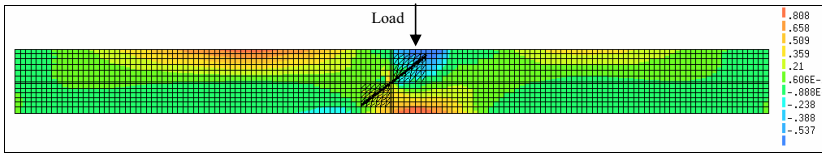

FIG. 7. Stress Contours for Cross Stitching Model (Case "R")

Slot Stitch

Slot stitching gave a maximum stress of approximately 130 psi (Figure 8).

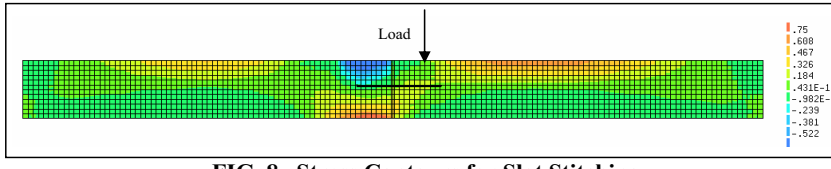

FIG. 8. Stress Contours for Slot Stitching

Staple

Stapling showed a maximum *s*tress of approximately 150 psi (Figure 9).

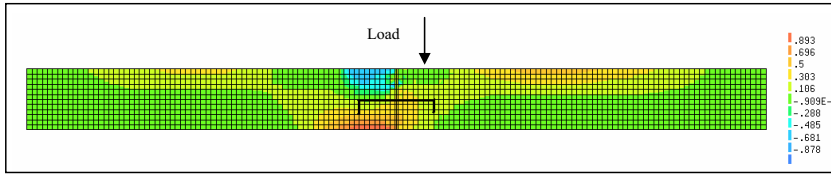

FIG. 9. Stress Contours for Stapling

Analysis of Results

In Figure 10, the results from the modeling are summarized. Since both load cases for cross stitching are present in the field, the worst case governs. As a truck wheel rolls along a joint that is cross stitched, the load will be transferred across the joint by several bars (the proportion of load sharing between the alternating stitch bars is an indeterminate structural analysis problem and is outside the scope of this study). Case "L" stress can be thought of as an upper bound solution, and Case "R" as a lower bound solution. The worst condition would be a wheel directly over a bar that Case "L" simulates, in which case the stress in the concrete would approach the 300 psi level. The least demanding condition would be when the wheel is directly over a bar of opposite orientation (Case "R"). Stress would approach the lower bound value of 140 psi in that case. Since the cross stitching is being evaluated from a global rather than local basis, the upper bound stress of 300 psi was used for comparison with other repair methods. Cross stitching showed the highest stress, followed by stapling. Slot stitching showed the lowest stress of the three repair methods. It should be noted, however, that the model did not consider aggregate interlock for narrow cracks for which cross stitching has been found to work well in the field.

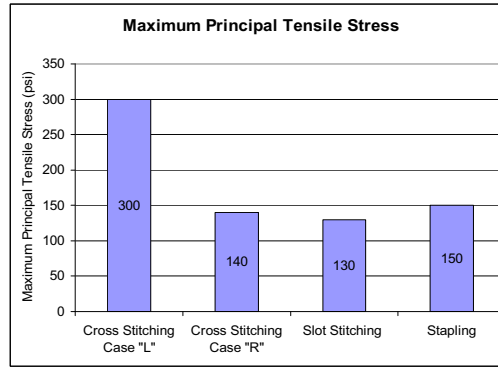

FIG. 10. Maximum Stress Values for Each Repair

The stress value for slot stitching (as opposed to the other two methods) is likely the most accurate reflection of what the repair would experience in the field. Repair materials used to fill the slots are typically rigid grouts, often portland cement-based, and have similar properties to concrete. Stapling, on the other hand, typically has a low-modulus elastomeric concrete in the slots. This difference would need to be accounted for when predicting ultimate failure loads of the repair. Because of this difference in repair materials, stapling would likely fail at a lower load than predicted by the FEM results, because the model assumed the slots to be filled with concrete. Results indicate that for the shear-type loading simulated in the analysis, slot stitching likely would perform best in the field. Cross stitching would likely perform worst.

CONCLUSIONS

Separated joints and cracks should be repaired as soon as possible, and before wide separations occur. Wide joints translate into high concrete stresses, high bending stresses in the repair bars, and lower stiffness (load transfer efficiency). From the FEM results, slot stitching had the smallest maximum principal tensile stress of the three methods tested and cross stitching had the highest stress when the wheel load was placed on the side with the diagonal bar nearest the surface. Cross stitching is recommended for repairing narrow cracks and slot stitching is recommended for wider cracks and joints.

REFERENCES

American Concrete Pavement Association (ACPA) (2001) Stitching Concrete Pavement Cracks and Joints. Special Report SR903P. American Concrete Pavement Association: Skokie, IL.

Analysis on Criterion for Void Identifying under Cement Concrete Pavement Corner

Sheng Zeng[1], Jia Xu[2], Xiaojun Zeng[2]

[1]Professor, School of Traffic and Transportation Engineering, Changsha University of Science & Technology, Hunan Changsha, 410076, P. R. China; (86) 731-2309339; zszs35@sohu.com
[2]Graduate Student, School of Traffic and Transportation Engineering, Changsha University of Science & Technology, Hunan Changsha, 410076, P. R. China; (86) 731-2309339; jilinxujia@sina.com

ABSTRACT: Based on deflections from theoretical analysis and falling weight deflectometer (FWD) at the slab center and corner, a method was established for the estimation of void size at the slab corner. Also, by modifying joint load-transfer capacity based on the theoretical slab corner deflection in infinite site slab under even supporting conditions, the theoretical slab corner deflection was calculated, and compared with FWD testing data to estimate the void conditions beneath the slab corner. A concept of void index was developed, which is defined as the ratio of deflections of testing in slab corner under FWD load against theoretical deflections. Through analyzing the relations between void index and other factors such as void size, slab modulus, slab thickness and foundation reaction modulus, the regression formula between void index and void size was established for the estimation of void size. The results of void identification using the method proposed in this study with the data from the test section at the Hunan Leiyi Expressway compare reasonably well with the actual condition, which proves the reasonableness and viability of the method proposed in this study.

KEYWORDS: Pavement engineering; Cement concrete pavement; Slab corner void; Criterion of judgment: Slab corner deflection

INTRODUCTION

Unless non-erodible subbases are utilized, plastic deformation and pumping will be developed in subbases under the slabs in Portland cement concrete (PCC) pavement due to repetitive applications of vehicle loads, which could lead to voids and accelerate the deterioration of PCC pavement condition. Extensive research positively identified the adverse effects that voids and non-uniform support have on PCC pavement performance. Even though substantial efforts have been made to evaluate voids under PCC pavement slabs using FWD, evaluation methods developed so far haven't been widely utilized due to the limitations of the methods in terms of accuracy and consistency. Further research is needed to address the limitations and

inconsistency in the current evaluation methods. The voids under PCC slabs often form in a slab corner first, and then extend to the center of the slab gradually by the repetitive effect of environmental loading (temperature and moisture variations in the slab) and vehicle loads. With the void size increasing, stresses and deflections in the slab will increase, resulting in slab cracking and pavement distresses. Voids normally form in the slab corner first and the extent of the voids is the largest in the slab corner. Meanwhile, the extent of the voids is minimal at the center for the slab. Therefore, the slab corner should be the FWD testing location for the detection of the voids. This paper presents a methodology for void detection using deflections from FWD applied at the slab corner.

THEORY OF VOID IDENTIFYING UNDER CCP CORNER DEFLECTION

There are a number of variables that have effects on slab deflections in PCC pavement, including the magnitude, contact area, and location of wheel load, the size, thickness, and modulus of the PCC slab, foundation condition, and joint load-transfer efficiency.

A few research studies have indicated that the effect of plane dimension on deflection can be neglected. When subbase is of even supporting condition that can be modeled by Winkler foundation and if temperature warping effect is ignored, the effect of joint load-transfer efficiency on the slab corner deflection could be characterized by the following equation;

$$\delta_c = \varepsilon_\omega \cdot \delta_{c\infty} \tag{1}$$

where,

δ_c — the theoretical slab corner deflection
$\delta_{c\infty}$: the slab corner deflection of infinite slab under even supporting conditions
ε_ω: the modified coefficient for joint load-transfer

THEORETICAL SLAB CORNER DEFLECTION IN INFINITE SLAB UNDER EVEN SUPPORTING CONDITIONS

Westergaard (1926) proposed a formula for slab deflection under round load acting on slab corner by a successive approximation method as shown below:

$$\Delta_c = \frac{P}{kl^2}[1.1 - 0.88(\frac{a\sqrt{2}}{l})] \tag{2}$$

where,

P: concentrated load (N)
h: pavement slab thickness (mm)
Δ_c: slab corner deflection (mm)
l: radius of relative stiffness (m)
a: the radius of tie contact area (m)

Radius of relative stiffness of the slab can be calculated by the follow formula:

$$l = [\frac{Eh^3}{12(1-\mu^2)k}]^{0.25} \tag{3}$$

where,

E: the elastic modulus of concrete pavement slab (MPa)

μ: concrete Poisson ratio

k: modulus of subgrade reaction (MN/m^3)

Estimation of Pavement Slab Modulus and Foundational Response Modulus

A new method for the estimation of the stiffness of the pavement structure is proposed in this study. It is based on the load stress distribution coefficient using FWD deflections at the slab center. Pavement slab modulus E and resilience modulus of foundation of elastic half-space E_0 can be estimated by (4) and (5).

$$E = 2(1-\mu^2)(q_0)a/(d_1 - d_{3/5h}) \tag{4}$$

where,

q_0: the stress in the center of FWD load plate application

d_1: the deflection in the center of FWD load plate application

$d_{3/5h}$: the deflection in the position 3/5h from the load plate center, which obtained from the linear interpolation

μ: the Poisson ratio of pavement slab

$$E_0 = 2(1-\mu_0^2)aq_0/(f_7 d_7) \tag{5}$$

where,

μ_0: the Poisson ratio of soil

d_7: the deflection of sensor at 160cm from the center of FWD load plate

f_7: load stress distribution coefficient 160cm from the center of FWD load plate

In general case, $f_7 = 2\times160/a = 21.333$ and the radius of FWD load plate $a = 15$cm.

Vesic and Saxena put forward (6) in 1974 that the connection between Winkler foundational response modulus k and resilience modulus of foundation of elastic half-space E_0 was established by pavement slab modulus E and the Poisson ratio of soil, which solved foundational response modulus.

$$k = (\frac{E_0}{E})^{\frac{1}{3}} \frac{E_0}{(1-\mu_0^2)h} \tag{6}$$

THE MODIFICATION OF THEORETICAL SLAB CORNER DEFLECTION ON LOAD TRANSFER CAPACITY

Research studies show that joint load-transfer capacity has a significant effect on slab corner deflection of PCC slab while having very little effect on deflections at the slab center. Joint load-transfer capacity is usually expressed by joint load-transfer coefficient ω (the ratio of the slab corner deflection under load to that of under no load). The ANSYS finite element program was used to analyze the deflection behavior of a standard slab (length to width ratio 5m×4m) and to study the effect of load-transfer capacity on slab corner deflection. Joint load-transfer can be simulated by selecting appropriate modulus of the joint element, and the load-transfer capacity change of joint dowel were often simulated by changing the material parameters of the joint dowel.

Calculated material parameters were as follows: pavement slab modulus E=30000MPa, Poisson ratio of pavement slab, semi-rigid base, and soil were 0.15, 0.25, and 0.35 respectively; pavement slab thickness h=0.25m, base modulus 5000MPa, base thickness 0.25m, Winkler foundational response modulus k=100MN/m3. The analysis results are provided in Table 1.

Table 1.The Influence of Load-transfer Capacity on Slab Corner Deflection

Winkler foundation stiffness radius l= 0.7804 m			**Winkler foundation stiffness radius l= 0.8386 m**		
Joint Load-transfer Coefficient ω /(%)	**Slab Corner Deflection /(0.01mm)**	**Load-transfer Modified Coefficient ε_ω**	**Joint Load-transfer Coefficient ω /(%)**	**Slab Corner Deflection /(0.01mm)**	**Load-transfer Modified Coefficient ε_ω**
0.00	70.36	1	0.00	62.14	1.000
5.67	66.56	0.946	3.28	59.97	0.965
9.89	64.31	0.914	7.33	57.98	0.933
17.45	60.65	0.862	11.89	55.87	0.899
29.91	55.23	0.785	21.17	52.01	0.837
34.27	53.61	0.762	24.22	50.89	0.819
42.18	51.15	0.727	32.54	47.97	0.772
49.85	49.11	0.698	40.81	45.49	0.732
58.34	47.35	0.673	49.74	43.37	0.698
62.67	46.58	0.662	55.22	42.26	0.680
75.23	44.68	0.635	69.18	40.39	0.650
83.22	43.488	0.618	76.53	39.27	0.632
86.98	42.99	0.611	81.24	37.72	0.607

Load-transfer modified coefficient is the ratio of slab corner deflection with load-transfer capacity to the one without load-transfer capacity. From Table 1 it can be

seen that slab corner deflection with load-transfer capacity decreased significantly compared with free slab, and load-transfer modified coefficient shows the same trend. Load-transfer modified coefficient and load-transfer coefficient have good correlation, which is shown as the regression formula below.

$$\varepsilon_{\omega} = 0.434\omega^2 - 0.809\omega + 0.99 \tag{7}$$

Based on the research above the theoretical slab corner deflection with even supporting conditions and different load-transfer capacity can be obtained by (1).

VOID SIZE ESTIMATION OF SLAB CORNER DEFLECTION

A large number of engineering practices show that void area of PCC slabs behave nearly as a triangle. In our discussion void area is assumed as an isosceles triangle, and void size is defined as the side length of the isosceles triangle L_V, which lies within 2m. So the paper introduces a concept of void index λ.

$$\lambda = \frac{\delta_c'}{\delta_c} \tag{8}$$

where,

δ_c: theoretical slab corner deflection

δ_c': test slab corner deflection

With the above definitions, the effect of different void sizes under slab corner on void index was analyzed. Part of the results obtained is shown in Table 2.

Table 2. Void Index in Different Dimension of Void under Single-round Load of Slab Corner

Void Size under Slab Corner L_V /m	Foundational Response Modulus k/ (MN/m^3)				
	100	150	200	250	300
0.00	1.000	1.000	1.000	1.000	1.000
0.40	1.261	1.311	1.352	1.388	1.419
0.80	1.521	1.621	1.704	1.775	1.839
1.20	1.782	1.932	2.056	2.163	2.258
1.60	2.043	2.243	2.407	2.550	2.678
2.00	2.303	2.553	2.759	2.938	3.097

h=0.25m, E=30000MPa, μ=0.15, P=50kN.

The results in Table 2 indicate that the void size under the slab corner has a notably significant effect on slab corner deflection. As expected, void index increases with

void size.

The analysis results, which are not presented due to space limitations, illustrate a good correlation between void index and not only void size but pavement slab modulus *E*, pavement slab thickness h, and foundational response modulus *k*. Pavement slab modulus *E* and thickness *h* have similar effects on void index λ. Void index decreases when E or *h* increases. On the other hand, it increases when *k* becomes larger. The variations in *E*, *h, or k* have similar sensitivity for the void index λ. The change curves of these factors approach a value of λ between 1.2 and 1.6 as *E*, *h, or k* approach large practical values. Foundational void conditions have the most significant effects on the void index.

Based on the analysis of the results discussed above, a regression formula for void index λ was obtained as (9).

$$\lambda = 1.272 L_V \left(\frac{Eh^3}{k}\right)^{-0.433} + 1 \tag{9}$$

After establishing the relation between the void index λ and void size L_V, comparing the test slab corner deflection with the calculated deflection in infinite slabs under even supporting conditions will determine the void index λ. With the void index information, the void size will be estimated from the Equation (9).

ENGINEERING EXAMPLE

Lei (yang) Yi (zhang) Expressway is a part of the Jingzhu national trunk highway in Hunan province. The slab size is 3.75m×5m. Some structural parameters used in the example analysis are; pavement slab thickness $h = 0.28$m, the Poisson ratio of pavement slab $\mu = 0.15$, and the Poisson ratio of soil $\mu = 0.35$.

A 50-m long section of Expressway was selected for field-testing to identify the slab cord void by using the methodology developed above. FWD testing was conducted at both the corner and the center of the slabs. The test deflection data is shown as Table 3. The results of the analysis using the methodology developed in this study are shown as Table 4.

Table 3. FWD Testing Data of CCP

Stake Number	Test Deflection of The Slab Center /(0.01mm)							Test Deflection of The Slab Corner /(0.01mm)			
	δ_1	δ_2	δ_3	δ_4	δ_5	δ_6	δ_7	δ_1	δ_2	δ_3	δ_4
K433+005	3.77	2.54	2.50	2.13	2.09	1.85	1.80	18.81	12.57	9.49	9.17
K433+010	4.23	3.67	3.54	3.74	3.02	2.64	2.51	16.11	11.32	7.04	5.66
K433+015	6.59	6.06	5.71	5.06	4.37	3.21	2.18	12.61	7.27	7.13	6.86
K433+020	6.69	6.53	5.66	5.20	4.16	3.04	2.04	12.35	9.7	9.7	8.1

K433+025	7.67	6.34	5.75	4.23	3.58	2.37	2.10	12.73	7.16	6.99	5.22
K433+030	7.82	7.05	5.81	4.83	3.90	3.24	2.76	22.98	14.52	10.11	7.95
K433+035	4.06	3.75	3.71	3.52	3.38	3.10	2.79	25.31	11.42	6.96	5.52
K433+040	4.62	4.13	4.07	3.75	3.69	4.42	3.13	17.63	9.91	8.38	8.27
K433+045	4.40	3.93	3.92	3.65	3.44	3.05	2.68	15.18	8.8	8.2	7.11
K433+050	5.12	4.94	4.77	4.53	4.26	3.64	3.00	18.21	10.9	9.3	7.88

Table 4. Void Identification Results underneath Slab Corner of CCP

Stake Number	***E*** **(MPa)**	E_0 **(MPa)**	***K*** **(MN/m^3)**	***l*****(m)**	$\delta_{c\infty}$ **(0.01mm)**	ω	ε_ω	δ_c **(0.01mm)**	λ	L_V **(m)**
K433+005	485	413	0.646	23.56	0.668	0.643	15.15	1.241	485	0.26
K433+010	348	204	0.938	25.13	0.703	0.636	15.98	1.008	348	No void
K433+015	400	242	0.911	22.32	0.577	0.668	14.90	0.846	400	No void
K433+020	428	177	1.328	15.35	0.785	0.622	9.55	1.292	428	1.09
K433+025	416	345	0.662	27.03	0.562	0.672	18.17	0.700	416	No void
K433+030	316	200	0.870	29.26	0.632	0.652	19.08	1.204	316	0.37
K433+035	313	145	1.183	23.16	0.451	0.713	16.52	1.532	313	1.62
K433+040	279	145	1.055	28.53	0.562	0.672	19.18	0.919	279	No void
K433+045	326	176	1.016	25.18	0.580	0.667	16.79	0.904	326	No void
K433+050	291	110	1.453	20.91	0.599	0.661	13.82	1.317	291	1.38

The results above were verified by core-drilling several locations in the test section and the largest error was 6.45% between the values from the analysis and actual measurements, which proves the viability of the method proposed in this study.

CONCLUSIONS

Based on the research effort in this study, the following conclusions were made:

1. Methods for joint load-transfer capacity evaluation and a void identification were developed in this study by comparing the theoretical and actual deflections at the slab corner. These methods overcome the limitations of the current method of single criterion using test deflections. The results from the void identification method developed in this study agree well with the actual data.

2. A concept of void index was proposed, which is defined as the ratio of measured deflections in the slab corner to theoretical deflections. Through the analysis of data between void index and void size, a regression formula between void index and void size was established for the estimation of void size. Void index decreases when E or *h* increases. On the other hand, it increases when *k* becomes larger. The variations in *E*, *h, or k* have similar sensitivity for the void index λ. The change curves of these factors approach a value of λ between 1.2 and 1.6 as *E*, *h, or k* approach large practical values. Foundational void conditions have the most significant effects on the void index.

The research shows that the void index decreases when E or *h* increases. On the other hand, it increases when *k* becomes larger. The effect degree on void index is equivalent in *E* and *h* and *k*. And foundational void condition has the most significant effect on the void index.

3. The results of void identification using the method proposed in this study with the data from the test section at the Hunan Leiyi Expressway compare reasonably well with the actual condition, which proves the reasonableness and viability of the method proposed in this study.

REFERENCES

Bradbury, R.D. (1938). "Reinforced concrete pavements". Wire Reinforcement Institute, Washington DC.

Cao, D.W. and Hu, C.S. (1998). "Research on determining whether the cavity beneath cement concrete slabs occurred". *Journal of Xi'an Highway University*. 18(3): 4-8.

Darter, M.I. Becker, J.M. Snyder, M.B. and Smith, R.E. (1985). "Portland cement concrete system pavement evaluation system (COPES)". *NCHRP Report 277, Transportation Research Board.*

Tang, B.M. (1992). "Detecion of voids beneath the rigid pavement slab". *China Journal of Highway and Transport*. 5(1): 40-44.

Vesic, A.S. and Saxena, K. (1974). "Analysis of structural behavior of AASHO road test rigid pavements". *NCHRP Report No.97*. Highway Research Board.

Westergaard, H.M. (1926). "Stresss in concrete pavements computed by theoretical analysis". *Public Roads*. 7(2): 25-35.

Yuan, S. (2004). "The analysis of dynamic response in CCP based on FWD". *Changsha: Changsha University of Science and Technology*. 37-50.

Zeng, S, Wang, G.M. Q.S. Zhang and et al. (2003). "Calculating modulus of pavement structure course directly using FWD load distribution coefficient". *Journal of Highway and Transportation Research and Development*. 20(4): 6-9.

Zeng, S. and Cheng, M.X. (2005). "Research on the concert pavement void and load transfer mechanism". *Journal of railway science and engineering*. 2(1): 68-72.

Zhang, N. Qian, Z.D. and Huang, W. (2004). "Void detection under PCC pavement". *Journal of Highway and Transportation Research and Development*. 21(1): 4-7.

Zhao, J. (2006). "Theory and method to identify and evaluate void scope beneath cement concrete pavement slabs". Shanghai: Tongji University. 30-77.

Differential Settlement Control Criterion of Bridge-approach on People-vehicle-road Interaction

Xiang-hua TAO[1]

[1]PhD, Henan Provincial Communications Quality Control Institute, Zhengzhou hanghai road 219, China, 450005; PH (86) 689-80331, taoxianghua@sina.com

ABSTRACT: The bump on bridge-approach has been an urgent worldwide problem on highways and bridges, caused by differential settlement between bridge abutment and approaching pavement. But the existing calculation models and methods of bridge-approach pavements could not describe and explain the mechanism of bump under vehicle dynamic load appropriately. So this paper adopts human weighed acceleration RMS (Root Mean Square) to evaluate ride comfort when the vehicle is passing through bridge-approach, and road unevenness model of bridge-approach is build up by exponential settlement curve, and effect factors of vehicle ride comfort are analyzed that velocity, the maximum differential settlement and settlement length have the important effect on people ride comfort. At last, the author builds up differential settlement control criterion of bridge-approach on people-vehicle-road interaction.

INTRODUCTION

The differential settlement control criterion not only concerns with the functional performance of pavements, but also the structural performance. Most countries provide different control criterions on the differential settlement of bridge approach, such as the peak differential settlement, the peak slope difference and the step height, but the criterions are not same because of many reasons. Obviously, the control criterion on the differential settlement should not be fixed because that the velocity, the load and passenger, have effect on ride comfort.

This paper sets up the suitable people-vehicle-road vibration model, and conducts computer procedure to analysis the effect on ride comfort, and aims to establish the differential settlement control criterion of bridge-approach according to ISO 2631.

EVALUATON METHOD AND INDEX ON RIDE COMFORT

At present, many evaluation criterions on ride comfort have existed in the worldwide. This paper adopts ISO 2631 as the basic evaluation criterion of ride comfort, and evaluates ride comfort with people average acceleration RMS (Root Mean of Square). The relationship between the comfort reactions and people average acceleration RMS is listed in **Table 1**. RMS may reflect people comfort, and it is easy to calculate, so this paper adopts acceleration RMS as the transient vibration index when the vehicles are passing the bridge approach.

Table 1. Comfort Reactions to Vibration Environments

Less than 0.315 m/s^2	not uncomfortable
0.315 m/s^2 to 0.63 m/s^2	a little uncomfortable
0.5 m/s^2 to 1 m/s^2	fairly uncomfortable
0.8 m/s^2 to 1.6 m/s^2	uncomfortable
1.25 m/s^2 to 2.5 m/s^2	very uncomfortable
Greater than 2 m/s^2	extremely uncomfortable

MATHEMATICAL MODEL OF VEHICLE VIARATION

Traditional quarter-car system model cannot reflect the relationship between front axle and behind axle. This paper adopts 2D five degrees of freedom vehicle model, and it is illustrated in **Fig.1.**

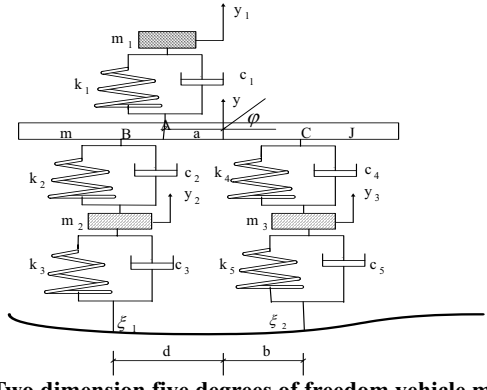

Fig.1. Two dimension five degrees of freedom vehicle model

The Newton-Euler equations are used in order to obtain the differential equations of motion of the system represented in **Fig. 1.** Governing equations of motion for this system are obtained directly as:

$$\begin{cases} m_1\ddot{y}_1 = -k_1(y_1 - y_a) - c_1(\dot{y}_1 - \dot{y}_a) \\ m_2\ddot{y}_2 = -k_2(y_2 - y_d) - c_2(\dot{y}_2 - \dot{y}_d) - k_3(y_2 - u_1) - c_3(\dot{y}_2 - \dot{u}_1) \\ m_3\ddot{y}_3 = -k_4(y_3 - y_b) - c_4(\dot{y}_3 - \dot{y}_b) - k_5(y_3 - u_2) - c_5(\dot{y}_3 - \dot{u}_2) \\ m\ddot{y} = -k_1(y_a - y_1) - c_1(\dot{y}_a - \dot{y}_1) - k_2(y_d - y_2) - c_2(\dot{y}_d - \dot{y}_2) - k_4(y_b - y_3) - c_4(\dot{y}_b - \dot{y}_3) \\ J\ddot{\varphi} = ak_1(y_a - y_1) + ac_1(\dot{y}_a - \dot{y}_1) + dk_2(y_d - y_2) + dc_2(\dot{y}_d - \dot{y}_2) - bk_4(y_b - y_3) - bc_4(\dot{y}_b - \dot{y}_3) \end{cases} \quad (1)$$

ROAD UNEVENESS MODEL

The road unevenness is defined as the deviation of a traveled surface from a true planar surface that has characteristic dimensions that affect ride comfort. The road unevenness can be described in a deterministic way or in a stochastic way by a power spectral density.

In this paper, local road irregularities as well as road roughness of bridge approach can be described by the exponential function; the exponential function is given by the following equation:

$$y = S_a + (S_b - S_a)\exp(-kx) \tag{2}$$

Where x is the distance along vehicle running direction, L is the settlement length of bridge approach, S_a is the settlement of abutment, S_b is the embankment settlement of length L, S_a-S_b is the differential settlement of bridge approach, and k is uncertain parameter.

Suppose the velocity v is a constant when the vehicles are running on the bridge approach. Road unevenness model can be described as follows:

$$u(t) = \begin{cases} h + h_0 + i_1 L_0 - i_1 vt & 0 \le t \le L_0 / v \\ (h_0 + h)\exp(-k(vt - L_0)) & L_0 / v < t \le (L_1 + L_0)/v \\ 0 & t > (L_1 + L_0)/v \end{cases} \tag{3}$$

Where h_0 is the settlement of abutment, h is the peak differential settlement, i_1 is the slope difference of bridge, L_0 is the length of bridge, other parameters are the same as forenamed parameters.

RCBA PROCEDURE AND RELATIVE PARAMETERS

A generic computer simulation procedure RCBA for obtaining people acceleration RMS is shown. Parameters should be obtained and used as input information. Also road unevenness model and road surface parameters must be obtained as the input into the procedure. People acceleration RMS can eventually be obtained by FFT and IFFT using two user subroutines roughness and weighs, and the results are saved in the computer.The relative parameters of vehicle model are listed in **Table 2.**

Table 2. Parameters of Vehicle Model

Parameter	Numerical	Parameter	Numerical
Body mass, m	9440 kg	Front tire stiffness, k_3	1900000 N/m
People and seat mass, m_1	50 kg	Behind tire stiffness, k_5	3800000 N/m
Body moment of inertia, J	75070 kg m^2	Front tire damping, c_3	1000 N s/m
Front axle mass, m_2	550 kg	Behind tire damping, c_5	1000 N s/m
Behind axle mass, m_3	1041 kg	Seat stiffness, k_1	10500 N/m
Front suspension spring	301840 N/m	Seat damping, c_1	240 N s/m

Behind suspension spring	607364 N/m	Front axle spacing, d	3.238 m
Front suspension damping, c_2	11901 N s/m	Behind axle spacing, b	1.462 m
Behind suspension damping, c_4	23691 N s/m	Front seat-body	2.238 m

PARAMETRIC ANALYSYS

When the running vehicles are passing the bridge approach, bumping will appear and people will feel uncomfortable. People comfortable reactions are caused by many reasons, the first reason is the differential settlement of bridge approach, the second is the running direction and the velocity, and the third is the vehicle parameters.

Effect of running direction

The vehicle response passing the bridge approach with constant velocity is investigated first using the values as the settlement length L=10 m, the peak differential settlement h=0.04 m, the velocity $v = 20$ m/s, and the bridge slope difference $i_1 = 0$. Effect of the running direction is considered to study the vehicle response. **Fig. 2** shows people acceleration RMS with time when the vehicles are passing along bridge entrance (left curve) and exit (right curve). People acceleration RMS amplitude will decrease with time, and the maximum RMS is the same regardless of the running direction. While the vehicles are passing through bridge entrance, the peak discomfort will appear on the bridge, it shows vibrations of the differential settlement will weaken when the vehicles reach the bridge. While the vehicles are passing through bridge exit, the peak discomfort will appear in the pavement, it shows vehicles vibrations will weaken when vehicles reach the pavement.

People acceleration RMS and comfort reactions are listed in **Table 3**, and it shows the running direction has no effect on people acceleration RMS and ride comfort, so this paper will establish the differential settlement control criterion of bridge approach along bridge exit.

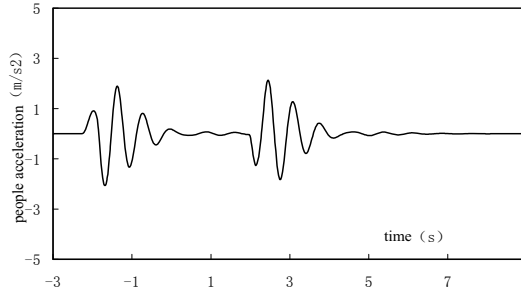

Fig. 2. Effect of running direction on people acceleration RMS with time

Table 3. Effect of Running Direction

Direction	People acceleration RMS (m/s^2)	People comfort reactions

bridge entrance	0.88	uncomfortable
bridge exit	0.89	uncomfortable

Effect of velocity

The velocity is one of most important factors to affect the ride comfort. The effect of the velocity on people acceleration RMS is observed in **Table 4** by using the values L=10 m, h=0.04 m, and $i_1 = 0$. As the velocity increases, the peak acceleration RMS increases sharply, and people is more and more uncomfortable, so velocity should be considered into the differential settlement criterion of bridge approach.

Table 4. Effect of Velocity

Velocity(m/s)	People Acceleration RMS (m/s^2)	People comfort reactions
10	0.253	not uncomfortable
12	0.322	a little uncomfortable
14	0.418	a little uncomfortable
16	0.531	a little uncomfortable
20	0.765	fairly uncomfortable
25	1.029	uncomfortable

Effect of load

Table 5 lists the effect of the vehicle load on the vehicle inherent frequency and the peak acceleration RMS. As the vehicle load increases, the inherent frequency of vertical vibration will reduce, and other inherent frequency has little change. The result shows people acceleration RMS changes little, it will decrease in some extent and people comfort will be improved with heavy load. Therefore it is easy for empty car to cause bump, and empty vehicle should be considered as standard vehicle when establishing the differential settlement control criterion of bridge approach.

Table 5. Effect of Vehicle Load

Load (kg)	body frequency(Hz)		Seat frequency (Hz)	Tire frequency(Hz)		People Acceleration RMS (m/s2)	People comfort reactions
	vertical vibration	rotational vibration		Front tire	Behind tire		
Empty (m=3500)	2.20	1.14	2.49	10.09	10.39	0.784	fairly uncomfortable
Half load (m=6470)	1.73	1.14	2.33	10.09	10.38	0.775	fairly uncomfortable
Full load (m=9440)	1.44	1.13	2.32	10.09	10.38	0.765	fairly uncomfortable
Overload (m=15000)	1.17	1.12	2.32	10.09	10.37	0.557	a little uncomfortable

Effect of geometry parameters of bridge approach

Table 6 shows the results corresponding to the different differential settlement. As the differential settlement increases, people acceleration RMS increases and people comfort reactions will be more and more uncomfortable. The relationship between RMS and the differential settlement is linear, so we can establish the

differential settlement control criterion by using the linear relationship.

Table 7 lists the effect of the settlement length on people acceleration RMS. It shows that the length increases, RMS will decrease and people comfort reactions will be more and more comfortable. Therefore the settlement length of bridge approach should be considered into the control criterion of differential settlement.

Table 6. Effect of Differential Settlement on People Acceleration RMS

Settlement (cm)	Slope Difference	People Acceleration RMS (m/s^2)	People comfort reactions
0.5	0.0005	0.116	not uncomfortable
1	0.001	0.231	not uncomfortable
2	0.002	0.462	a little uncomfortable
3	0.003	0.693	fairly uncomfortable
4	0.004	0.925	uncomfortable
5	0.005	1.156	uncomfortable

Table 7. Effect of the Settlement Length

Settlement length (m)	Slope difference	Acceleration RMS (m/s^2)	People comfort reactions
4	0.0100	1.543	very uncomfortable
6	0.0067	1.349	uncomfortable
8	0.0050	1.138	uncomfortable
10	0.0040	0.925	uncomfortable
12	0.0033	0.728	fairly uncomfortable
15	0.0027	0.503	a little uncomfortable

DIFFERENTIAL SETTLEMENT CONTROL CRITERION

The results in the previous sections are used to establish the differential settlement control criterion. According the relationship between people comfort reactions and the velocity, the settlement length, the differential settlement and load, this paper adopts the empty vehicle as standard vehicle, and establishes the differential settlement control criterion, as shown in **Table 8**. When the velocity changes from 120 km/h to 20 km/h, the corresponding peak differential settlement will change from 1.4 cm to 16.3 cm.

Table 8. Differential Settlement Control Criterion of Bridge-approach

Settlement length (m)	Peak Differential Settlement (cm)				
	Expressway	Arterial highway	The second class highway	The third class highway	The fourth class highway
4	≤1.4	≤1.9	≤2.0	≤3.2	≤3.9
6	≤2.3	≤2.6	≤3.2	≤5.3	≤7.0
8	≤3.0	≤3.6	≤4.1	≤6.5	≤8.6

10	≤3.5	≤4.5	≤5.3	≤9.1	≤12.7
12	≤4.5	≤5.6	≤6.8	≤11.0	≤15.2
15	≤5.4	≤7.1	≤9.2	≤13.6	≤16.3

CONCLUSIONS

This paper establishes 5 degrees of freedom vibration model based on people-vehicle-pavement interaction, and compiles RCBA procedure to calculate people acceleration RMS. At last the differential settlement control criterion of bridge approach is established by using the peak differential settlement or the slope difference as the control index.

A numerical example demonstrates the influence of the running direction, velocity, vehicle load, the differential settlement and the settlement length of bridge approach. The results show that the running direction has no effect on ride comfort. As the velocity increase, the peak people acceleration RMS increases. While vehicle load is beneficial to improve ride comfort in some extent, this paper adopts the empty vehicle as standard vehicle. The differential settlement has the linear relationship with the acceleration RMS. At the same time, the settlement length of bridge approach increases, and people acceleration RMS will decrease.

The differential settlement control criterion of bridge approach in this paper can be used as the embankment differential settlement control criterion, and provides the basis on solving bump and constructing bridge approach.

REFERENCES

FENG Guang-le, XU Zhi-hong, LING Tian-qing (2005). “Study on Settlement Criterion Basing on Serviceability at Bridge Approach”. *Journal of Highway and Transportation Research and Development,* Vol. 22(2): 35-38. (in Chinese)

DU Zhi-gang, PAN Xiao-dong, WANG Fu-gui (2007). “Analysis and Evaluation of Vehicle Bumping at Bridge-head of Mountain Highway Based on Ergonomics” *Journal of Central South Highway Engineering*, (1): 20-23. (in Chinese)

FENG Zhong-ju, FANG Yi-li, GONG Jian-cheng (1999). “Analysis of the Harmful Effect of Vehicle Bump at Bridge head of the Highway and Its Mechanism”. *Journal of Xi’an Highway University*, Vol. 19(4): 33-35. (in Chinese)

Mechanical vibration and shock - Evaluation of human exposure to whole-body vibration (1997), ISO 2631-1, 1997.

TAO Xiang-hua (2006). “Differential settlement control criterion of bridge-approach and people-vehicle-road interaction”. *Doctoral dissertation of Southeast University*. China: 27-40. (in Chinese)

Deflection and Stress Analysis of Concrete Slab under Temperature and Axle Load Coupling

Xinkai Li[1], Songlin Ma[2], Xiangshen Hou[3]

[1] PHD Student, School of Transportation Science and Engineering, Harbin Institute of Technology, Harbin, 202 Haihe Road, Nangang District, Harbin 150090, P.R. China Tel. 86-451-86282120; lxkhit@126.com

[2] Professor, School of Transportation Science and Engineering, Harbin Institute of Technology, Harbin, 202 Haihe Road, Nangang District, Harbin 150090, P.R. China Tel. 86-451-86282837; masonglin@hit.edu.cn

[3] Professor, School of Transportation Science and Engineering, Harbin Institute of Technology, Harbin, 202 Haihe Road, Nangang District, Harbin 150090, P.R. China Tel. 86-451-86282837; houxiangshen@126.com

ABSTRACT: A concrete slab edge will tend to curl up when it is subjected to a negative temperature gradient extending through the slab thickness. The tendency to curl up can induce tensile stresses on the top of slab as the pavement is restrained by its weight or other factors. At present in cement concrete pavement design in China the total stress as a result of load stress plus temperature stress results in transverse crack from the bottom to top of the slab is the only transverse crack considered. In recently many researchers have noticed top-down cracks in concrete pavement slab, and the top-down cracking has been observed in China through coring. Therefore, in order to understand the influences of coupling curling and loading stress on slab cracking, the single slab resting on elastic foundation with frictionless interface is simulated by finite element model (FEM). In FEM the axle load positions from an edge of the slab to another edge are considered and the negative temperature gradients are considered also. From the calculated results when a negative temperature gradient is combined with an axle load, high tensile stress will occur on the top of slab, so top-down cracking will occur. Therefore, in concrete pavement design the top-down cracking in concrete pavement should be considered in the design.

INTRODUCTION

It has been recognized that slabs tend to curl up due to complicated environmental influences such as temperature differentials, moisture differentials, built-in temperature stresses, differential shrinkage and so on (Rao, et. al, 2005 and Hiller, et. al,2002). Therefore, a slab in service is not flat any more. Through FEM calculations high stress are predicted at the top of slab due to differential shrinkage and temperature (Health, et,al, 2000). However, in China in concrete pavement design a slab resting on a foundation is assumed to be flat, so the maximum load-induced stress in a slab occurs at bottom and cracking should develop from bottom to up (JTG-D40-2002). Top-down

cracking in concrete pavement is not considered. Recently, many longitudinal and corner cracks were observed in concrete pavement in Heilongjiang province, China. The cracking develops from top to down as observed by coring different highways. See Figure 1.

a) Longitudinal cracks **b) Top-down cracking through coring**

FIG.1. Longitudinal cracks and top-down cracking in Heilongjiang Province

In Chinese concrete pavement design, the load induced stress and thermal stress are computed separately and then added together at the bottom of the slab to calculate the critical stress. Therefore, the analysis of slabs under combined temperature and axle load is needed to develop the cracking model. In jointed plain concrete pavement (JPCP) the transverse joints are commonly saw-cut and no dowels are placed in transverse joints. The dowels will be instrumented for very heavy traffic. Therefore, for general JPCP the joint's load transfer efficiency (LTE) is contributed to by aggregate interlock, but in winter the contribution of aggregate interlock for LTE will decrease. As a result, the LTEs of adjacent slab are not considered. The single slab with frictionless interface between slab and foundation is simulated using a three dimensional finite element procedure. The deflection and stress of slab are calculated under temperature gradient and self-weight of slab, and then the FEM results are validated through comparing with the closed-form solution of slab. The deflection and stress of slab under combined negative temperature gradient and axle load are analyzed through FEM, and the different axle load positions on the slab are considered.

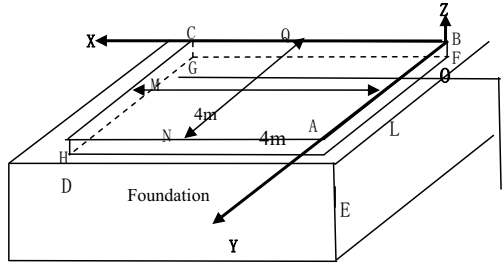

FIG. 2.The sketch map of model

THE FINITE ELEMENT MODEL

The parameters in FEM

The single slab resting on elastic foundation is modeled using the finite element program ABAQUS and the sketch map are listed as following figure 2.

The interface between slab and foundation is very complicated and important to concrete pavement and in this FEM the interface is assumed to be frictionless (unbonded). In ABAQUS the frictionless interface is simulated through contact elements which can simulate the separation of slab and foundation as slab edge curling up (S. N. Shoukry et al. 2007, Tianxi Tang et al. 1993). In this model the sizes of slab are 4m×4m×0.2m (length × width × height) and the values of parameters in FEM are listed in Table 1.

Table 1.The values of parameters in FEM

Parameters	Elastic Modulus (MPa)	Possion's ratio	Density (Kg/m^3)	Thermal conductivity (W/mK)	Coefficient of Thermal Expansion	Thickness of Slab (cm)
Slab	30000	0.15	2400	6	$5e^{-6}$	
Foundation	400	0.30	2000	0	0	0

Temperature Gradient

In the FEM, the temperature gradient is assumed to be linear along thickness of the slab. The negative temperature gradient for the slab edge curling is considered only because slab edge curl up is more common and seriously affects slabs, especially in northeast China. The heat change between slab and foundation is ignored. At northeast of china the minimum temperature in winter can arrive at -30℃ for several months, so in FEM the temperature gradient is assumed to be -1.5℃/cm, and the temperature difference between bottom and surface of slab can arrive at 30℃.

Axle Load

In FEM the standard axle load for concrete pavement design in China, BZZ-100, is employed. The axle load applies on slab from one edge to another and the different axle load positions are presented in Figure 3.

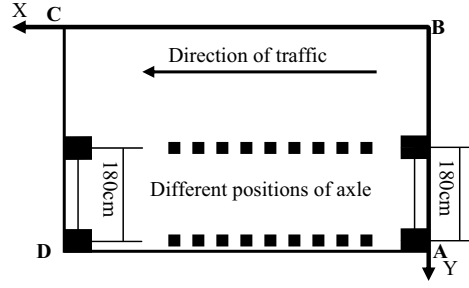

FIG.3.The positions of axle load applying on slab

Element Mesh

The three dimensional eight nodes continuum is employed in the FEM. In the course of element meshing of the FEM the number of elements will influence the precision of calculated results, but more elements will take more time to calculate, so the appropriate element size should be selected. Through comparison of different element sizes the number of elements of slab, 20×20×2 (length × width × height), was selected.

Verification of FEM

The calculated results of FEM need to be verified. If the self weight of slab is ignored, the closed-form solution of single slab curling up due to temperature gradient can be calculated by Equation (1) (Yao Zu-kang et al. 1981). Therefore, this case is selected to validate the FEM. Equation (1) can be derived through slab geometrical relationship.

$$\delta = \frac{\alpha \Delta F L^2}{2h} \qquad (1)$$

Where: δ — The vertical displacement of arbitrary point in slab; α — Coefficient of thermal expansion of concrete; ΔF — Temperature gradient along slab thickness; h — Slab Thickness L — The distance from arbitrary point to slab center.

Through Equation (1) if the self weight of slab is closer to zero the results should converge to the results of Equation (1). Therefore, the results from decreasing self weight converging to the closed-form solution can be used to validate the FEM. In FEM the slab weight is assumed to be W. When slab weight ranges from W to 0.001W, the calculated results of FEM due to negative temperature gradient are presented in Figure 4.

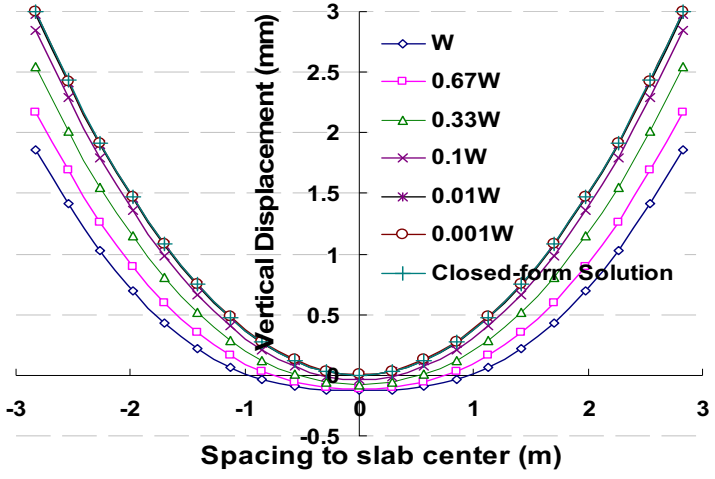

FIG.4.The vertical displacement as different slab self weights

In Figure 4 as the slab self weight decreases, the vertical displacement of the curling corner increases. When the self weight converges to zero the calculated results from the FEM is very close to close-form solution from Equation (1).

THE RESULTS UNDER TEMPERATURE AND AXLE LOAD COUPLING

Under a negative temperature gradient the slab edge curls up, and then the axle load, BZZ-100, is applied from the slab edge AB to symmetrical line QN in Figure 2. When load and temperature combine, the responses at each load position in Figure 3 are calculated by FEM, and the stress in Y direction contour plots of slab are presented in Figure 5.

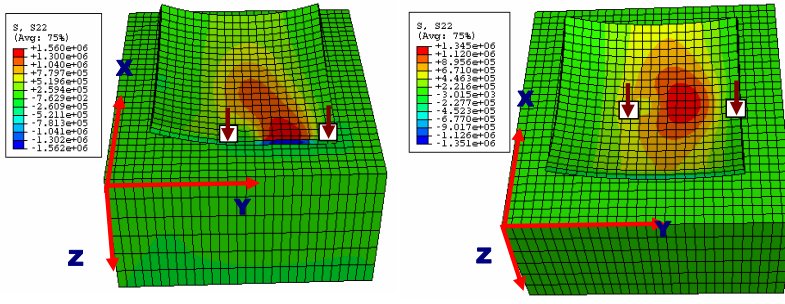

a) Axle load position: Slab edge AB **b) Axle load position: Slab center QN**

FIG.5.Stress in Y direction as axle load applying on different positions

When the negative temperature gradient exists along slab thickness, no matter where the axle load applies, the maximum tensile stress occurs on the top of slab, so the cracking will develop from top to down. The maximum stress in X and Y direction on the top of slab for the axle load in different positions is plotted in Figure 6.

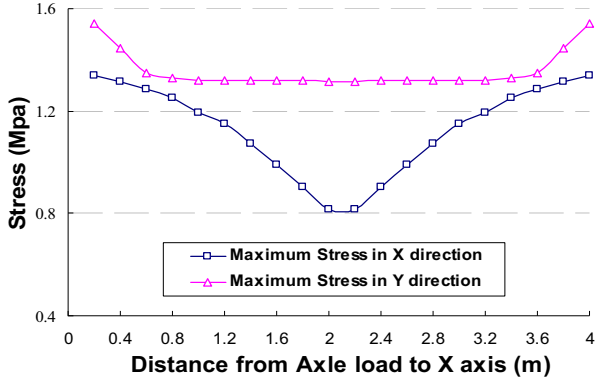

FIG.6.The maximum tensile stress at different axle load positions

Figure 6 presents the maximum tensile stress on the top of the slab in X and Y directions for the axle load in different positions. From Figure 6, it is clear that the maximum stress in Y direction is larger than the stress in X direction as the axle load moves from one slab edge to another. When the axle load acts upon the slab edge, the stress in the Y direction maximizes. From the results of the slab under combined temperature and axle load the following conclusions can be drawn.

1) The slab edge will tend to curl up because of negative temperature gradients. When the axle load is applied to the curling slab, the maximum tensile stress is on the top of the slab, not at the bottom of the slab. This will cause slab cracking from top to bottom.

2) When the axle load in on the slab edge, the stress at the slab edge is larger than other cases, so the initial cracking induced by axial load should begin at the slab edge.

3) The top stress in Y direction is always larger than stress in X direction no matter what the axle load position. This suggests that the longitudinal cracks are dominating the damage caused by slab edge curl up.

CONCLUSIONS

Under combined negative temperature gradient and axle load, the responses of a single slab are calculated using a finite element procedure. From the results, the maximum tensile stress is on the top of the slab, not at the bottom of the slab. This will cause cracking development is from the top down. At the same time, the results show that the longitudinal top-down cracking is the dominating damage under combined negative temperature gradient and axle load. However, top-down cracking is not considered in concrete pavement design in China. In this paper only a single slab is

considered for analysis, so the responses of multi-slabs under combined temperature and axle load will be researched in the future.

REFERENCES

Shreenath. Rao, Jeffery R. Roesler.(2005). "Characterizing Effective Built-in Curling from concrete pavement field measurement." *Journal of Transportation Engineering*, vol.131(04): 320~326.

Hiller.J.E, Roesler.J.R.(2002). "Transverse joint analysis for mechanistic-empirical design of rigid pavements." *Transport Research Record*,n1809:42~51.

Health. A.C., Roesler.J.R.(2000). "Top-down cracking of rigid pavements constructed with fast-setting hydraulic cement concrete." *Transport Research Record*,n1712:3~12.

JTG-D40-2002. *Specifications of Cement Concrete Pavement Design for Highway*. Ministry of Communications of People Republic of China, China Communications Press, 2002, Peking.

S. N. Shoukry, M. Fahmy, J. Prucz, G . William. (2007). "Validation of 3DFE Analysis of Rigid Pavement Dynamic Response to Moving Traffic and Nonlinear Temperature Gradient Effects." *International Journal of Geomechanics*,vol.7(01): 16-24.

Tianxi Tang, Dan G. Zollinger, and Sanjaya Senadheera.(1993). "Analysis of Concave Curling in Concrete Slab." *Journal of Transportation Engineering,*vol.04: 618-633.

Yao Zu-kang .(1981). "Thermal Warping Stresses in Concrete Pavements." *Journal of Tongji University*, vol. 119(04): 44-55.

Tan Zhi-ming,Zhou Yu-min, Liu Bo-ying. (2004). "Calculation of Thermal Warping Stresses in Cement Concrete Pavement Slabs." *Highway*, vol.11(11): 63-67.

Robert Y. Liang, Yan-Zhou Niu.(1998). "Temperature and Curling Stress in Concrete Pavement." *Journal of Transportation Engineering,* vol..124(01): 91-100.

Sensitivity Analysis of Transverse Cracking for Continuously Reinforced Concrete Pavement

Xudong Zha[1]

[1]Professor, School of Traffic and Transportation Engineering, Changsha University of Science & Technology, Hunan Changsha, 410004, P. R. China; xdzha@tom.com

ABSTRACT: Sensitivity analyses for transverse cracking of Continuously Reinforced Concrete Pavement (CRCP) were investigated for the CRCP structure of Lei-Yi (Leiyang to Yizhang) Expressway in Hunan Province, China. The investigation included 13 main parameters (slab thickness, elastic modulus of steel, temperature shrinkage coefficient of steel, drying shrinkage strain, compression strength, creep coefficient of concrete, elastic modulus of concrete, temperature shrinkage coefficient of concrete, diameter and spacing of longitudinal reinforcement, base friction coefficient, reinforcement bond strength and temperature differences) at 5 different levels. The average crack spacing, the average crack width and the maximum reinforcement stress were simultaneously calculated with the iterative algorithms according to the one-dimension nonlinear analysis method. It considered the creep action and the nonlinear boundary properties that took into account the bond-slip between reinforcement and concrete, and the friction-slip between slab and base. The sensitivities of CRCP transverse cracking influenced by each factor were analyzed with the relative comparison method quantitatively and qualitatively. The results show that the main factors impacting the CRCP transverse cracking included shrinkage properties of concrete, concrete grade, spacing and diameter of reinforcement, and the grade and type of reinforcement.

KEYWORDS: Continuously Reinforced Concrete Pavement (CRCP); Transverse cracking; Sensitivity; Crack spacing; Crack width; Reinforcement stress

INTRODUCTION

CRCP has been widely used on the heavy traffic pavements in Europe, U.S., Japan, Australia and other developed countries due to its fine qualities and performance (Zha et al. 1999). Forty kilometers of CRCP paved in 2001 on the Lei-Yi (Leiyang to Yizhang) Expressway in Hunan Province was investigated, and it is the first CRCP on expressways in China (Zha et al. 2003). Because CRCP lacks transverse joints, the concrete slabs produce transverse cracking over time due to temperature and moisture shrinkage of the concrete. When these cracks become too wide, they can lead to concrete spalling, erosion and reinforcement rusting. In addition, when crack spacing is too dense, punchouts can develop (Kohler et al. 2006; Xiao et al. 2006). In order to

control CRCP transverse cracking, the crack spacing (1-2.5m), the crack width (≤1mm) and the reinforcement stress (≤ reinforcement yield strength) are used as design indexes of CRCP in the specifications and guidelines for pavement design (JTG D40-2002; AASHTO 1995).

There are many influential factors involved in CRCP transverse cracking (Li et al. 2003). Many theoretical analyses have been applied in China and abroad with linear elastic theories, linear boundary properties and static methods, but the developments of CRCP transverse cracking remain unpredictable (Cao et al. 2001; Kim et al. 2000). To analyze the sensitivities of various factors influencing CRCP transverse cracking, a nonlinear analysis method was used to simultaneously solve crack spacing, crack width and reinforcement stress, while considering nonlinear boundary properties under the effects of temperature and moisture shrinkage for the CRCP structure of the Lei-Yi Expressway in Hunan Province. (Xiao et al. 2004).

SELECTION OF VALUE LEVELS OF PARAMETERS

According to the CRCP structure in Lei-Yi Expressway, the 13 main parameters at five different levels were investigated as shown in Table 1.

Table 1. Value Levels of Parameters

Category	Parameters		Value Levels				
			1	2	3	4	5
Material	Concrete	E_c (GPa)	20	25	30	35	40
		α_c ($\times 10^{-5}$/°C)	0.2	0.4	1.0	1.4	1.8
		ε_{sh} ($\times 10^{-4}$)	2.0	2.5	3.0	3.5	4.0
		R (MPa)	20	30	40	50	60
		ϕ	0.4	0.6	0.8	1.0	1.2
	Reinforcement	E_s (GPa)	100	150	200	250	300
		α_s ($\times 10^{-6}$/°C)	3	6	9	12	15
	Boundary	k_c (kPa/mm)	5	10	20	40	80
		k_s (MPa)	3.3	4.3	5.31	6.3	7.3
Load	ΔT (°C)		10	20	30	40	50
Geometric	Variant ρ (%)		0.4	0.5	0.606	0.7	0.8
	Slab	h_c (cm)	42.4	33.9	28	24.2	21.2
	Reinforcement	d_s (mm)	14.6	16.4	18	19.3	20.7
		b (cm)	22.7	18.2	15	13.0	11.4
	Invariant ρ (%)		0.606				
	Reinforcement	d_s (mm)	14	16	18	20	22
		b (cm)	9.1	11.8	15	18.5	22.4

In Table 1, the 13 main parameters include one load parameter (i.e. temperature differences ΔT), three geometric parameters (i.e. slab thickness h_c, reinforcement diameter d_s and reinforcement spacing b) and nine material parameters which have five concrete parameters (i.e. elastic modulus E_c, temperature shrinkage coefficient α_c,

drying shrinkage strain ε_{sh}, compression strength R and creep coefficient ϕ), two reinforcement parameters (i.e. elastic modulus E_s and temperature shrinkage coefficient α_s) and two boundary properties (i.e. base friction coefficient k_c and reinforcement bond strength k_s), but the reinforcement ratio ρ are combined with the three geometric parameters.

Because the three geometric parameters have mainly influenced the ρ, the two cases are considered, i.e. the variant ρ and the invariant ρ. For the variant ρ, when the influences of one of the geometric parameters are analyzed, the other two parameters are kept invariant as level three, and its levels are determined from the ρ value levels. For the invariant ρ, five value levels are selected according to the combination of d_s and b.

The creep is analyzed with the concrete effective modulus E_{ca} by Eq. 1, and the tensile strength R_f is calculated by Eq. 2 (Nicholas et al. 1995). The bond-slip between reinforcement and concrete as well as the friction-slip between concrete slab and base are analyzed by Eq. 3 and Eq. 4 with the section linear models, respectively (Kim et al. 2000).

$$E_{ca} = E_c/(1+\phi) \tag{1}$$

$$R_f = 0.33\sqrt{R} \tag{2}$$

$$\tau_s = \begin{cases} 36.38sk_s & (s \le 0.025) \\ (0.82 + 3.48s)k_s & (0.025 < s \le 0.051) \\ (1.65 - 12.74s)k_s & (0.051 < s \le 0.102) \\ 0.35k_s & (s > 0.102) \end{cases} \tag{3}$$

$$\tau_c = \begin{cases} k_c u & (u \le u_y) \\ k_c u_y & (u > u_y) \end{cases} \tag{4}$$

where,

τ_s, s: bond stress (MPa) and relative slip (mm) between reinforcement and concrete, respectively

τ_c, u, u_y: frictional force (kPa), relative slip (mm) and critical relative slip (mm) between slab and base, respectively, and u_y is selected as 0.7mm for the slurry seal

SENSITIVITY ANALYSIS

While analyzing the influences of one of the parameters, other parameters are selected as the middle values in Table 1 (level 3), but for the analysis of geometric parameters under the invariant ρ, the combinations of d_s and b are selected. Therefore, the results of the average crack spacing, l, the average crack width, w, and the maximum reinforcement stress, σ_s, are obtained under different value levels of various parameters with the one-dimension nonlinear iteration analysis method, and the

change curves of the major parameters are as shown in FIG. 1 as the limitation of pages.

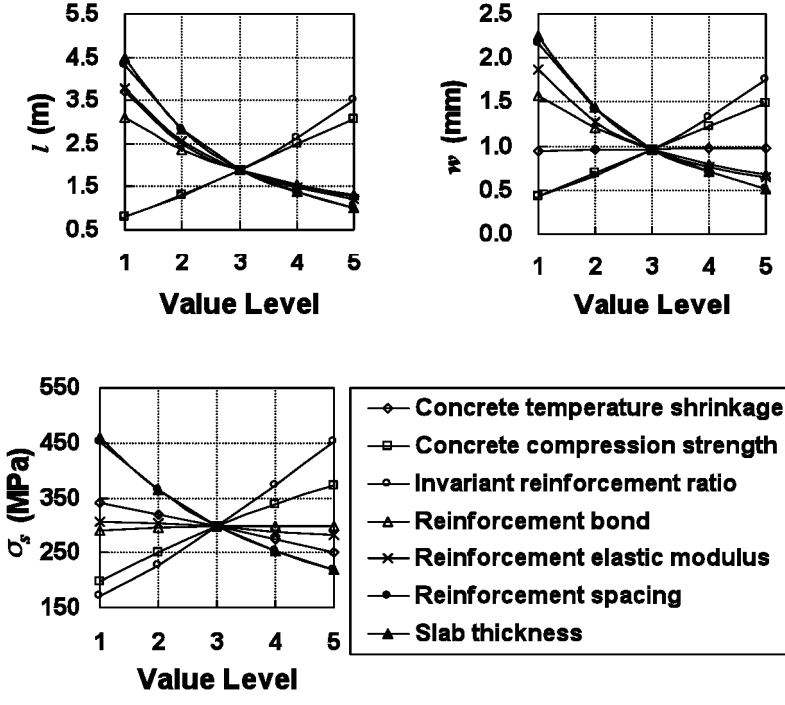

FIG. 1. Influence curves of parameters

Because the parameters have different units and physical meanings, it is difficult to accurately evaluate the influence degrees of various parameters on CRCP transverse cracking. With the 10% of changing the middle values (level 3) for various parameters, the average relative variations of three design indexes could represent the relative influence of various parameters. In order to analyze the significance degrees of various parameters of influence on the design indexes qualitatively, the significance grades are defined according to the ranges of absolute value C of the average relative variations of the design indexes in Table 2, and the corresponding analysis results are shown in Table 3.

Because the material parameters and the load parameters are analyzed under the invariant ρ, the significance degrees of sensitivity of the 10 parameters for influence on CRCP transverse cracking can be obtained with the comparison method, and the

order from largest to smallest about the design indexes will be as shown: 1) the average crack spacing l: $E_s > k_s > R > \alpha_c > \Delta T > \varepsilon_{sh} > E_c > \phi > k_c > \alpha_s$; 2) the average crack width w: $E_s > k_s > R > E_c > \phi > \alpha_c > k_c > \Delta T > \varepsilon_{sh} > \alpha_s$; 3) the maximum reinforcement stress σ_s: $R > \varepsilon_{sh} > \alpha_c > \alpha_s > E_c > E_s > k_s > \phi > k_c > \Delta T$.

Table 2. Significance Definition of Influence on Design Indexes

C (%)	$C < 0.1$	$0.1 \le C < 1$	$1 \le C < 5$	$5 \le C < 10$	$C \ge 10$
Significance Degree	Not Influence	Not Marked	Less Marked	Marked	Very Marked
Significance Grade	V	IV	III	II	I

Table 3. Average Relative Variations and Significance Grades of Design Indexes

Category	Parameters		C (%) and Significance Grades		
			l	w	σ_s
Material	Concrete	E_c	–3.20 (III)	–0.80 (IV)	–0.90 (IV)
		α_c	–8.03 (II)	0.27 (IV)	–1.87 (III)
		ε_{sh}	–6.31 (II)	0.18 (IV)	–1.92 (III)
		R	12.07 (I)	10.83 (I)	5.94 (II)
		ϕ	1.20 (III)	0.31 (IV)	0.35 (IV)
	Reinforcement	E_s	–13.58 (I)	–12.81 (I)	–0.87 (IV)
		α_s	0.00 (V)	0.00 (V)	1.82 (III)
	Boundary Properties	k_c	–0.26 (IV)	–0.25 (IV)	–0.13 (IV)
		k_s	–12.45 (I)	–12.45 (I)	0.39 (IV)
Load	ΔT		–7.36 (II)	0.20 (IV)	–0.09 (V)
Geometric	Variant ρ	h_c	24.42 (I)	23.63 (I)	10.76 (I)
		d_s	–11.60 (I)	–11.52 (I)	0.35 (IV)
		b	23.35 (I)	22.66 (I)	10.42 (I)
	Invariant ρ	d_s	31.85 (I)	30.67 (I)	21.31 (I)
		b	15.93 (I)	15.34 (I)	10.66 (I)

For the material parameters and the load parameters, E_s, k_s and R are the key factors of influence on l and w, and their influence ratios on the design indexes are more than their own changes. R is the marked factor of influence on σ_s. The results show that the suitable selection of grade and type of reinforcement as well as concrete grade are the primary measures to control CRCP transverse cracking. α_c, ε_{sh} and ΔT are the marked factors of influence on l. Because ΔT depends on the local climate and environment, the control of shrinkage properties of concrete is the important measure to ensure the reasonable cracking in CRCP. α_c, ε_{sh} and α_s are the important factors of the influence on σ_s, so the control of material shrinkage properties is beneficial to the working of reinforcement. E_c, ϕ and ΔT have a certain influence on l, but have no influence on w and σ_s. k_c has very small influence on CRCP transverse cracking and can be ignored.

While analyzing the influence of the three geometric parameters on CRCP

transverse cracking, two cases should be considered, i.e. the variant ρ and the invariant ρ.

For the variant ρ, all the order of significance degrees for the three parameters of influence on the three design indexes from largest to smallest are: $h_c > b > d_s$. The influence of the variant ρ on CRCP transverse cracking is very marked. The effects of the changing h_c are similar to that of b and very marked. In fact, h_c is determined by the AESALs, and generally does not change much. Therefore, the changing b will be beneficial to control CRCP transverse cracking. Changes in d_s will be beneficial to control l and w, and its influence on σ_s is very small.

For the invariant ρ, we mainly consider the combinations of d_s and b. The influence of different reinforcement on the three design indexes was marked. Along with the change of reinforcement way from small combination of d_s and b to large combination of d_s and b, l, w and σ_s will all increase remarkably. In fact, the reinforcement way of small combination of d_s and b will provide the larger bond area between reinforcement and concrete, and it can enhance the constraint action of reinforcement to concrete. Then, the way will influence CRCP transverse cracking remarkably and make l decrease, and w and σ_s will be decrease obviously.

Therefore, when the ρ and the other parameters could not be changed, there must be a reasonable range for the combination of d_s and b to meet the control requirements of the three design indexes, and the combination is too large or too small to meet the design requirements. d_s and b are smaller, the constraint action of reinforcement to concrete will be larger, but it will also make l too small and easily cause CRCP punchouts under the traffic loads. Meanwhile, the too dense reinforcement will possibly make the concrete under and below the reinforcement mat separate and break. Otherwise, the too large combination will increase l to cause the increase of w and σ_s, and it will easily produce concrete spalling, rain erosion and reinforcement tensile fracture. Therefore, for the reinforcement in CRCP in Lei-Yi Expressway according to the standard reinforcement size, the reasonable way is the combination of d_s = 16mm and b = 12cm or d_s = 18mm and b = 15cm, and the second way is selected in the real applications.

Through the investigation of the CRCP trial road in Lei-Yi Expressway in December 29, 2006, the average crack spacing has been 2.91m for 5.5 years of applications (Zha 2008). The forecasted final average crack spacing will be 2.22m, and the result shows that the reinforcement way is more reasonable.

CONCLUSIONS

According to the CRCP structure of Lei-Yi Expressway in Hunan Province, the sensitivities of various parameters of influence on CRCP transverse cracking were analyzed with the one-dimension nonlinear iteration method. The results show that sensitivities of various parameters have different influences on different design indexes. In order to control CRCP transverse cracking, the most critical factors are material shrinkage properties, grade and type of reinforcement, and concrete grade. Under the variant reinforcement ratio, the proper selection of reinforcement spacing is beneficial, and using different bar diameters could be effective for crack spacing and crack width control. Under the invariant reinforcement ratio, the reasonable selection

of reinforcement for the combination of diameter and spacing is very important.

ACKNOWLEDGMENTS

The author appreciates the support of Scientific Research Fund of Hunan Provincial Education Department.

REFERENCES

AASHTO. (1995). "AASHTO guide for design of pavement structure". Published by the AASHTO.

Cao, D. and Hu, C. (2001). "Analysis of thermal stress for continuously reinforced concrete pavement (CRCP)". *Journal of Xi'an Highway University*. 21(2): 1-5.

JTG D40-2002. (2002). "Specifications for design of highway cement concrete pavement". Beijing: People Communications Publishing House.

Kim, S. M. Won, M. C. and McCullough, B. F. (2000). "Three-dimensional nonlinear finite element analysis of continuously reinforced concrete pavements". *Report FHWA/TX-00/1831-1*. The University of Texas at Austin.

Kohler, E. and Roesler, J. (2006). "Crack spacing and crack width investigation from experimental CRCP sections". *International Journal of Pavement Engineering*. 7(4): 331-340.

Li, Z. Zha, X. and Zhang, Q. (2003). "Analysis of early transverse cracking for continuously reinforced concrete pavement". *Journal of China & Foreign Highway*. 23(2): 26-28.

Nicholas, J. C. and James, R. C. (1995). Prediction of cracking in reinforced concrete structures". *NISTIR 5634*. National Institute of Standards and Technology. U.S.A.

Xiao, Q. Zha, X. and Zhang, Q. (2004). One-dimensional nonlinear analysis of continuously reinforced concrete pavements". *Journal of Changsha Communications University*. 20(3): 20-26.

Xiao, Q. and Wang, W. (2006). "Evaluation of crack width of continuously reinforced concrete pavement based on extension method". *Journal of Railway Science and Engineering*. 3(1): 87-91.

Zha, X. Wang, Y. and Han, C. (1999). "Summary of cement concrete pavement in Europe". *Journal of Foreign Highway*. 19(3): 16-22.

Zha, X. Zhang, Q. and Li Y. et al. (2003). "Study of construction technology for continuously reinforced concrete pavement in expressway". *Journal of China & Foreign Highway*. 23(1): 1-4.

Zha, X. (2008). "Development laws of transverse cracking for Continuously Reinforced Concrete Pavement". *Journal of Traffic and Transportation Engineering*. 8(2): 65-68.

Estimation of the Compressive Strength of Concrete Using Shear Wave Velocity

Ji-Hwan An[1], Jeong-Hee Nam[2], Soo-Ahn Kwon[3], and Sung-Ho Joh[4]

[1]Researcher, Highway Facility Research Division, Korea Institute of Construction Technology, jenix@kict.re.kr
[2]Senior Researcher, Highway Facility Research Division, Korea Institute of Construction Technology, archnam@kict.re.kr
[3]Research Fellow, Highway Facility Research Division, Korea Institute of Construction Technology, sakwon@kict.re.kr
[4]Professor, Chung-Ang University, shjoh@cau.ac.kr

ABSTRACT

Compressive strength of concrete is a very important parameter in the quality control of both new and existing concrete pavement. It has been widely used to evaluate the concrete strength both in the laboratory and in the construction field regardless of whether numerous mix designs or identical mixtures are used.

Errors usually happen in the compressive strength test even if the mixture is evenly mixed and compacted into test specimens. This is caused by either by the hand-operated testing machine or by the eccentricity between the specimen and the testing machine.

If concrete specimens with identical mix design need to be tested at various curing ages every time concrete is used in the construction field, the result is significant waste of time, money and efforts are required.

Consequently, there is a real need to replace the repeated compressive strength tests with the introduction of nondestructive tests to estimate compressive strength of concrete.

In this study, a nondestructive test method using elastic waves was used because shear wave velocity is not affected by restraint conditions. The compressive strength of concrete was estimated according to various curing ages as well. In the results, shear wave velocity was very closely related to the compressive strength. The results further showed that the estimation of compressive strength of concrete using shear wave velocity is very effective and reliable.

INTRODUCTION

Strength has been used to characterize concrete in the design and quality control of concrete because a strength test is easier than other test methods. Particular characteristics such as elastic modulus, impermeability, and long-term pavement performance are dependent on strength and calculated from strength data.

Compressive strength of concrete is generally three to nine times greater than flexural strength and seven to eleven times greater than indirect tensile strength. Most

concrete structures are designed with the biggest compressive strength measured. In fact, concrete structures undergo compressive strength, tensile strength, and flexural strength from all direction simultaneously. Among these strengths, the 28-day compressive strength of concrete is tested most easily in the laboratory and is accurate enough to be accepted as a concrete strength indicator (Mehta, 2006).

Flexural strength, however, is used in concrete pavement design because the fracture of a concrete pavement slab under traffic load occurs by the combined actions of compressive stress and tensile stress on both the top and bottom respectively.

From the studies conducted by Westergaard in the 1940's to Picket, most research of concrete pavement analysis have suggested that slab stress is proportional to the amount of traffic load and it can be represented as a function of: slab thickness, the elastic modulus and the Poisson ratio. But it is difficult to measure the flexural strength of the existing pavement road directly for the purpose of pavement quality control. So, the flexural strength was calculated indirectly from the correlation of flexural strength to the compressive strength.

Usage of compressive strength is divided into two categories: in the laboratory and in the field. In the laboratory, compressive strength is measured to see if it achieves the target strength for ensuring quality control of material production and development of new mix design. In the field, compressive strength of concrete core samples is measured to evaluate the concrete strength of existing pavement.

However, to ensure the quality control or develop a new mix design, numerous tests are required in the laboratory. In the field, obtaining core sample consumes plenty of time, money and effort and it can deteriorate concrete pavement. Therefore, nondestructive testing needs to be introduced in order to eliminate both the problems in the laboratory and in the field.

This study focuses on the correlation of compressive strength of concrete to shear wave under the influence of various factors that include: normal conditions, different curing conditions, and different aggregate amounts. The results are compared and analyzed systematically to show the correlation between their effects on the shear wave and the compressive strength of concrete. Materials used in this study are obtained from the construction site of concrete pavement. Experiments were conducted in the laboratory where the shear wave, which is one of elastic waves, was used to analyze the correlation between the shear-wave velocity and the compressive strength of concrete at different curing ages.

INTRODUCTION OF ELASTIC WAVE AND RESEARCH TRENDS

When elastic wave signals propagate through a medium and meet an interface boundary, a part of them are refracted or reflected. The basic principle of measurement using an elastic wave is to receive these signals and analyze them to investigate a structure. Using nondestructive testing of concrete pavement to evaluate its engineering characteristics is based on this theory of elastic wave propagation. Elastic waves are categorized into body waves and surface waves. Body waves are further subdivided into a P-Wave (Primary Wave, Compression Wave) and an S-wave (Secondary Wave). Surface waves are subdivided into a Love wave and a Rayleigh wave (FIG. 1). The energy sources which generate elastic waves can be classified into

three categories: impact type, impulse type and vibration type.

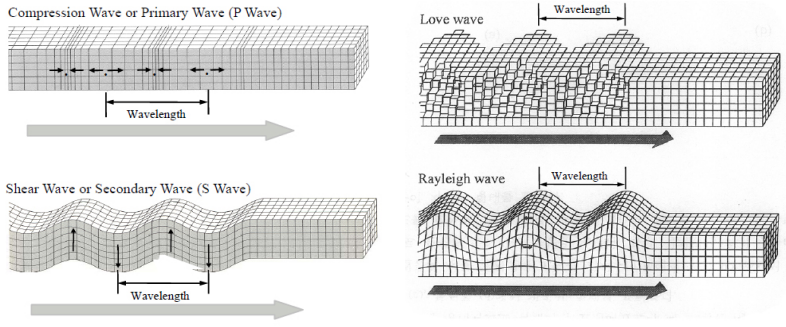

(a) Body Wave (b) Surface Wave

FIG. 1. Body Wave and Surface Wave.

Nondestructive testing of concrete structures is based on the p-wave resonance and the surface wave propagation. In previous research, Professor Sansalone at Cornell University studied p-wave resonance and Professors Stokoe and Roesset at the University of Texas studied surface wave propagation. Nondestructive testing equipment widely used in U.S. are based on these theories. Nondestructive testing using elastic wave has two essential methods that include the Impact-Echo Method and the Spectral-Analysis-of-Surface-Waves (SASW) Method. The Impact-Echo Method is based on the p-wave resonance and SASW Method is based on surface wave propagation. Each of them has its advantages and disadvantages such that applying either method exclusively is unreliable and ineffective to evaluate the integrity of concrete pavement. This study, therefore, introduces a new elastic wave method that combines the merits of both existing methods to better ensure quality control and to more effectively evaluate the integrity of concrete pavement.

Much research has been conducted to predict concrete strength using nondestructive testing in a variety of different ways. These include a study on factors affecting the correlation between ultrasonic velocity and concrete compressive strength in which the factors are a type of course aggregate, maximum size, aggregate content, curing conditions, and water content (Yuan et al., 2003). Pessiki and Carino studied the concrete setting time and concrete strength using Impact-Echo Method. They found no difference in the correlation between ultrasonic velocity and concrete compressive strength when the water-cement ratio ranged 0.57~0.5, whereas the aggregate content had an influence on their correlation (Lee et al., 2003). Pessiki and Johnson used the Impact-Echo Method and succeeded in predicting early age concrete strength used in plate-like structures such as slabs and walls (Pessoki et al., 1996).

Another study used the Impact-Echo Method to develop the correlation formula between ultrasonic velocity and concrete compressive strength. The correlation formulae were developed for two ranges after setting standard water-cement ratio at 0.35, under 0.35 and in the range of 0.35 to 0.58. This study discovered a slight

difference in the correlation between ultrasonic velocity and concrete compressive strength according to the existence of Fly Ash (Lee et al., 2003). For various types and ages of aggregates, the study showed different elastic moduli and the flexural strength of concrete calculated from the moduli was predictable with a high degree of accuracy (An, 2000). Transformation of wave propagation and the water content of concrete have no influence on the shear wave. Unlike the compression wave, the shear wave is not affected by restraint conditions of concrete. Therefore, measuring the shear wave velocity provides more reliable and constant results than measuring the compression wave (Cho, 2007).

In this study, the correlation between the shear wave velocity and the compressive strength of concrete is investigated using a shear wave.

TEST PLAN AND TEST METHOD

Specimens were made in the field and tested to measure elastic wave and compressive strength according to various curing ages. The J.J Pickel Research Campus in the U.S. and the Seoul Beltway in Korea were chosen for field tests by the American Center for Transportation Research (CTR). The mix design are identical for all three test fields; however one of them had different curing conditions than the other two field tests with standard curing condition (Table 1). Despite the fact that the mix designs of the CTR and the Seoul beltway were different, because their design strengths were the same, the behavior of the elastic wave velocity and strength according to various curing ages could be compared.

Table 1. Mix Design

Field	Flexural strength	Max Agg.	Slump	Air Void	Water	Cement	W/C	S/a	Sand	Aggregate		AE
	kg/㎠	m/m	cm	%	kg/m3	Kg	%	%	kg/m3	32mm	19mm	kg
CTR	45	32	7.6	4.9	79	278	28.2	45	898	1098		0.742*
Seoul Beltway 1st	45	32	2.5	5.5	127	334	38	41	762	678	452	1.002
Seoul Beltway 2nd	45	32	2.5	5.5	127	334	38	41	762	678	452	1.002

* High efficiency AE water-reducer was used.

Table 2. Curing Methods

Test Field	Curing Method
CTR	standard, sand
Seoul Beltway 1st	standard
Seoul Beltway 2nd	standard

In field curing, specimens are buried in the sand around the field and water is given once a day to for the purpose of simulating the moist environmental conditions of the field. (FIG. 2(a))

The specimen sizes were 150x300mm Cylinder type specimens at each of the fields except the CTR field where the specimen sizes were 100x200mm Cylinder type specimens. Specimens made at the field were moved to the laboratory only after they were partially cured and were safe to move. After the strength increased enough for safe demolding, specimens were submerged into the 20 water (FIG. 2(b)). Specimens were picked up just before the tests and the elastic wave test and the compressive strength test were then performed.

(a) Sand curing around field (b) Standard curing in laboratory

FIG. 2. Curing Methods.

At the same time, elastic wave tests and compressive strength tests were conducted periodically since the minimum strength of concrete was developed. The demolding time was different according to field weather conditions and mixture conditions and three specimens were tested for each single test. For the first two days, tests were conducted occasionally; however, tests were performed based on curing ages of: 3-days, 7-days, 14-days, and 28-days.

Test equipment for the elastic wave test included: a computer for analysis, a NI-DAQ CARD for signal analysis, an impact hammer, an accelerometer sensor, and an analysis program (FIG.3).

Figure 4 showed the velocity measurement of the ROD wave and the shear wave in the screen and test equipment. In figure 5, the ROD wave was measured at one end of specimen by attaching an accelerometer at the center and hitting the center of the specimen at the other end. When measuring the shear wave, the accelerometer and the impact hammer were placed at the same distance from both ends of specimen which was calculated to obtain an optimum shear wave.

After completion of the elastic wave test, the compressive strength test was conducted according to the compressive strength test method specified in KS F 2405.

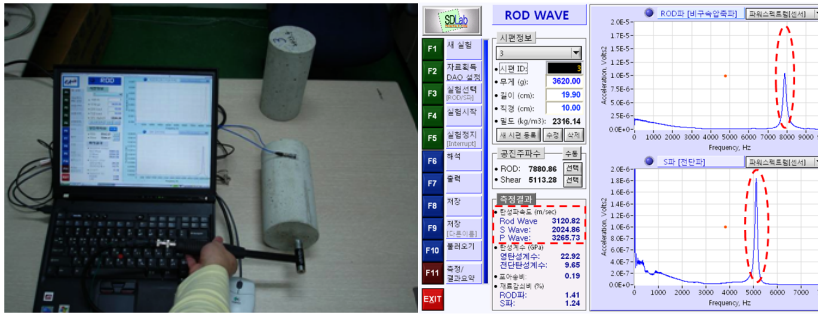

FIG. 3. Test method (Left: measuring equipment, Right: output)

FIG. 4. Elastic wave test method (Left: ROD wave, Right: shear wave)

RESULTS OF LABORATORY TESTS

The compressive strength of the concrete specimens based on the curing method and curing ages was compared in the CTR field.

The inner temperature of the specimens was measured and compared for 10 days according to different curing conditions (FIG. 5). The inner temperature of the specimen in standard curing condition was constant after early hydration reaction, whereas the temperature in sand curing condition in the field was altered by the temperature variation of atmosphere.

If this temperature data was converted to concrete maturity, the maturity of sand cured specimen in the field was 8791.9 hr· and the maturity of standard cured specimen was 8420.0 hr· . The temperature difference was 370 hr· which is considered similar.

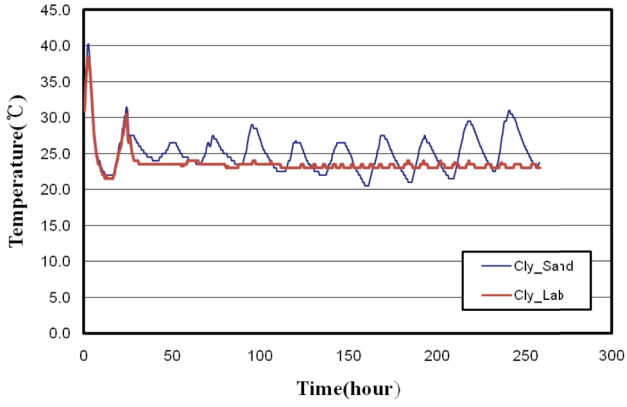

FIG. 5. Temperature Record according to the curing method (CTR)

The compressive strength of the concrete specimens in the CTR field based on the curing method and curing ages is shown in FIG. 6. The compressive strength of specimens within 48 hours after making them was marked with CTR_Ini. Specimens demolded after 24 hours of their making were cured in sand and water and three of them were tested for compressive strength according to curing ages.

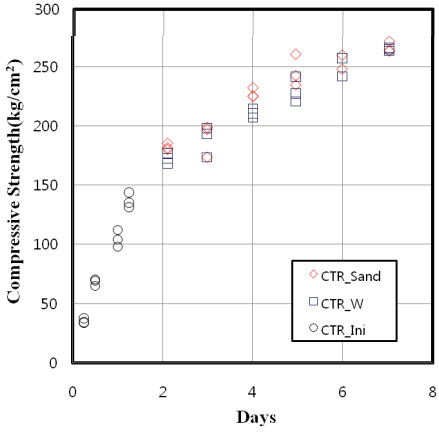

FIG. 6. Compressive strength according to the curing method by curing ages (CTR)

As a result, the compressive strength measured according to the curing ages was similar and the correlation between the elastic wave velocity and the compressive strength was same regardless of curing conditions (FIG. 7).

Consequently, even if the curing conditions were different, the correlation between elastic wave velocity and compressive strength appeared to be the same when the

mixture was the same and the maturity was similar.

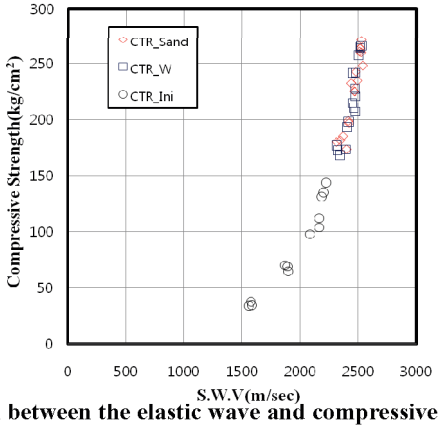

FIG. 7. Correlation between the elastic wave and compressive strength according to the curing method (CTR)

Figure 8 shows compressive strength according to the different fields. The materials and mixtures were identical in the field of Seoul Beltway 1 and Secul Beltway 2. The compressive strength of the 14-day specimen (Seoul Beltway 2) was 75% lower than the others. The deviation in compressive strength increased as the curing ages increased. The lower compressive strength of Seoul Beltway 2 might have been caused by the field temperature and the mixture error at the time they were made. The specimens were made on October 9 and November 6 for Seoul Beltway 1 and Seoul Beltway 2 respectively.

Figure 9 shows the core temperature of the specimens. The specimen temperature of Seoul Beltway 2 was lower than that of Seoul Beltway 1. After 24 hours, the temperature of the specimen was maintained in 18□ water.

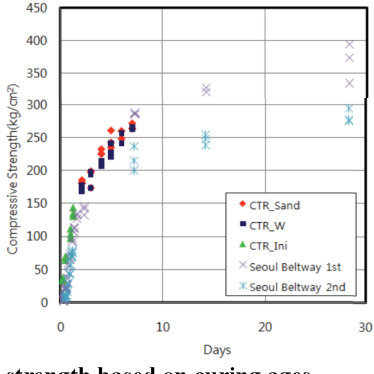

FIG. 8. Compressive strength based on curing ages

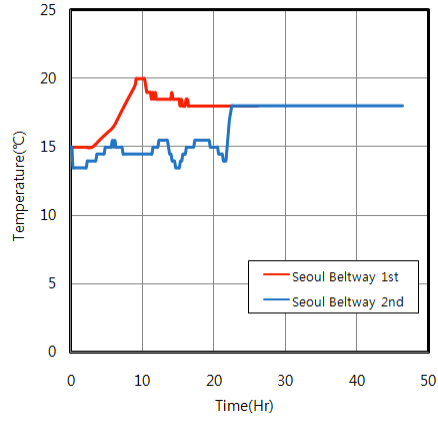

FIG. 9. Specimen Temperature

Figure 10 shows that the correlation between elastic wave and compressive strength was high regardless of curing ages. It shows the correlation between shear wave velocity and compressive strength, which are influenced by the specimen density level as a curing condition, not by the curing age. If compressive strength is high in the same curing age, then the elastic wave velocity appears high, and vice versa.

The correlation between the compressive strength and the shear wave was very high, especially in the early curing ages. Because of the characteristics of exponential functions, the change in compressive strength relative to the change of shear wave velocity was small at first, but it increased at the end.

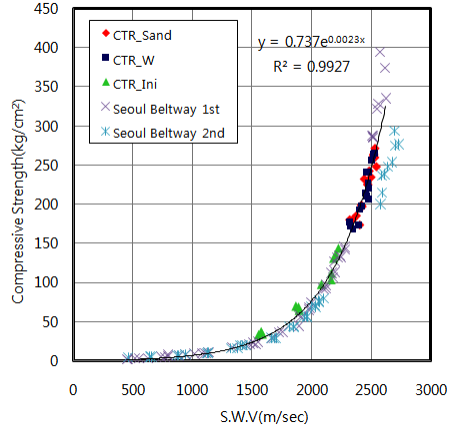

FIG.10. Correlation between shear wave and compressive strength based on curing age

CONCLUSION

The Resonance Analyzer Test, a type of nondestructive test, was conducted to analyze the correlation between the shear wave and the compressive strength according to various curing ages in different fields. The test results are summarized as follows.

1. The correlation between shear wave and compressive strength was very high and it was given by an exponential function.
2. Compressive strength appeared to be the same when the concrete maturity was similar, even if the curing conditions are different.
3. Under similar mixture conditions but different environmental conditions, compressive strength appeared to be different. However, the correlation between the elastic wave and compressive strength was similar. If the compressive strength in the same curing age was high, the elastic wave velocity appeared to be high, and vice versa.
4. Due to the characteristics of compressive strength, early age concrete strength hardly had deviations. However, as concrete aged, the deviation became higher. Therefore, the estimation of compressive strength using shear wave would be more accurate in the early curing ages.

This study discovered that the correlation between the shear wave and the compressive strength was high. From this fact, it is possible to estimate the compressive strength of desired curing ages (especially, at the early curing ages) without testing numerous specimens.

Further research will study the correlation between the shear wave velocity and compressive strength according to the various curing conditions with identical mixtures. It will also be desirable to study the change of shear wave velocity based on different aggregate content because this is expected to have an effect on the shear wave velocity.

ACKNOWLEDGMENTS

This study is part of the task "Eco-friendly pavement material and design development", supported by Ministry of Land, Transport and Maritime Affairs. Thanks to SPRC (Sustainable Pavement Research Center).

REFERENCES

An, Ji-Hwan (2000), "Material Properties for Estimation of Flexure Strength in Concrete Pavement", Master's Thesis, Chung-ang University.

A.M.Neville (1995), "Properties of Concrete, 4th", Longman

D. Yuan, S. Nazarian and A. Medichetti (2003), "A Methodology for Opening of PCC Pavements to Traffic", TX-01 4188-2, TxDOT.

Hoi-Keun Lee, Hyunjune Yim, Kwang-Myong Lee (2003), "Velocity-Strength Relationship of Concrete by Impact-Echo Method", *ACI Material Journal*, V. 100, No. 1, January-February 2003.

Heisey, S., K. H. Stokoe, II, and A. H. Meyer. (1988), " Moduli of Pavement Systems from Spectral Analysis of Surface Waves", In *Transportation Research Record 852*, TRB, National Research Council, Washington, D.C.

Hoi-keun Lee, Hyunjune Yim and Kwang-Myong Lee (2003), "Velocity-Strength Relationship of Concrete by Impact-Echo Method," *ACI Material Journal*, V.100, No. 1, January-February, 2003.

Mi-Ra Cho, Sung-Ho Joh. etc.,(2007), "Nondestructive In-Place Strength Profiling of Concrete Pavements by Resonance Search Technique" *86th Annual Meeting of the Transportation Research Board* Washington, D.C.

P.Kumar Mehta and Paulo J.M.Monteiro (2006) , "Concrete Microstructure, Properties, and Materials", McGraw Hill

Pessiki, S.., and Johnson, M. R.(1996), "Nondestructive Evaluation of Early-Age Concrete Strength in Plate Structures by Impact-Echo Method,", *ACI Material Journal*, V. 93, No. 3, May-June 1996.

Soheil Nazarian, Deren Yuan (2003), "A Methodology for Optimizing Opening of PCC Pavements to Traffic," Texas DOT, Research Report 4188-2, 2003.

V.M. Malhotra, N. J. Carino (2004), "Nondestructive Testing of Concrete", CRC Press.

Performance of Continuously Reinforced Concrete Pavement Containing Recycled Concrete Aggregate

Seongcheol Choi[1] and Moon Won[2], M. ASCE

[1]Research Engineer, Center for Transportation Research, The University of Texas at Austin, Texas, 78705 USA; seongcheol.choi@gmail.com,
[2]Associate Professor, Department of Civil & Environmental Engineering, Texas Tech University, Lubbock, Texas, 79409 USA; moon.won@ttu.edu

ABSTRACT: This paper presents the performance of continuously reinforced concrete pavement (CRCP) constructed in 1995 that utilized recycled concrete aggregate (RCA) as both coarse and fine aggregates. The project is Houston on a section of IH-10 between Loop 610 W and IH-45. In this project, no virgin aggregates were used. Concerns were raised regarding the performance of CRCP containing RCA. Detailed study was conducted to evaluate concrete material properties containing RCA. The properties of recycled aggregate measured in this study compared with virgin aggregate are consistent with those reported elsewhere: low specific gravity, higher water absorption, sulfate soundness loss, LA abrasion loss, and thermal coefficient. Little variation was observed in the paving operation due to the use of 100 % recycled coarse and fine aggregates. The moisture control of recycled aggregate, especially fine aggregate, is critical in producing consistent and workable concrete. The short-term and long-term performance of the reconstructed CRCP has been excellent, with tight crack widths and little spalling. Between concrete with virgin aggregates and concrete with recycled aggregates, there is no significant difference in thermal coefficient and permeability; however, there are significant differences in modulus of elasticity, compressive and indirect tensile strength, and water absorption. The low modulus of RCA concrete and good bond between recycled coarse aggregates and new mortar appear to be the key ingredients for good pavement performance. After more than 10 years of service under heavy traffic, the CRCP section containing 100% RCA is still providing excellent performance with no single structural distress.

Background

In 1995, TxDOT's Houston District began a rehabilitation project on a 9.3 km (5.8 miles) section of IH-10 between IH-45 and Loop 610 West to replace the distressed pavement as well as to provide high-occupancy vehicle (HOV) lanes. There are two typical sections. One is a 28 cm (11 in) concrete slab on top of a 2.5 cm (1 in) bond breaker, which sits on the existing CRCP. The other is a 36 cm (14 in) concrete slab on top of a 7.5 cm (3 in) bond breaker, which sits on 15 cm (6 in) of lime-treated subgrade. The original CRCP was constructed in 1968 and served heavy traffic for almost 30 years.

The contractor decided to utilize demolished concrete from the existing pavement for concrete aggregate. The decision was primarily based on economic reasons. All the aggregates used in this project, both coarse and fine, are recycled aggregates, with no virgin aggregate used. This is the only CRCP project to date where all the aggregates used in concrete, both coarse and fine, were recycled aggregates. TxDOT required that the recycled aggregate meet the same specification requirements as virgin aggregates. The performance of the section has been excellent, with tight crack widths, few minor spallings, and no punchouts. The original aggregate in the crushed concrete was siliceous river gravel (SRG). Normally, meandering cracks and spalling problems have been observed within a few years when SRG is used as coarse aggregate in CRCP. It has been a pleasant surprise to TxDOT that the typical meandering cracks and spalling associated with the use of SRG have not taken place in this project after more than 10 years of service under heavy traffic of IH-10 in Houston. TxDOT is so pleased with the performance of this CRCP section that it specifically allowed the use of recycled coarse aggregate for pavement concrete in its 2004 specifications.

This paper presents the findings obtained from the evaluations of the properties of concrete materials containing RCA and the performance of CRCP utilizing the concrete with RCA.

Summary of Recycled Concrete Aggregate Properties

The details of the study results are presented in the report (*1*) and part of the findings are repeated over here. Table 1 summarizes the material properties of recycled concrete aggregates. Most of the values are in agreement with those reported elsewhere. A summary of the general properties are described below:

1. Recycled coarse aggregates have lower specific gravity, higher water absorption, LA abrasion loss, thermal coefficient, and sulfate soundness loss compared with those of virgin aggregates.
2. Recycled fine aggregates have lower specific gravity and higher water absorption than virgin siliceous sand.
3. The amount of old mortar attached to the original virgin aggregate is about 30 % by volume of total recycled coarse aggregate.
4. Freeze-thaw of RCA is comparable to that of lightweight aggregates.
5. ASR potential of this specific coarse recycled aggregate as evaluated by ASTM C1260 is less than the limit (0.1 %).
6. Recycled fine aggregates are more angular than virgin siliceous river sand as evaluated by the National Aggregate Association method.

TABLE 1 Material Properties of Recycled Concrete Aggregates

material	properties	test method	test result for RCA	typical value for virgin gravel or siliceous sand
coarse aggre-gate	specific gravity	ASTM C127	2.45 ~ 2.48	~ 2.6
	mortar content	*	about 30 %	n/a
	water absorption	ASTM C127	3.9 ~ 4.1 %	< 2 %
	sodium soundness loss	ASTM C88	1 ~ 9 %	1 ~ 2 %
	magnesium soundness loss	ASTM C88	1 ~ 4 %	2 ~ 6 %
	LA abrasion	ASTM C131	32 ~ 38 %	mostly < 20 %
	thermal coefficient	*	16 ~ 26 /C	**
	freeze-thaw loss	Tex-433C	11.5 %	**(lightweigh t agg ~9%)
	alkali-silica reactivity	ASTM C1260	0.023 %	varies
fine aggre-gate	specific gravity	ASTM C128	2.37	about 2.6
	water absorption	ASTM C128	7.9 %	about 1 %
	angularity	NAA Method	38.6 %	34.5 %

* no standardized method exisits.
** not available

Evaluation of In-situ Concrete Properties

A total of 15 cores were taken representing the entire project. The detailed information has been reported elsewhere (*1*), and part of the findings are presented here. In-situ concrete properties considered to affect CRCP performance were evaluated. These properties were compared with the in-situ properties of concrete with virgin aggregates. These properties include:

Strength;
Modulus of elasticity;
Thermal coefficient of expansion;
Chloride and Sulfate;
Density; and
Permeability.

Strength – The 28-day compressive strength values range from 29.4 MPa (4260 psi) to 36.3 MPa (5270 psi) with an average of 31.8 MPa (4615 psi). It has been observed that concrete strength does not correlate well with pavement performance in terms of spalling and punchouts in CRCP. For example, concrete with SRG has higher strength than concrete with limestone or lightweight aggregate; however, the CRCP performance of concrete with SRG is generally poorer than that with limestone or lightweight aggregates *(2,3).* As with limestone or lightweight aggregate, the lower

strength of concrete with RCA should not be equated with it being an inferior material or a poor performer.

Modulus of Elasticity – The average value was 17.8 X106 MPa (2.58 million psi), which is much lower than that of normal concrete and is comparable to that of lightweight aggregate concrete. It has been observed that the CRCP performance depends to a great extent on the modulus of elasticity of concrete. The lower the modulus of the concrete, the better the performance. Low modulus values of concrete with RCA are expected since RCA contains old mortar, which is less stiff than virgin aggregates. A low modulus of concrete results in lower concrete stress due to environmental loading (drying shrinkage or thermal volume change), resulting in fewer cracks.

Coefficient of Thermal Expansion (CTE) – Since the early cracks in CRCP develop due to drying shrinkage and temperature changes, the thermal coefficient of expansion of concrete has a significant effect on early cracking in CRCP *(4)*. CTE was measured in accordance with Test Method Tex-428-A *(5)*. The average values range from 8.5 to 9.5 /C (4.7 to 5.3 /F). This value is comparable to that of concrete with virgin aggregates and much lower than the value reported previously *(1)*. Since mortar has higher CTE values than aggregates, and RCA concrete has 36 % more mortar volume than concrete with virgin aggregates, it was expected that concrete with RCA would have higher CTE values *(6)*. However, the values obtained in this study are comparable to or slightly lower than those of concrete with SRG.

Chloride and Sulfate Content – One of the concerns raised regarding the use of RCA was the potential deterioration of concrete with RCA due to high chloride and sulfate content. The chloride and sulfate values were obtained in accordance with Test Methods Tex-617J and Tex-620J, respectively *(5)*. The average sulfate value obtained is 1436 ppm and the average chloride content is 0.03 kg/m^3 (0.04 lb/cy). Chloride and sulfate contents in concrete with virgin aggregates were evaluated from cores off of new bridge decks. The average chloride value from 98 specimens was 0.005 kg/m^3 (0.007 lb/cy) with a standard deviation of 0.011 kg/m^3 (0.015 lb/cy). For the typical concrete mixtures normally used in practice, the threshold chloride content to initiate corrosion is in the range of 0.6 to 0.9 kg/m^3 (0.8 to 1.2 lb/cy) *(7)*. Even though it contains more chloride than the concrete in new bridge decks, the chloride content of the RCA concrete is much lower than the threshold value for steel corrosion. However, this result does not mean that chloride might not be a potential problem for RCA concrete in locations where deicing salts are used. Normally, deicing salts are not needed in the Houston area, which explains the low chloride content in RCA concrete. In northern states where deicing salts are used extensively, the use of recycled aggregates might result in higher chloride contents in concrete.

Density – Since the RCA has lower specific gravity than virgin aggregate due to the mortar volume attached to the original aggregate, it is expected that the density or unit weight of concrete will be lower than that of normal concrete. The densities of concrete from several mix designs for this project range from 2.16 to 2.21, which are lower than that of concrete with virgin aggregates. The density obtained from the cores range from 2.19 to 2.36, with an average of 2.24, which indicates the consolidation of concrete during construction was satisfactory, as further evidenced by few honeycombs and by limited segregation of aggregates.

Permeability **–** The permeability of concrete was evaluated in accordance with ASTM C 1202. The values from eight specimens ranged from 366 to 628 Coulomb, with the average value of 466 Coulomb. These values are surprisingly small compared with those from normal concrete. The values for the concrete from high performance concrete bridge decks vary from 1050 to 1150 Coulomb at one year. This bridge deck concrete had 6 sacks of cement with 30 % Class C fly ash. It was expected that the larger volume of mortar in RCA concrete would make it more permeable; however, this test result showed that was not the case. According to the criteria stipulated in ASTM C 1202, RCA concrete is classified as very low in chloride penetrability, whereas concrete from high performance concrete bridge decks is classified as low in chloride penetrability.

Pavement Performance

Pavement performance was evaluated in terms of transverse crack spacing, crack widths, and spalling. The average crack spacing evaluated in 1999 was 2.19 m (7.19 ft) with a standard deviation of 1.36 m (4.45 ft). This crack spacing is larger than that of SRG concrete and is comparable to that of limestone concrete *(8)*. Low modulus of elasticity and medium CTE of this concrete appear to offset the effect of low concrete strength on cracking behavior of this concrete. Crack width was measured in the shoulder. Overall, cracks were tight, with the majority of crack widths ranging from 0.2 mm (0.008 in) to 0.7 mm (0.028 in). For the CRCP to perform satisfactorily, cracks need to be kept tight. Tight crack width provides good load transfer and minimizes the water intrusion into cracks. Even though the measured crack widths are small, the variability in the crack width measurements can be substantial, mainly due to the changes in crack width along a crack. The variability is also due to the temperature effect. In an experiment in this study, crack width was measured every 3 inches along the crack. In one crack, the crack width varied from 0.4 mm (0.016 in) to 0.8 mm (0.031 in). Therefore, during the crack width measurement, caution was taken to measure representative crack width.

Over the last 10 years, spalling has not been a problem in this project. As mentioned earlier, spalling has been the major problem in CRCP in Houston when virgin SRG is used as a coarse aggregate. Petrographic analysis shows a good bond between old mortar and original siliceous river gravel aggregate in coarse RCA. It appears that once the bond between mortar and SRG surface survives the volume change strains and stresses during the hardening stages of concrete without cracking, good bond will eventually develop. There is a good bond between old and new mortar, as shown in Figure 1. It is believed that this good bond is responsible for the minimal spalling problems in this project. The condition of the pavement is shown in Figure 2, which was taken in 2009, more than 10 years after the construction. Under heavy traffic, it appears that the pavement section provided excellent performance.

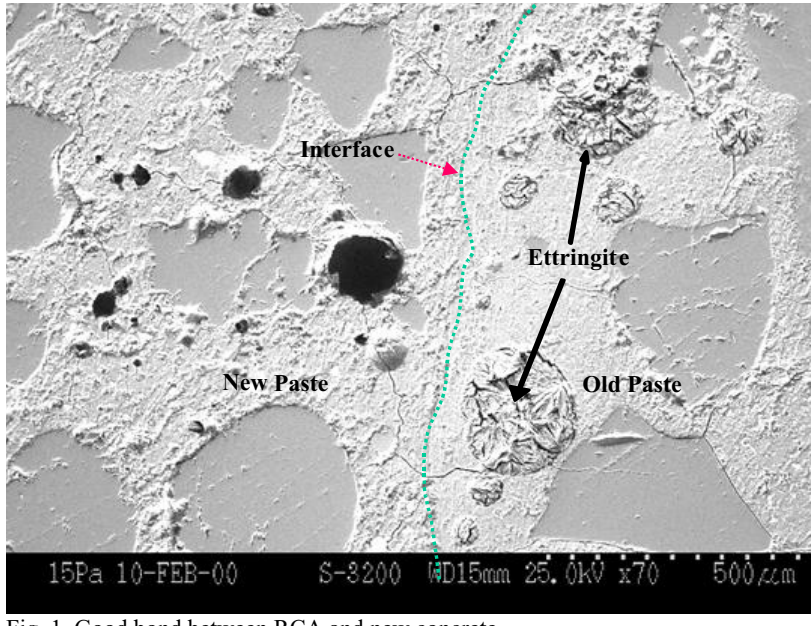

Fig. 1. Good bond between RCA and new concrete

Fig. 2 Condition of CRCP with RCA in 2009

CONCLUSIONS

Based on the results of this study, the following conclusions are made:

1) recycled concrete aggregate properties

- Recycled coarse aggregates have lower specific gravity, higher water absorption, LA abrasion loss, thermal coefficient, and sulfate soundness loss compared with those of virgin aggregates.
- Recycled fine aggregates have lower specific gravity and higher water absorption than virgin siliceous sand.
- The amount of old mortar attached to the virgin aggregate is about 30 % by volume of total recycled coarse aggregate.
- Freeze-thaw of RCA is comparable to that of lightweight aggregates.
- ASR potential of this specific coarse recycled aggregate as evaluated by ASTM C1260 is less than the limit (0.1 %).
- Recycled fine aggregates are more angular than virgin siliceous river sand as evaluated by National Aggregate Association method.

2) In-situ properties of concrete containing 100 % recycled coarse and fine aggregates

- Compressive and indirect tensile strengths are lower than that of concrete with virgin aggregates.
- Modulus of elasticity is much lower than that of concrete with virgin aggregates.
- Coefficient of thermal expansion is comparable to that of concrete with virgin aggregates.
- Chloride content is higher than that in the concrete with virgin aggregates.
- Sulfate content is comparable to that in concrete with virgin aggregates.
- Density is lower than that of concrete with virgin aggregates.
- Permeability is classified as “very low” according to ASTM C 1202.

3) performance of CRCP with 100 % recycled aggregates

- The pavement has performed well. No structural distresses have taken place.
- The transverse crack spacing distributions are comparable to those in concrete with virgin limestone.
- Low modulus of concrete and good bond between recycled coarse aggregate and new mortar appear to be the key ingredient of good pavement performance.
- The large amount of old mortar in recycled coarse aggregate does not appear to have an adverse effect on CRCP performance.

References

(1) Won, M. Use of Crushed Concrete as Aggregate for Pavement Concrete. 7th Annual Symposium Proceedings, International Center for Aggregate Research, The University of Texas at Austin, April 1999.

(2) McCullough, B.F., Won, M., and Hankins, K. Long-Term Performance Study of Rigid Pavements. Proceedings, 4th International Conference on Concrete Pavement Design and Rehabilitation. Purdue University. West Lafayett, IN 1990.

(3) McCullough, B.F., Zollinger, D., and Dossey, T. Evaluation of the Performance of Texas Pavements Made with Different Coarse Aggregates. Research Report 3925-1, Center for Transportation Research, The University of Texas at Austin. September 1998.

(4) Suh, Y.C., Hankins, K., and McCullough, B.F. Early-Age Behavior of Continuously Reinforced Concrete Pavement and Calibration of the Failure Prediction Model in the CRCP-7 Program. Research Report 1244-3, Center for Transportation Research, The University of Texas at Austin. March 1992.

(5) Texas Department of Transportation. Manual of Testing Procedures. Volume III, Austin, Texas, September 1995.

(6) Neville, A.M. Properties of Concrete. 4th ed. John Wiley & Sons, Inc. New York, NY, 1996.

(7) Mehta, K. and Monteiro, P. Concrete. Second Edition, Prentice Hall, Englewood Cliffs, New Jersey 1993.

(8) Gutierrez, M. and McCullough, B.F. Summary Report for 1978 CRCP Condition Survey in Texas. Research Report 177-20, Center for Transportation Research, The University of Texas at Austin. January 1981.

Author Index

Page number refers to the first page of paper

An, Ji-Hwan, 154, 107
An, ZuOg, 101

Bae, Jong-Oh, 101

Cen, Guo-ping, 93
Chen, Dar Hao, 119
Chen, Yu-liang, 35, 75
Cho, Yoon-Ho, 101
Choi, Seongcheol, 165
Crawford, Taylor, 119

Fowler, David W., 119
Fu, Hongyuan, 85

Gaul, Robert, 1
Guo, Zhongyin, 52

Hou, Xiangshen, 140
Huang, Wei, 9
Huang, Xiaoming, 61

Jeon, Sungil, 107
Jin, Shu-yang, 68
Jirsa, James, 119
Joh, Sung-Ho, 154

Kim, Hyung Bae, 19
Kuang, Bo, 85
Kwon, Soo-Ahn, 107, 154

Lee, Kwang-Ho, 19
Lee, Seung Woo, 101
Li, Le, 93
Li, Xinkai, 140
Li, Xue-lian, 35, 75
Ling, Chen, 52
Liu, Yun, 28
Luo, Bing, 68

Ma, Songlin, 140

Nam, Jeong-Hee, 107, 154
Nam, Jung-Hee, 101

Pan, Youqiang, 52
Park, Min-Young, 101

Qian, Zhendong, 9, 28

Ryu, Sung Woo, 101

Stringer, Megan, 119

Tao, Xiang-hua, 133

Whitney, David, 119
Won, Moon, 119, 165

Xu, Jia, 125
Xu, Tao, 61

Yang, Jian-jun, 45

Zeng, Sheng, 125
Zeng, Xiaojun, 125
Zha, Xudong, 147
Zhang, Lei, 9, 28
Zhang, Wen-xian, 68
Zhang, Yang, 85
Zheng, Jian-long, 45

This page intentionally left blank

Subject Index

Page number refers to the first page of paper

Aggregates, 165
Aging, 101
Airport runways, 93
Asphalt pavements, 1

Bonding, 35
Bridge construction, 68
Bridge decks, 1, 9, 19, 35, 45, 52, 61, 75
Bridge design, 9
Bridges, arch, 35
Bridges, concrete, 35
Bridges, highway, 9, 19, 28, 45, 61, 133
Bridges, long span, 9
Bridges, steel, 9, 75

Cements, 75
China, 1, 28, 45, 52, 140
Composite materials, 75
Compressive strength, 154
Concrete, 107, 154
Concrete construction, 68
Concrete pavements, 52, 85, 93, 101, 119, 125, 147, 165
Concrete slabs, 85, 140
Coupling, 140
Cracking, 119, 140, 147

Deflection, 125, 140
Deterioration, 52

Fatigue, 75, 93
Fiber reinforced materials, 68
Finite element method, 61
Fly ash, 107

Joints, 119

Korea, South, 101

Mechanical properties, 35, 45, 61, 68
Moisture, 19

Optimization, 9
Orthotropism, 1, 75

Parameters, 61, 93
Particle size, 107
Pavement design, 61
Pavement overlays, 101
Pavements, 9, 19, 28, 45, 75
Physical properties, 107
Portland cements, 85

Quality control, 154

Recycling, 165
Rehabilitation, 19, 119
Reinforced concrete, 68, 101, 147, 165

Sensitivity analysis, 93, 147
Settlement, 133
Shear stress, 28
Shear waves, 154
Slabs, 125
Stress analysis, 85, 140
Structural analysis, 35

Temperature effects, 140

Vehicles, 133
Velocity, 154
Voids, 85, 125